Industria Textilă

ISSN 1222-5347

2/2016

Revistă **cotată ISI** și inclusă în **Master Journal List** a Institutului pentru Știința Informării din Philadelphia – S.U.A., începând cu vol. 58, nr. 1/2007/
ISI rated *magazine, included in the* ***ISI Master Journal List*** *of the Institute of Science Information, Philadelphia, USA, starting with vol. 58, no. 1/2007*

Editată în 6 nr./an, indexată și recenzată în:
Edited in 6 issues per year, indexed and abstracted in:
Science Citation Index Expanded (SciSearch®), Materials Science Citation Index®, Journal Citation Reports/Science Edition, World Textile Abstracts, Chemical Abstracts, VINITI, Scopus, Toga FIZ technik ProQuest Central

Recunoscută în România, în domeniul Științelor inginerești, de către **Consiliul Național al Cercetării Științifice din Învățământul Superior** (C.N.C.S.I.S.), în **grupa A** /
Aknowledged in Romania, in the engineering sciences domain, by the ***National Council of the Scientific Research from the Higher Education*** *(CNCSIS), in* ***group A***

it Sumar

Contents

EDITORIAL STAFF

Editor-in-chief: Dr. eng. Emilia Visileanu
Graphic designer: Florin Prisecaru
e-mail: visilean@ns.certex.ro

Journal edited in colaboration with **Editura AGIR**, 118 Calea Victoriei, sector 1, Bucharest, tel./fax: 021-316.89.92; 021-316.89.93;
e-mail: editura@agir.ro, www.edituraagir.ro

A comparison for the physical properties of cotton, modal and acrylic yarns spun in ring and OE-rotor spinning systems

GONCA BALCI KILIC AYŞE OKUR

REZUMAT – ABSTRACT

Comparație între proprietățile fizice ale firelor de bumbac, modale şi acrilice filate în sistemele cu inele şi cu capăt liber OE

Scopul acestui studiu a fost de a analiza efectele materiei prime şi ale sistemului de filare asupra proprietăților fizice ale firelor. În acest scop, au fost analizate fire din fibre: naturale (100% bumbac), regenerate (100% modale) şi sintetice (100% acrilice). Firele au fost realizate utilizând sistemele de filare cu inele şi capăt liber (OE). Neuniformitatea firelor, neuniformitatea optică, imperfecțiunile, proprietățile structurale cum ar fi densitatea, CVFS% (rugozitatea), forma (rotunjimea) etc., pilozitatea, frecarea fir-fir, frecarea fir-ceramică şi frecarea fir-metal au fost evaluate în scopul realizarii acestui studiu. La evaluarea efectului sistemelor de filare, rezultatele au arătat că valorile neuniformității, imperfecțiunilor, diametrului şi rugozitatii, în cazul firelor filate cu capăt liber (OE), sunt ridicate. Pe de altă parte, s-a constatat că valorile densității, factorului de formă, pilozității şi coeficienţilor de frecare pentru firele filate cu capăt liber (OE) sunt mai mici decât în cazul firelor filate cu inele, pentru toate tipurile de materiale. Mulți cercetători afirmă că efectul materiei prime asupra proprietăților firelor este important. Cu toate acestea, în acest studiu, se remarcă faptul că valorile neuniformității, imperfecțiunilor, pilozității şi coeficienţilor de frecare ale firelor modale şi acrilice din fibre cu aceeaşi lungime şi finețe sunt apropiate.

Cuvinte-cheie: fire filate cu inele, fire filate cu capăt liber, fire acrilice, fire modale, metoda Capstan, metoda cu dublă răsucire, frecarea firului, pilozitatea firului

A comparison for the physical properties of cotton, modal and acrylic yarns spun in ring and OE-rotor spinning systems

In this study, it was aimed to analyze the effects of raw material and spinning system on physical properties of yarns. For this purpose, natural (100% cotton), regenerated (100% Modal) and synthetic (100% acrylic) yarns were analyzed. Yarns were produced systematically in ring and open-end rotor (OE-rotor) systems. Yarn unevenness, optical unevenness, imperfections, structural properties such as density, CVFS% (roughness), shape (roundness) etc., yarn hairiness, yarn-to-yarn friction, yarn-to-ceramic friction and yarn-to-metal friction properties were evaluated in the scope of the study. When the effect of spinning systems is evaluated, results show that the values of unevenness, imperfections, diameter and roughness for OE-rotor yarns are higher. On the other hand, values of density, shape factor, hairiness and friction for OE-rotor yarns are found lower than ring yarns for all material types. Many researchers state that the effect of raw material on yarn properties is important. However, in this study, it is remarkable that unevenness, imperfections, hairiness and friction values of Modal and acrylic yarns made of fibres with the same length and fineness are fairly close to each other.

Keywords: ring yarns, open-end rotor yarns, acrylic yarns, Modal yarns, Capstan method, twisted strand method, yarn friction, yarn hairiness

INTRODUCTION

Raw material and spinning system are known to be the most important factors which determine physical properties of yarns. Although different spinning systems developed in recent years, conventional spinning systems (ring and OE-rotor) are still commonly used. Ring and OE-rotor spinning systems constitute approximately 90% of yarn production in the world [1].

Many researchers have studied the effect of raw materials and spinning systems on yarn properties [2–8]. Mohamed et al. analyzed the hairiness and diameter of 100% cotton, 100% polyester and cotton-polyester ring and open-end yarns and stated that OE yarns are more bulky but less hairy than corresponding ring yarns. On the other hand, they found that the hairiness of OE yarns have a higher coefficient of variation than ring yarns [9]. Jackowska-Strumillo et al. studied the quality of cotton yarns spun using ring-, compact-, and rotor-spinning machines and found that the rotor yarns are characterized by lower hairiness, unevenness and tenacity [10]. Kilic and Okur investigated the effect of structural, physical and mechanical properties of ring, compact and vortex spun yarns. They found that hairiness values of ring yarns are the highest and vortex yarns are the lowest [11]. Soe et al. investigated the structure and properties of vortex spun yarns and compared with ring and open-end rotor spun yarns. They measured

yarn properties such as evenness, hairiness, bulkiness, tenacity, compression and bending properties and concluded that vortex yarns are stiffer than ring and open-end rotor spun yarns, while ring yarns have the highest tenacity values [12]. Ghosh et al. investigated yarn-to-yarn (YY) and yarn-to-metal (YM) friction coefficients of yarns which were produced in different spinning systems (ring, rotor, air-jet, open-end, friction) by using viscose fibres. The results indicate that in case of YM friction, ring yarns have higher friction values than rotor yarns [13]. Balci Kilic and Sülar investigated the frictional properties of 100% cotton, 100% Tencel LF, %50:50 cotton/Tencel LF blended yarns spun in ring-, compact- and vortex-spinning systems. Results show that the lowest YY friction coefficient values belong to the vortex yarns. However, the highest YM and YC friction coefficient is observed for vortex yarns [14]. Tyagi et al. studied the response of cotton ring- and rotor-spun yarns to mercerization treatment. The results show that yarn-to-metal frictional coefficient of OE-rotor-spun yarns are significantly lower than ring-spun yarns for both mercerized and grey yarns [15]. Nair et al. also examined the relationship between physical properties and frictional properties of cotton fibres and yarns and showed coarser and more compressible yarns have higher coefficients of friction values [16].

Systematically spun ring and OE-rotor yarns made of natural (100% cotton), regenerated cellulose (100% Modal) and synthetic (100% acrylic) fibres were preferred in the scope of this study. The fibre length and fibre fineness also directly affect the physical properties of yarns. Most of the studies carried out to investigate the yarn properties have ignored this fact. In this kind of studies, yarns have to contain fibres with the same length and fineness for better comparison. For this reason, Modal and acrylic fibres with the same length and fineness, cotton fibres have different length and fineness due to its natural structure were used in the study. Cotton fibres were preferred as reference raw material which is traditionally used to evaluate the effects of spinning systems.

EXPERIMENTAL WORK

Materials and methods

In this study, natural (100% cotton), regenerated (100% Modal) and synthetic (100% acrylic) ring and OE-rotor yarns were analyzed. Properties of cotton, Modal and acrylic fibres are given in table 1 and table 2. Acrylic and Modal fibres have same cut length and fineness (table 2). All yarns were produced systematically in both spinning systems. The slivers that have the same properties were used in ring and OE-rotor spinning systems. The fibres of all yarns were passed through the same production steps for both spinning systems to analyze the effect of raw material and spinning system accurately. The cotton fibres passed through the combing process.

Unevenness, imperfections, diameter, density, roughness, shape, hairiness and yarn friction (yarn-to-yarn, yarn-to-metal and yarn-to-ceramic) were measured in the study. For 100% cotton yarns, the effect of spinning system and for 100% acrylic and 100% Modal yarns that have the same fibre length and fibre fineness, also the effect of raw material were investigated. Moreover, yarn hairiness and yarn-to-yarn friction values were measured using two different methods for each. The effect of measuring method on frictional properties of yarns is also analyzed.

Unevenness, imperfections, diameter, density, roughness and shape values of yarns were measured by using Uster Tester 5 S800. Every test was performed at 400 m/min test speed throughout 2.5 minutes. Hairiness value of yarns (H) was measured by using Uster Tester 5 S800 with at 400 m/min test speed throughout 2.5 minutes. Hairiness value was also measured by using Uster Zweigle Hairiness Tester 5 (UZHT5) with 5 cN pretension with 50 m/min test speed and 4 minutes test duration. The hairiness value of the UT5 is called *H*, whereas the hairiness values of the UZHT5 is called *S3*. UZHT5 also measures S1+2 value. The H value is total length of protruding hairs per centimeters, *S3* value is the sum of all protruding fibres 3 mm and longer (cumulative) and S1+2 value is the total amount of the fibres shorter than 3 mm [17–18]. Measurement of yarn-to-yarn (YY), yarn-to-metal (YM) and yarn-to ceramic (YC) friction were performed by using Lawson Hemphill CTT Dynamic Friction Tester with a constant speed of 100 m/min. The friction testing device used in the experiments has a tension arm and the input tension is set at constant value by this arm. The output tension is measured by the tension meter and the friction coefficient is calculated by software through input and output tensions [19]. YY, YM and YC tests were

Table 1

PROPERTIES OF COTTON FIBRES (HVI RESULTS)	
Fibre fineness (micronaire)	3.6
Fibre length (mm)	29.5
Tenacity (cN/tex)	29.0
Elongation (%)	4.85
Uniformity (%)	82.5
Maturity	0.88
SFI (%)	8.50

Table 2

PROPERTIES OF MODAL AND ACRYLIC FIBRES		
Parameters	Modal	Acrylic
Fineness (dtex)	1.3	1.3
Cut length (mm)	38	38
Tenacity (cN/tex)	35	30
Elongation (%)	13	35.4
Tenacity in wet state (cN/tex)	20	35.8
Elongation in wet state (cN/tex)	15	36.4

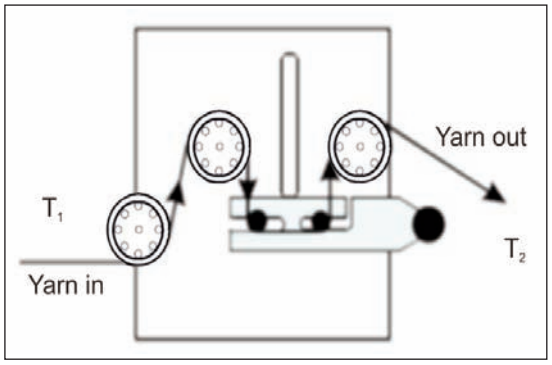

Fig. 1. The position of yarns during yarn-to-material friction tests

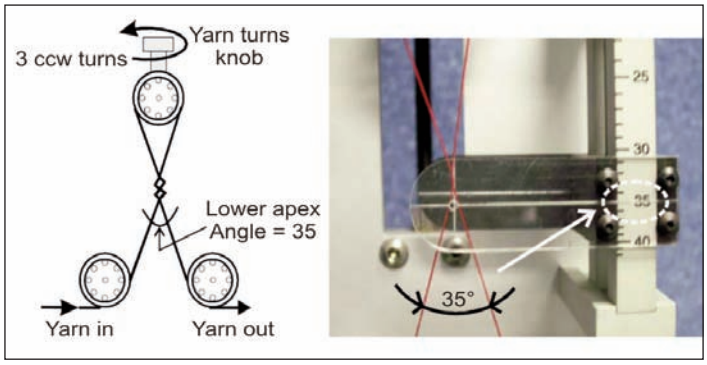

Fig. 2. The position of yarns during yarn-to-yarn friction tests (twisted strand method)

performed by using 5 cN input tension. When the literature is examined, it could be seen that input tension in knitting process ranges from 3 to 10 cN [20–22]. In this study, input tension is selected as 5 cN which is equal to pretension in UZHT5.

Yarn is allowed to run over friction surfaces such as stainless steel or ceramic pin with a specified wrap angle in yarn-to-material (YM and YC) test and the method is called "Capstan Method". YM and YC friction tests are performed with the same test fixture by changing friction pins. The software calculates the coefficient of yarn-to-material friction (μ) using the Capstan formula given in equation 1 [23]:

$$\mu = \frac{\ln\left(\frac{T_2}{T_1}\right)}{\theta} \quad (1)$$

μ is the coefficient of yarn-to-material friction; T_2 – the output tension; T_1 – the input tension; θ – the cumulative wrap angle (radian) (figure 1).

Yarn is wrapped around itself in YY friction test and it is named "Twisted Strand Method". Output tension on the yarn changes during the test and is measured by tension meter. The software calculates the coefficient of yarn friction using the input and output tension values as well as the number of wraps and apex angle (figure 2). The coefficient of YY friction using the formula given in equation 2 [24]:

$$\mu = \frac{\ln\left(T_2/T_1\right)}{4\pi(n - 0.5)\sin\beta/2} \quad (2)$$

where μ is the coefficient of YY friction; T_2 – the output tension; T_1 – the input tension; β is 35° (lower apex angle between two yarns); and n – the number of wraps ($n = 3$).

Yarn-to-material (YM and YC) and YY friction tests are performed by different methods and the coefficients of friction are calculated by different formulas as mentioned above. In the study, YY tests also performed with Capstan Method. Yarn is wrapped around on fixed frictionless pulleys and cumulative wrap angle is measured (225°) for every test in this method and friction coefficient of yarn is calculated using the Capstan Formula (figure 3).

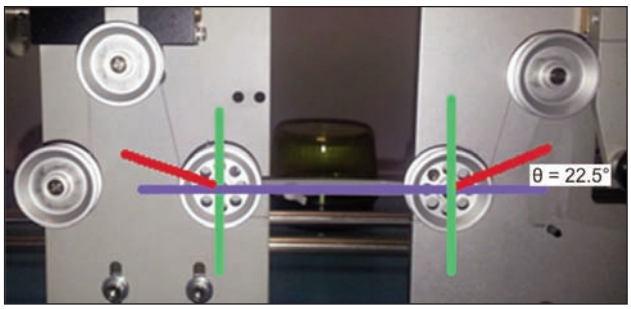

Fig. 3. The position of yarns during yarn-to-yarn friction tests (Capstan method)

RESULTS AND DISCUSSION

In this section, effects of raw material and spinning system on yarn properties were evaluated in terms of unevenness, imperfections, structural properties (density, CVFS%, shape etc.), hairiness and frictional properties. The test results were evaluated by SPSS 20 software to compare the main effects. Analyses of variance (ANOVA) were performed for $\alpha = 0.05$ significance level

Unevenness and Imperfections

Unevenness (CVm%), optical unevenness (CV2D 0.3 mm%), values of thin places (–50 %/km), thick places (+50 %/km) and neps (+200 %/km, +280 %/km) of 100% cotton, 100% Modal, 100% acrylic ring and OE-rotor yarns are given in table 3. Unevenness and optical unevenness results are shown in figure 4 and ANOVA results are shown in table 4. It is seen that the effect of spinning system is statistically significant on both yarn unevenness and imperfections for cotton, Modal and acrylic yarns ($p \leq 0.05$). The OE-rotor yarns have higher values for all parameters.

When the effect of raw-material on unevenness and optical unevenness is evaluated, it is seen that cotton yarns have the highest values for both ring and OE-rotor spinning technologies as expected (figure 4). Acrylic yarns have lower values than Modal yarns for both ring and OE-rotor spinning technologies. For ring yarns, differences are not statistically significant between Modal and acrylic raw materials ($p = 0.073$). The number of fibres in yarn cross-section and the

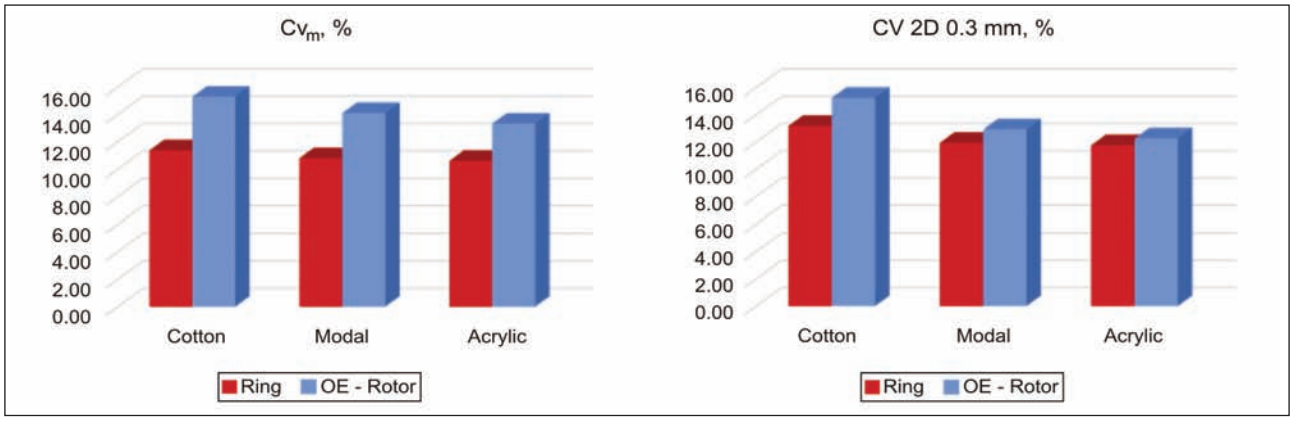

Fig. 4. CVm % and CV 2D 0.3 mm% values of ring and OE-rotor yarns

Table 3

UNEVENNESS AND IMPERFECTION VALUES OF RING AND OE-ROTOR YARNS						
Parameters	**RING**			**OE-ROTOR**		
	Cotton	**Modal**	**Acrylic**	**Cotton**	**Modal**	**Acrylic**
Cvm%	11.40	10.82	10.63	15.32	14.12	13.36
CV2D 0.3 mm	13.19	11.95	11.78	15.26	12.94	12.28
Thin places –50%	0.0	0.0	0.8	67.5	14.2	13.8
Thick places +50%	5.8	4.6	1.3	82.9	44.6	14.2
Neps +200%	13.3	12.9	0.8	340.4	121.7	27.9
Neps +280%	1.0	0.0	0.0	15.2	6.5	11.5

Table 4

ANOVA RESULTS FOR Cv_m (%) AND CV2D 0.3 mm(%)					
Parameters	**Spinning System**	**Sum of Squares**	**Mean Square**	**F**	**Sig.**
Cvm (%)	RING	1.967	0.983	33.713	0.000
	OE-ROTOR	11.728	5.864	287.856	0.000
CV2D 0.3 (%)	RING	7.180	3.590	58.356	0.000
	OE-ROTOR	29.432	14.716	422.849	0.000

fibre length are the main parameters which effect yarn unevenness [25]. In the study, Modal and acrylic fibres have the same linear densities (1.3 dtex) and fibre lengths (38 mm). This is the main factor to get statistically the same unevenness values for Modal and acrylic yarns. For OE-rotor yarns, it is seen that differences between the Modal and the acrylic raw materials are also statistically significant ($p \leq 0.05$). The main factor for this situation is thought to be the differences between the spinning technologies. In ring spinning, distances between the drafting rollers take effect for unevenness. On the other hand, in OE-rotor spinning system fibres become individual elements after opening roller and form a yarn structure by the help of frictional forces in the rotor groove. Because the frictional forces between the acrylic fibres are higher, yarn formation stage is more controlled when the yarn is pulled out of the navel [26].

If the effect of raw material on imperfections is examined, it is seen that effect of raw material is not statistically significant for ring yarns in terms of thin places (–50 %/km), thick places (+50 %/km) and neps (+200 %/km). On the other hand, the effect of raw material on imperfections is statistically significant for OE yarns. However, OE-rotor acrylic yarns have lower values of thin places (–50 %/km), thick places (+50 %/km) and neps (+200 %/km) because of the effect of their surface properties related with frictional forces.

Structural Parameters

Diameter (2DØ mm), density (D g/cm^3), roughness (CV FS %) and optical shape (roundness) values of cotton, Modal and acrylic yarns spun in ring and open-end systems are shown in table 5 and bar charts of these parameters are shown in figures 5 and 6.

Table 5

STRUCTURAL PARAMETERS OF RING AND OE-ROTOR YARNS						
Parameters	**RING**			**OE-ROTOR**		
	Cotton	**Modal**	**Acrylic**	**Cotton**	**Modal**	**Acrylic**
2DØ (mm)	0.23	0.21	0.22	0.26	0.23	0.24
D (g/cm^3)	0.46	0.57	0.51	0.38	0.47	0.42
CV FS (%)	8.84	8.11	7.21	10.46	8.93	8.50
Shape	0.83	0.84	0.85	0.76	0.78	0.80

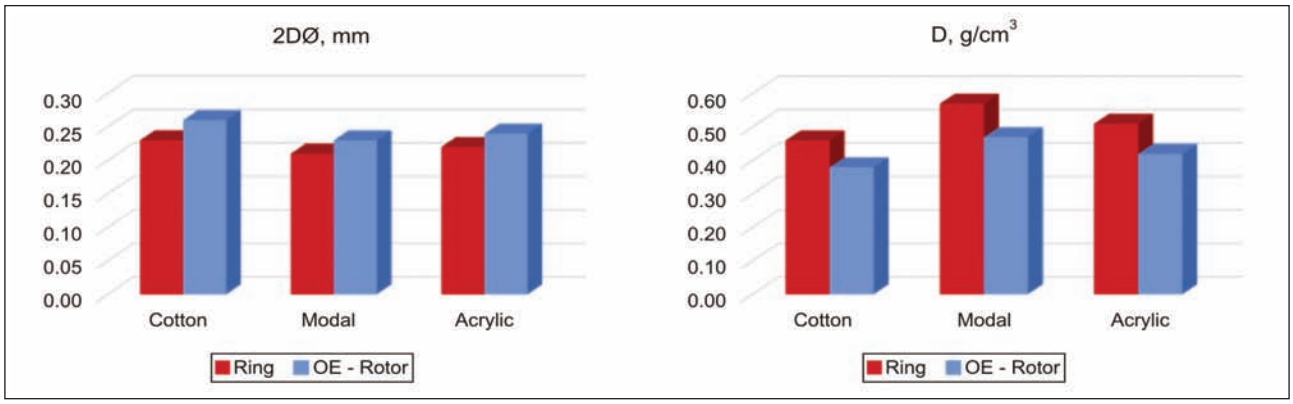

Fig. 5. Diameter (mm) and density (g/cm^3) values of ring and OE-rotor yarns

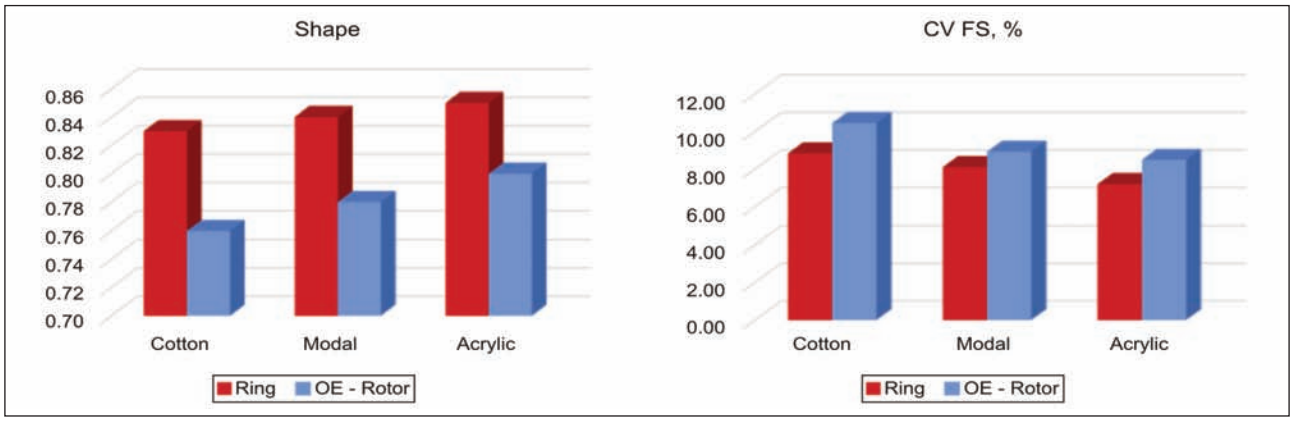

Fig. 6. Shape and roughness (CV FS %) values of ring and OE-rotor yarns

Upon a general evaluation of the spinning systems, the effect of spinning system is found to be statistically significant on diameter (2DØ mm), density (D g/cm^3), roundness (Shape) and roughness (CV FS %) values ($p \leq 0.05$). Density (D g/cm^3) and roundness (Shape) values of ring yarns are higher than OE-rotor yarns for all of the raw material types. Furthermore, roughness (CV FS %) and diameter (2DØ mm) values of OE-rotor yarns are higher than ring yarns. These are all due to the differences between ring and OE-rotor spinning technologies. Since the fibers are located through a helical way in a ring yarn, ring yarns have denser structures than OE-rotor yarns. This means lower diameter, but higher density for ring yarns. In addition, helical settlement causes more regular and round shape for ring yarns. In terms of roughness property, rotor yarns have higher values because of the wrapper structure. Figure 7 shows the cross-sectional images of ring and OE-rotor yarns that were processed by image analysis tools.

The effect of raw material is also found to be statistically significant on structural parameters ($p \leq 0.05$) (table 6 and table 7). When a comparison is done between Modal and acrylic yarns, 100% Modal yarns have lower diameter and higher density values for both spinning systems. This would be due to the trilobal cross-sectional shape of Modal fibres. It is thought that trilobal fibres packed closer and this would cause a denser structure (figure 7).

Roughness (CV FS%) is CV of fine structure of a yarn and it means irregularity increase between

Table 6

ANOVA RESULTS FOR 2DØ (mm) AND D (g/cm^3)					
Parameters	**Spinning System**	**Sum of Squares**	**Mean Square**	**F**	**Sig.**
2DØ (mm)	RING	0.002	0.001	206.430	0.000
	OE-ROTOR	0.002	0.001	260.071	0.000
D (g/cm^3)	RING	0.040	0.020	230.192	0.000
	OE-ROTOR	0.024	0.012	182.672	0.000

Table 7

ANOVA RESULTS FOR SHAPE AND ROUGHNESS (CV FS%)					
Parameters	**Spinning System**	**Sum of Squares**	**Mean Square**	**F**	**Sig.**
Shape	RING	0.002	0.001	29.400	0.000
	OE-ROTOR	0.005	0.002	28.562	0.000
Roughness (CV FS %)	RING	7.952	3.976	34.963	0.000
	OE-ROTOR	12.773	6.386	236.281	0.000

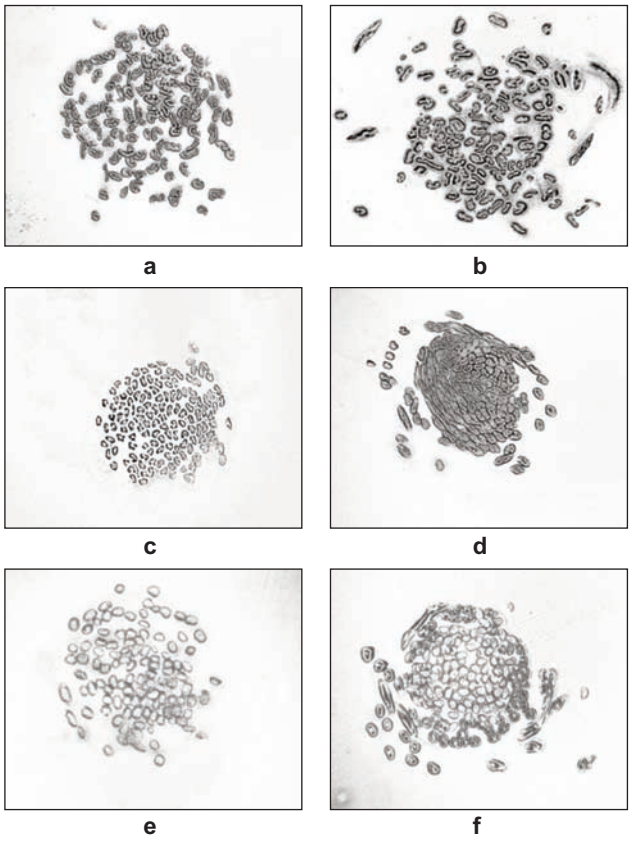

Fig. 7. Cross-sectional images of ring and OE-rotor yarns: *a* – cotton-ring; *b* – cotton-rotor; *c* – Modal-ring; *d* – Modal-rotor; *e* – Acrylic-ring; *f* – Acrylic rotor

0.3 mm and 8 mm cut length taken into account. On the other hand, shape is a factor which indicates the average yarn roundness of the yarn. Roughness value corresponds to the ratio of the short-to the long main axis of an ellipse (1 = circular, 0.5 = ellipse ½ as wide as long) [17]. If a general evaluation is made for shape and roughness values of yarns, it is seen that yarn roughness (CV FS%) decreases while the shape (roundness) factor increases for both spinning systems. It is seen that acrylic yarns have higher shape and lower roughness values for ring and OE-rotor spinning systems.

Yarn hairiness

Yarn hairiness values (S1+2, S3 and H) of ring and open-end spun cotton, modal and acrylic yarns are shown in figure 8. ANOVA results are given in table 8. When a general evaluation is made in terms of spinning technologies and raw material, it is seen that the effect of spinning system and the effect of raw material are statistically significant on yarn hairiness, whether the hairiness is measured by different principles such as UZHT5 (S1+2, S3) or UT5 (H) ($p \leq 0.05$). OE-rotor yarns have lower hairiness values than ring yarns for all types of materials [9, 10]. It is seen that the hairiness values of cotton yarns are the highest and acrylic yarns are the lowest for ring yarns. On the other hand, hairiness values of acrylic yarns are the highest and cotton yarns are the lowest for OE-rotor yarns. The main factor for this situation is the fibre properties acting differently for each spinning technology. Fibre fineness, fibre length and fibre length uniformity are the main factors for hairiness of ring yarns [27]. Higher linear density, shorter length and lower length uniformity values of fibres cause higher hairiness. Cotton fibres used in the study have higher linear density, shorter fibre length and lower length uniformity than Modal and acrylic fibres, which cause higher hairiness values of cotton ring yarns. In addition, because the wrapper fibres mainly cause the hairiness in OE-rotor yarns, acrylic yarns, which have higher bending stiffness, have the highest hairiness [28–29]. Higher hairiness values of acrylic yarns may be due to the electrostatic forces occurs by the fibre-to-metal and fibre-to-fibre frictions in production. Acrylic fibres have the highest tendency to be loaded by static electric [30]. Moreover, parts of OE-rotor

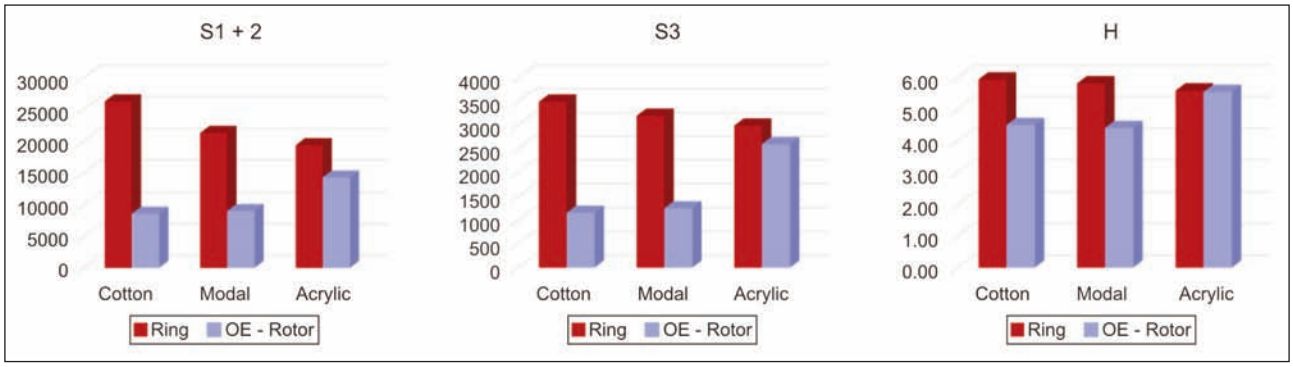

Fig. 8. Yarn hairiness values of ring and OE-rotor yarns

Table 8

ANOVA RESULTS FOR YARN HAIRINESS

Parameters	Spinning System	Sum of Squares	Mean Square	F	Sig.
S1+2	RING	153508494.4	76754247.2	47.698	0.000
	OE-ROTOR	118119434.1	59059717.04	119.918	0.000
S3	RING	772605.068	386302.534	11.809	0.001
	OE-ROTOR	7762760.083	3881380.042	55.487	0.000
H	RING	0.398	0.199	3.633	0.052
	OE-ROTOR	4.839	2.419	345.077	0.000

machine such as opening roller, rotor groove, navel etc. make fibres to rub either the metal surfaces or each other excessively.

Yarn friction

The mean values of yarn friction coefficients for cotton, Modal and acrylic yarns spun in ring and open-end systems are given in table 9 and figure 9. Results of variance analysis of these values are shown in table 10.

A general assessment of spinning systems shows that the effect of spinning technologies is statistically significant on frictional properties of yarns ($p \leq 0.05$). Friction coefficients of ring yarns are higher than OE-rotor yarns for yarn-to-metal, yarn-to-ceramic and yarn-to-yarn friction and for all of the raw materials. The possible reason for this situation could be the increasing surface area. The fibres are located in a helical path in ring spun yarns. In OE-rotor yarns, fibres are located randomly and hold together by the aid of wrapper fibres. When a contact occurs between friction surface and yarns, in ring yarns all the surface fibres contact with friction surface and they will be subjected to the frictional forces, whereas

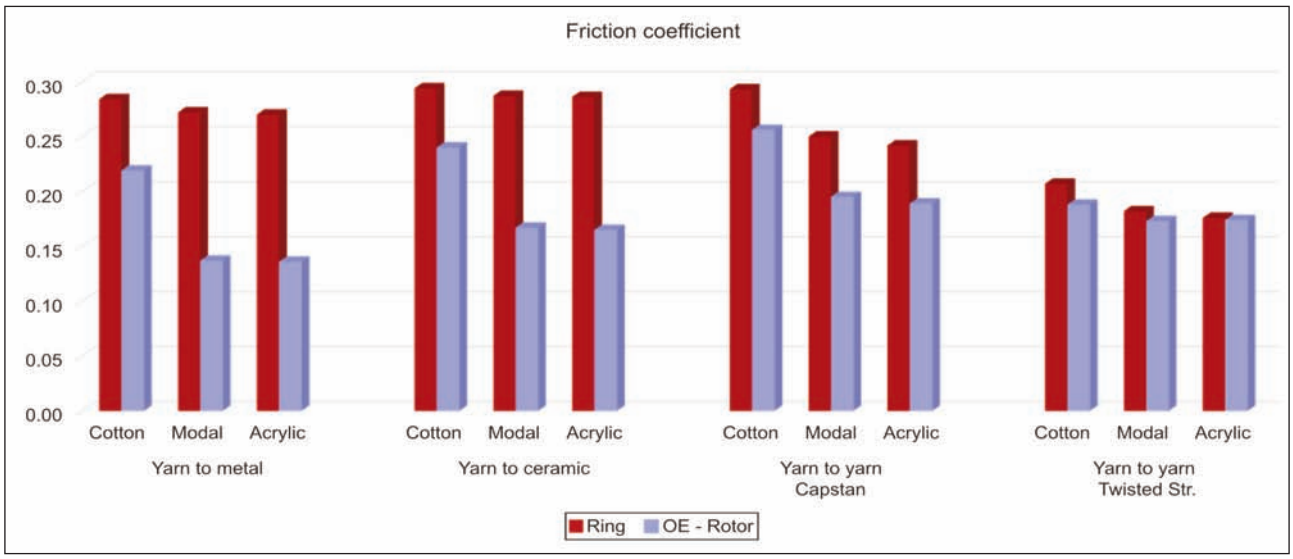

Fig. 9. YM, YC and YY friction coefficient values of ring and OE-rotor yarns

Table 9

FRICTION COEFFICIENT VALUES OF RING AND OE-ROTOR SPUN YARNS						
Friction Coefficient	**RING**			**OE-ROTOR**		
	Cotton	**Modal**	**Acrylic**	**Cotton**	**Modal**	**Acrylic**
Yarn-to-metal	0.284	0.272	0.270	0.219	0.137	0.136
Yarn-to-ceramic	0.294	0.287	0.286	0.240	0.167	0.165
Yarn-to-yarn (Capstan)	0.293	0.250	0.242	0.256	0.195	0.189
Yarn-to-yarn (Twisted Str.)	0.207	0.182	0.176	0.188	0.173	0.174

Table 10

ANOVA RESULTS FOR YARN FRICTION					
Parameters	**Spinning System**	**Sum of Squares**	**Mean Square**	**F**	**Sig.**
Yarn-to-metal	RING	0.001	0.000	74.494	0.000
	OE-ROTOR	0.027	0.013	210.253	0.000
Yarn-to-ceramic	RING	0.000	5.579E-0.05	13.913	0.000
	OE-ROTOR	0.022	0.011	300.779	0.000
Yarn-to-yarn (Capstan)	RING	0.009	0.004	294.806	0.000
	OE-ROTOR	0.017	0.008	156.266	0.000
Yarn-to-yarn (Twisted Str.)	RING	0.003	0.002	458.371	0.000
	OE-ROTOR	0.001	0.000	72.826	0.000

in OE-rotor yarns only the wrapper fibres. This situation will cause increasing asperities, real contact area and friction force for ring spun yarns. In addition, higher hairiness values of ring yarns should be taken into consideration as another factor increasing real contact area and frictional forces.

Upon a general evaluation of the friction measurement methods, it is seen that coefficient of yarn-to-yarn friction measured by twisted strand method, differences between the friction coefficients of ring and OE-rotor yarns are quite smaller than other surfaces. The main factor for this situation is thought to be the differences between measurements of yarn friction. Difference between the yarn-to-yarn friction coefficients of ring and OE-rotor yarns are higher for Capstan method such as yarn-to-metal and yarn-to-ceramic friction.

It is seen that the friction coefficients of Modal and acrylic yarns for both spinning systems and all friction surfaces are very close to each other and generally the differences between the friction coefficients of Modal and acrylic yarns are not statistically significant ($p > 0.05$). Despite the fact that fibre-to-surface friction of acrylic is high, relatively lower values of yarn-to-yarn and yarn-to-material frictions of acrylic yarns are remarkable. It can be due to the lower roughness and higher shape factor of acrylic yarns. Although it is known that fibre friction is one of the most important parameter that effects yarn friction, it is also known that yarn friction is a complex phenomenon and unevenness and structural properties of yarns highly affect the friction.

CONCLUSION

The effects of raw material and spinning technology on physical properties of yarns were investigated in the scope of this study. Natural (100% cotton), regenerated (100% Modal) and synthetic (100% acrylic) fibres were chosen as raw materials. Yarns were produced systematically in both ring and OE-rotor spinning systems. Physical properties of yarns such as unevenness, imperfections, diameter, density, roughness, shape, hairiness and friction (yarn-to-metal, yarn-to-ceramic and yarn-to-yarn) were evaluated to compare the effects of spinning system and raw material. The results indicated that raw material and spinning system take important role on physical properties of yarns.

The effect of the spinning system was found statistically significant on unevenness and imperfections values. Unevenness and imperfection values of OE-rotor yarns were found higher than ring yarns for all raw material types. Moreover, the results show that OE-rotor yarns have higher diameter and roughness; on the other hand, they have lower density, shape factor, hairiness and friction values for cotton, Modal and acrylic yarns. OE-rotor yarns have lower hairiness values than ring yarns for all types of materials. Therefore, it is possible to say that OE-rotor yarns are more bulky. Permeability properties of fabrics produced from OE-rotor yarns are better due to the high volume and low hairiness of these yarns. Friction coefficients of ring yarns are higher than OE-rotor yarns for yarn-to-metal, yarn-to-ceramic and yarn-to-yarn friction for cotton, Modal and acrylic

yarns. Ring yarns have higher friction coefficient values than OE-rotor yarns due to the higher real contact area. This situation is the similar for the fabrics that were produced from these yarns.

When the effect of raw material was investigated, it was observed that cotton yarns have higher unevenness, imperfections, diameter, roughness, hairiness and friction due to having shorter fibre length and coarser fibre fineness. Acrylic yarns have the lowest values for both ring and OE-rotor spinning systems by considering the unevenness and optical unevenness. Many researchers state that the effect of raw material on yarn properties is important. However, the results showed that unevenness, imperfections, hairiness and friction values of Modal and acrylic yarns which have the same fibre length (38 mm) and the same fibre fineness (1.3 dtex) are very close to each other, especially for ring yarns. In this case, it can be concluded that the effect of fibre fineness and fibre length have higher importance than the effect of raw material for Modal and acrylic yarns.

The findings in this study emphasized the effects of raw materials and spinning systems on yarn physical properties. Therefore, this will contribute to the preference of manufacturers for a specific product or area of usage.

Acknowledgements

Thanks to TÜBİTAK (2211 National Doctorate Scholarship Program) and Kipaş Holding A.Ş. for their contributions to the study.

BIBLIOGRAPHY

[1] Bange, M.P., Constable, G.A., Gordon, S.G., Long, R.L., Naylor, G.R.S. and van der Sluijs, M.H.J. *FIBREpak from seeds to good shirts,* In: The Cotton Catchment Communities CRC, 2009, Australia

[2] Huh, Y., Kim, Y.R. and Oxenham, W. *Analyzing Structural and Physical Properties of Ring, Rotor, and Friction Spun Yarns,* In: Textile Research Journal. 2002, vol. 72, issue 2, pp. 156–163

[3] Rameshkumar, C., Anandkumar, P., Senthilnathan P., Jeevitha R. and Anbumani, N. *Comparitive Studies on Ring, Rotor and Vortex Yarn Knitted Fabrics*, In: AUTEX Research Journal, 2008, vol. 8, issue 4, pp. 100–105

[4] Sirang, Y., Dinfon, G. and Behery, H.M. *A Study of Hairiness and Diameter of Open-End Yarn Processed Through Single- and Double-Cylinder Carding Machines and Its Comparison with Ring Yarn*, In: Textile Research Journal, 1982, vol. 52, issue 4, pp. 274–279

[5] Barella, A., Manich, A.M., Castro, L. and Hunter, L. *Diameter and Hairiness of Ring and Rotor Polyester-Cotton Blended Spun Yarns,* In: Textile Research Journal, 1984, vol. 54, issue 12, pp. 840–844

[6] Ortlek, H. G., Kilic, G., Bilgin, S. *Comparative study on the properties of yarns produced by modified ring spinning methods*, In: Industria Textila, 2011, vol. 62, issue 3, pp. 129-133

[7] Erdumlu, N., Ozipek, B., Oztuna, A.S. and Cetinkaya, S. *Investigation of Vortex Spun Yarn Properties in Comparison with Conventional Ring and Open-end Rotor Spun Yarns*, In: Textile Research Journal, 2009, vol. 79, issue 7, pp. 585–595

[8] Chattopadhyay, R., Banerjee S. *The Frictional Behaviour of Ring-, Rotor-, and Friction-spun Yarn,* In: Journal of Textile Institute, 1996, vol. 87, issue 1, pp. 59–67

[9] Mohamed, M.H., Lord, P.R. and Saleh, H.A. A *Comparison of the Hairiness and Diameter of Ring and Open-End Yarns,* In: Textile Research Journal, 1975, vol. 45, issue 5, pp. 389–395

[10] Jackowska-Strumillo, L., Cyniak, D., Czekalski, J. and Jackowski, T. *Quality of Cotton Yarns Spun Using Ring, Compact-, and Rotor-Spinning Machines as a Function of Selected Spinning Process Parameters*, In: Fibres & Textiles in Eastern Europe, 2007, vol. 15, issue 1, pp. 24–30

[11] Kilic, M. and Okur, A. *The Properties of Cotton-Tencel and Cotton-Promodal Blended Yarns Spun in Different Spinning Systems*, In: Textile Research Journal, 2011, vol. 81, issue 2, pp. 156–172

[12] Soe, A.K., Takahashi, M., Nakajima, M., Matsuo, T. and Matsumoto, T. *Structure and Properties of MVS Yarns in Comparison with Ring Yarns and Open-End Rotor Spun Yarns*, In: Textile Research Journal, 2004, vol. 74, issue 9, pp. 819–826

[13] Ghosh, A, Patanaik A., Anandjiwala, R.D. and Rengasamy, R.S. *A Study on Dynamic Friction of Different Spun Yarns*, In: Journal of Applied Polymer Science, 2008, vol. 108, pp. 3233–3238

[14] Balci Kilic, G. and Sülar, V. *Frictional Properties of Cotton-Tencel Yarns Spun in Different Spinning Systems*, In: Textile Research Journal, 2012, vol. 82, issue 8, pp. 755–765

[15] Tyagi, G. K., Goyal, A., Dhanda K. *Frictional and Mechanical Properties of Mercerized Ring- and Rotor-Spun Yarns*, In: Indian Journal of Fibre & Textile Research, 2004, vol. 29, issue 3, pp. 357–361

[16] Nair, A. U., Sheela, R., Vivekanandan, M.V., Patwardhan, B. A., Nachane, R. P. *Studies on Friction in Cotton Textiles: Part I – A Study on the Relationship Between Physical Properties and Frictional Characteristics of Cotton Fibres and Yarns*, In: Indian Journal of Fibre & Textile Research, 2012, vol. 38, issue 3, pp. 244–250

[17] *Uster Tester 5 S800 Application Handbook*, 2006

[18] *Uster Zweigle Hairiness Tester 5 Application Handbook*, 2009

[19] *Lawson Hemphill CTT User Manual,* 2008

[20] Henshaw, D.E. *Cam Forces in Weft Knitting*, In: Textile Research Journal, 1968, vol. 3, issue 6, pp. 592–598

[21] Srdjak M., Vrljicak, Z. *Applying Discrete Fourier Transform to the Knitting Process*, In: Textile Research Journal 2001; 71; pp. 384–387

[22] Koo Y., Seok, K. *Yarn Tension Variation on the Needle During the Knitting Process*, In: Textile Research Journal, 2004, vol. 74, issue 5, pp. 314–317

[23] ASTM D3108/3108M-13, *Standard test method for coefficient of friction, yarn to solid material,* 2013

[24] ASTM D3412/3412M-13, *Standard test method for coefficient of friction, yarn to yarn*, 2013

[25] Lawrence, C. A. *Fundamentals of Spun Yarn Technology*. 2003, CRC Press, USA

[26] Lewin, M. *Handbook of Fiber Chemistry (Third Edition),* 2007, CRC Press, London, England

[27] Barella, A., Manich, A.M. *Yarn Hairiness: A Further Update. Textile Progress,* In: Journal of Textile Institute, 2002, vol. 31, issue 4

[28] Kilic, M. and Okur, A. *Different Hairiness Testers for Cotton-Tencel Blended Yarns*. In: Indian Journal of Fibre & Textile Research, 2014, vol. 39, issue 1, pp. 49-54

[29] Cook, J., G. *Textile Fibres Vol. II- Man-Made Fibres*, 2009, Woodhead Publishing, England

[30] Morton, W. E., Hearle, J. W. S. *Physical Properties of Textile Fibres,* 2008, CRC Press, New York

Authors:

GONCA BALCI KILIC[1]
AYŞE OKUR[1]

Dokuz Eylül University
[1]Faculty of Engineering, Department of Textile Engineering

Tinaztepe Campus-35397
Buca-Izmir-TURKEY
e-mail: gonca.balci@deu.edu.tr, ayse.okur@deu.edu.tr

Corresponding author:

GONCA BALCI KILIC
gonca.balci@deu.edu.tr

Diversity of spun yarn properties sized *with* and *without* prewetting

STANA KOVAČEVIĆ IVANA GUDLIN SCHWARZ ZENUN SKENDERI

REZUMAT – ABSTRACT

Diversitatea proprietăților firelor încleiate cu și fără înmuiere prealabilă

Obiectivul lucrării a fost de a investiga proprietățile mecanice ale firelor cu finețe diferită și cu coeficienţi similari de torsiune din fibre Tencel, încleiate cu și fără înmuiere prealabilă, folosind concentrații diferite de încleiere. S-a constatat că firul încleiat cu înmuiere prealabilă are întotdeauna un grad de stoarcere mai mic decât firul încleiat fără înmuiere prealabilă și proprietăți relevante mai bune (rezistență mai mare la abraziune și frecvență mai mică a pilozității). Acest lucru este de o importanță deosebită, datorită avantajelor exprimate în termeni ecologici și economici, deoarece aceleași proprietăți sau proprietăți mai bune sunt obținute cu un grad de stoarcere mai mic.

Cuvinte-cheie: încleiere, înmuiere prealabilă, stoarcere, proprietățile firului

Diversity of spun yarn properties sized *with* and *without* prewetting

The goal of the paper was to investigate mechanical properties of yarns with various fineness and with similar twist factors made of Tencel fibers, sized with and without prewetting sizing process, using different size concentrations. It was found that the yarn sized with prewetting has always a lower size pick-up than the yarn sized without prewetting, as well as better relevant properties (greater abrasion resistance and lower frequency of protruding fibers). This is of paramount importance because of the advantages in ecological and economical terms, since the same or better properties are achieved with a lower size pick-up.

Keywords: sizing, prewetting, size pick-up, yarn properties

INTRODUCTION

Yarn properties are defined with raw material composition and its structure. Yarn structure for an approximately equal twist factor greatly depends on the arrangement of fibers both in the cross section and in the length direction. For a specific spinning process (carding, half-combing and combing) it is not always possible to obtain a sufficiently uniform structure of the yarn. Therefore, spun yarns have a certain unevenness (total unevenness, thick and thin places and neps), resulting in a different distribution of the size pick-up in the yarn. It is therefore of great importance to know yarn structure and propertied well in order to optimize size pick-up in the sizing process [1–4].

The single yarn used in the warp should be sized to enhance strength, smoothness and abrasion resistance and to reduce static electricity, reducing the frequency of weak places. In the weaving process warp threads are exposed to higher dynamic forces which can cause breaks reducing the efficiency of weaving machines and fabric quality. To achieve high quality sizing, it is necessary to keep the equal quality of size pick-up constant from the beginning to the end of sizing, which is often a complicated task. By applying a greater amount of size the sizing process becomes uneconomical. Substance balance is used to define several influential parameters of the sizing process. According to the previous investigations of substance balance three parameters that can be monitored and corrected continuously are important, and they directly affect size pick-up. These are: inlet and outlet warp moisture and size concentration [5–8].

In order to reduce sizing costs, to achieve greater environmental protection and to obtain optimum quality of the sized warp, the sizing with warp prewetting was investigated. It is known that in sizing without prewetting the size pick-up becomes thicker for two reasons: the yarn absorbs water more easily than the size and one part of the water from the size evaporates. By immersing the warp with prewetting into the size one part of the water is released and the size is diluted which affects the parameters of the sized warp. When sizing the wet warp the size remains longer on the surface creating a surface film around the yarn which protects the yarn sufficiently against dynamic forces and abrasion in the weaving process [9–12].

Thick places have an opener structure and a lower twist level than thin places so that the size penetrates them more easily. Depending on own friction properties and abrasion resistance as well as on surface characteristics of friction elements, the yarn wears more or less, deforms and changes the surface which can result in breaks. In case of testing abrasion resistance, as a measure of resistance the number of yarn passages over the abrading element is used so that the sizing effect can be evaluated by measuring abrasion resistance [13, 14]. The goal of sizing is to protect the yarn in the weaving process against destruction, especially in weak places, which is achieved by sticking the fibers to the yarn body.

EXPERIMENTAL

Yarns of counts 14, 16, 20, 28 and 35 tex spun from 100% Tencel fibers were used for the purposes of this research. The following parameters were tested:

- size pick-up
- breaking properties on the Statimat M (Textechno) strength tester according to standard ISO 2062;
- yarn twist was tested on the MesdanLab Twist tester according to standard 17202;
- abrasion resistance was tested on a Zweigle G-551 abrasion tester; simultaneously 20 threads were tested under a load of 20 g; the yarn was abraded by moving the roller back and forth which is coated with sand paper with a fineness of 800 over the thread surface over 7 cm until thread breakage;
- hairiness before and after sizing was tested on a Zweigle G 565. The instrument measures the total number of protruding fibers at specified distances, in our case of $n_1 = 2$ mm; $n_2 = 4$ mm, $n_3 = 6$ mm and $n_4 = 8$ mm from the yarn edge. The yarn speed was 50 m/min and the length of yarn tested was 25 m.

An increase in yarn strength caused by sizing was determined according to the equation (1):

$$I = \frac{\sigma\ (sized\ yarn) - \sigma\ (unsized\ yarn)}{\sigma\ (unsized\ yarn)} \times 100\ (\%) \quad (1)$$

where: I (%) is strength increase by sizing; σ (cN/tex) – tensile strength.

Sizing was performed on a specially designed sizing machine (figure 1) without and with water prewetting. The laboratory sizing machine consists of a creel for cross-wound bobbins with possible yarn tension control, a box for prewetting warp before sizing, a size box, a contact dryer and a winder of the sized yarn (figure 1). The prewetting box consists of an immersion roller and a pair of squeezing rollers with possible water heating up to 100 °C and control of squeezing water from the warp. The size box consists of a pre-box and a working box with two pairs of immersion rollers and two pairs of rollers for size squeezing. The role of the pre-box is to keep size levels in the working box constant, namely continuous size circulation from the working box to the pre-box with natural flow, and from the pre-box to the working box using a pump. During the sizing process it is possible to keep water temperature constant in the pre-wetting box and size temperature in the size box with integrated heaters and thermostats, which indirectly warm up the water and size through the walls of the boxes. Drying the sized yarn is performed by contact, by passing across the two heated cylinders of the contact dryer. Sizing speed can be kept constant using the winder and an additional speed controller.

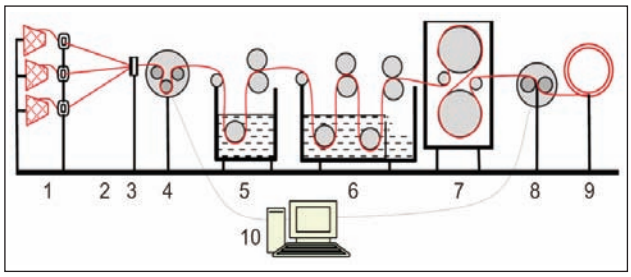

Fig. 1. Laboratory sizing machine: 1 – creel for cross wound bobbins, 2 – thread guide and brake, 3 – comb, 4 – tension meter, 5 – pre-wetting box with hot water, 6 – size box, 7 – dryer, 8 – humidity measuring instrument, 9 – winder of the sized yarn, 10 – computer

Concentrations, recipes and technological sizing conditions were as follows:

- concentration 5%, recipe: 1 l of water + 50 g Tuboflex PVA80 + 4 g Tubowax 24,
- concentration 10%, recipe: 1 l of water + 100 g Tuboflex PVA80 + 8 g Tubowax 24,
- concentration 15%, recipe: 1 l of water + 150 g Tuboflex PVA80 + 12 g Tubowax 24,
- size temperature 75–80 °C; sizing speed 2 m/min; temperature of contact cylinder drying 135 °C,
- pressure on the back part of the pair of the rollers at the exit of the working box 0.66 N/cm^2,
- warp moisture before sizing 6.5%; warp moisture after the exit of the prewetting box 72%; warp moisture after the exit of the size box 80%; warp moisture after drying 5%.

The applied sizing agents were made by Bezema Company. Yarn tension was measured with a tension meter Schmidt Model ETM which had been reconstructed with the aim of measure and to save data continuously. A computer was used to record the measurements of output yarn moisture after drying and yarn tension after the creel. A Zeiss Jena handheld refractometer was used to measure size concentration.

When sizing yarn without prewetting on the laboratory sizing machine, the prewetting box with hot water with a temperature 50 to 60 °C (mark 5 in figure 1) is removed.

The size pick-up in relation to the sized yarn was determined according to equation (2):

$$S = \frac{m_s - m_u}{m_s} \times 100\ (\%) \quad (2)$$

where: S (%) is the size pick-up, m_s (g) – mass of the dry sized yarn, m_u (g) – mass of the dry unsized yarn.

Twist factor a_{tex} was determined according to equation (3):

$$\alpha_{tex} = T \times \sqrt{T_t} \quad (3)$$

where: T (twist/m) is the number of twists, T_t (tex) – yarn count.

RESULTS AND DISCUSSION

Yarn twist

The number of twists changed with changing yarn counts so that the finest yarn 14 tex had the highest number of twists (871 twist/m), while the coarsest yarn 35 tex had the lowest number of twists (581 twist/m) (table 1). Yarn twist factor was 3140.0 for the yarn of 16 tex to 3437.2 for the yarn of 35 tex.

Table 1

YARN TWIST PARAMETERS					
Parameters	**T_t (tex)**				
	14	**16**	**20**	**28**	**35**
T (twist/m)	871	785	755	639	581
CV(T) (%)	2.8	3.3	2.7	3.6	6.6
a_{tex} – twist factor	3258.9	3140.0	3376.5	3381.3	3437.2

Table 2

SIZE PICK-UP WITHOUT AND WITH PREWETTING						
Size pick-up	**C (%)**	**T_t (tex)**				
		14	**16**	**20**	**28**	**35**
S_{wo} (%) – without prewetting	5	6.58	6.83	6.75	7.09	9.41
	10	7.91	8.28	8.31	9.94	12.84
	15	12.17	12.33	12.90	15.00	18.01
S_w (%) – with prewetting	5	5.21	5.32	5.44	7.03	8.22
	10	6.11	7.41	8.17	9.83	12.40
	15	10.09	11.99	12.47	14.77	17.05

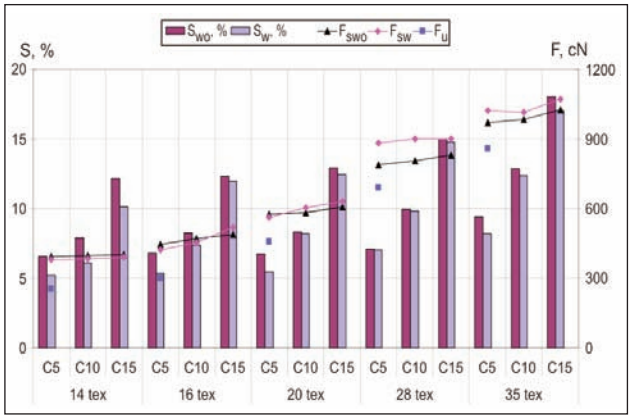

Fig. 2. Dependence of size pick-up and breaking force of the yarn on concentration and yarn count: F_{swo} (%) – breaking force of the yarn sized without prewetting, F_{sw} (cN) – breaking force of the yarn sized with prewetting, F_u (cN) – breaking force of the unsized yarn; C5, C10, C15 – size concentration of 5%, 10% and 15%

Size pick-up

The size pick-up increased with increasing yarn count and size concentration (C) in both sizing processes for all tested yarns (table 2, figure 2). Thus, the finest yarn (14 tex) sized with and without prewetting had the lowest size pick-up for all concentrations. These results suggest that despite similar twist factor, after being subjected to sizing process under the same conditions, finer yarns maintain a smaller percentage of size, i.e. size penetration into the spaces between fibers is much harder as well as retaintion of size on the surface of the yarn with a smaller diameter. Size pick-up of yarns sized with prewetting in relation to yarns sized without prewetting are significantly lower. That difference is particularly pronounced at small size concentration (5%) for all yarns and also at finer yarns (14 tex, 16 tex) sized with all size concentration (in average for almost 20%). All the above confirms that the sizing with prewetting is more economical.
Parameters of breaking properties of all tested unsized and sized yarns are shown in tables 3–5.

Table 3

PARAMETERS OF THE UNSIZED YARN					
Parameters	**T_t (tex)**				
	14	**16**	**20**	**28**	**35**
F (cN) – breaking force	253.5	301.4	455.6	691.5	859.7
CV(F) (%)	12.5	10.1	7.2	6.2	5.0
ε (%) – elongation at break	6.1	6.4	6.9	8.1	8.3
CV(ε) (%)	9.2	9.0	8.2	5.9	5.6
W (cNxcm) – work to rupture	472.6	594.4	974.6	1647.6	2120.8
CV(W) (%)	20.0	17.9	13.9	11.6	10.0
σ (cN/tex) – tensile strength	18.1	18.8	22.8	24.7	24.6

Table 4

PARAMETERS OF THE YARN SIZED WITHOUT PREWETTING						
Parameters	**C (%)**	**T_t (tex)**				
		14	**16**	**20**	**28**	**35**
F (cN)	5	394.8	446.0	575.9	787.1	969.1
	10	396.9	470.1	582.9	806.0	985.1
	15	399.5	487.2	608.6	830.7	1024.0
CV(F) (%)	5	6.4	6.1	5.7	11.6	7.1
	10	8.4	7.6	7.5	8.5	7.4
	15	11.5	8.9	5.4	21.9	5.2
ε (%)	5	3.6	4.0	4.1	4.3	4.0
	10	3.8	4.7	5.2	5.2	5.1
	15	4.0	5.0	4.8	5.1	5.2
CV(ε) (%)	5	8.7	9.9	8.5	16.6	11.8
	10	12.0	11.5	15.1	13.2	8.8
	15	22.5	17.9	7.6	27.2	8.9
W (cNxcm)	5	486.1	758.6	889.7	1411.3	1948.0
	10	507.2	746.7	1000.1	1386.8	1969.6
	15	528.7	674.4	1041.5	1261.2	1655.2
CV(W) (%)	5	14.8	14.9	14.1	24.2	18.4
	10	18.4	19.9	17.4	20.5	14.3
	15	31.4	25.5	12.5	35.4	14.2
σ (cN/tex)	5	28.4	27.9	30.5	28.8	29.3
	10	28.5	29.4	29.2	29.7	27.7
	15	28.2	30.5	28.8	28.1	28.2
I (%) – strength increase by sizing	5	56.6	48.0	33.7	16.6	19.1
	10	57.7	56.0	28.0	20.1	12.7
	15	55.8	61.7	26.4	13.8	14.6

Tensile strength

By reducing yarn count (increasing fiber number in the cross section) in an narrower range of twist factor (3140.0 to 3437.2) the strength of the unsized yarn increases for 27% (from 18.1 cN/tex to 24.7 cN/tex) (table 3). By sizing yarn strength and breaking force increases as expected (tables 4 and 5). By reducing the yarn count from 14 tex to 20 tex an increase in strength for all size concentrations of the sized yarn without prewetting was observable, by an average of 3.1 %. By further reducing the yarn count from 20 tex to 35 tex the strength of the sized yarn is reduced, by an average of 1.7%. According to the obtained results of tensile strength between yarns sized with two processes, a great similarity is observable. A strength reduction in the sized yarn with prewetting does not start at 20 tex as in the sized yarn without prewetting, but it starts at the yarn count of 28 tex to 35 tex. Therefore, it can be concluded that there are limits of yarn fineness over which the strength of sized yarns no longer increases and these are 20 tex yarn in sizing without prewetting and 28 tex yarn in sizing with prewetting.

Strength increase of the yarn sized with both sizing process in relation to the unsized yarn indicates that in case of rougher yarns (28 tex and 35 tex) strength values amounts from 12.7% to 37.4%, while in case of finer yarns (14 tex and 16 tex) it is much higher and ranges from 40.5% to 72.4%. A lower size pick-up of the yarn sized with prewetting at lower concentrations reflected in a lower increase in yarn tensile strength due to sizing, but only at lower concentrations (5% and 10%). At higher size concentration (15%) an increase in tensile strength of the yarn sized with prewetting is mainly higher. This indicates that an increase in the size concentration increases strength of the yarn sized with prewetting.

Elongation at break

Elongation at break of the unsized yarn increases with reducing yarn count from 14 tex to 35 tex, in average for 27% (values range from 6.1 % to 8.3%) and follows the course of breaking forces. Generally, the sizing process reduces the elongation at break for all tested yarns. The yarns sized without prewetting have elongation at break in the range from 3.6% to 5.2%, while in case of sizing with prewetting it ranges from 3.1% to 5.8%. Elongation at break of the yarn slightly increases by reducing yarn count at all concentrations and with both sizing processes. It was

Table 5

PARAMETERS OF THE YARN SIZED WITH PREWETTING						
Parameters	**C (%)**	**T_t (tex)**				
		14	**16**	**20**	**28**	**35**
F (cN)	5	378.5	423.2	560.3	883.7	1021.5
	10	383.6	452.0	605.1	898.8	1016.6
	15	390.4	519.5	632.15	900.6	1071.5
CV(F) (%)	5	4.8	27.1	8.9	16.4	15.4
	10	7.6	17.3	13.0	22.2	3.4
	15	13.8	6.6	6.1	6.4	7.1
ε (%)	5	4.9	4.9	5.2	5.7	5.8
	10	4.6	4.6	4.8	5.3	5.4
	15	3.2	3.1	3.7	3.8	4.3
CV(ε) (%)	5	9.5	23.3	13.5	5.1	26.0
	10	6.7	24.8	24.7	16.3	5.9
	15	18.6	12.6	18.0	12.7	18.2
W (cNxcm)	5	610.2	558.8	1035.4	1702.6	1942.7
	10	575.6	713.7	885.7	1465.2	2048.8
	15	414.9	510.5	744.1	1079.6	1643.4
CV(W) (%)	5	13.0	40.1	21.5	43.8	29.9
	10	13.0	32.7	30.6	26.2	8.5
	15	29.1	19.0	22.6	18.9	21.9
σ (cN/tex)	5	27.4	26.5	30.3	34.0	29.2
	10	27.0	28.3	28.0	28.0	29.1
	15	27.9	32.5	31.6	32.1	30.6
I (%)	5	51.4	40.5	32.8	37.4	18.7
	10	49.4	50.0	23.0	13.3	18.3
	15	54.1	72.4	38.7	30.0	24.6

noted that yarn elongation by increasing size concentration from 5% to 15% decreases in case of sizing with prewetting, while in case of sizing without prewetting this occurrence was not observed. By sizing the fibers within the yarn structure are fixed to a certain extent, the yarn becomes more compact, stronger and stiffer, resulting in a reduction of elongation at break and representing a negative feature of the yarn after sizing.

Work to rupture

Changed structure of the sized yarns changes the properties of work to rupture, being very important parameter in the production in terms of defining the weaving conditions. According to the obtained results, it is evident that sizing without prewetting of rougher yarns (28 tex and 35 tex), with all size concentrations, decreases the values of work to rupture. Also, that kind of work decrease of yarns sized with prewetting in regard to unsized yarns was evident for all yarn counts sized with a 15% size concentration; for yarn counts of 20 tex, 28 tex and 35 tex sized with a 10% size concentration; and for a yarn count of 35 tex sized with a 5% size concentration. Regardless of the increase in breaking force of rougher yarns caused by the increase in the number of fibers in the cross section and also caused by sizing procedure, lower breaking elongation of sized yarns significantly affected on the reduction of the work of the above listed yarn counts and size concentrations.

Abrasion resistance

It is known that higher yarn abrasion resistance reduces the number of warp breakages in the weaving process. Rougher unsized yarns have substantially higher abrasion resistance than finer yarns. Thus, a yarn of a count of 14 tex has abrasion resistance 36.6 cycles to breakage, while the yarn with a count of 35 tex has 197.5 cycles to breakage, which is 440% more (table 6, figure 3). Sizing process results in substantially higher yarn abrasion resistance, for both sizing process. By reducing yarn count abrasion resistance increases mainly in both sizing processes and at all three size concentration levels. It was observed that in case of rougher yarn counts of 28 tex and 35 tex abrasion resistance is the highest when applying 10% size concentration in both sizing processes, regardless of a higher size pick-up on the yarns sized with a 15% size concentration. It points to the fact that abrasion resistance increases with the size pick-up only to a certain limit.

Table 6

ABRASION RESISTANCE OF THE YARN (AVERAGE NUMBER OF CYCLES TO BREAKAGE)						
T_t (tex)	Abrasion					
	h_u – average No. of abrasion cycles to breakage – unsized yarn	C (%)	h_{swo} – average No. of abrasion cycles to breakage – without prewetting	k_1 – quotient of the increase in abrasion resistance of the yarn sized without prewetting in relation to the unsized yarn	h_{sw} – average No. of abrasion cycles to breakage – with prewetting	k_2 – quotient of the increase in abrasion resistance of the yarn sized with prewetting in relation to the unsized yarn
14	36.6	5	193	4.3	384	9.5
		10	292	7.0	416	10.4
		15	237	5.5	577	14.8
16	46.5	5	335	6.2	354	6.6
		10	392	7.5	496	9.7
		15	531	10.4	516	10.1
20	92.2	5	261	1.8	428	3.6
		10	460	4.0	730	6.9
		15	473	4.1	486	4.3
28	160.9	5	407	1.5	617	2.8
		10	779	3.8	1155	6.2
		15	594	2.7	676	3.2
35	197.5	5	676	2.4	846	3.3
		10	1085	4.6	1777	7.9
		15	910	3.6	1698	7.6

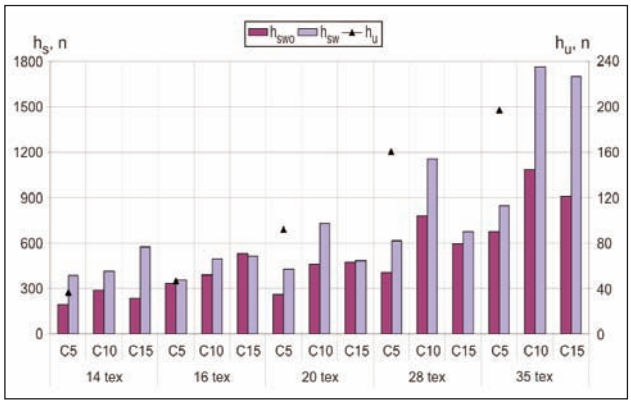

Fig. 3. Abrasion resistance of the unsized and sized yarns

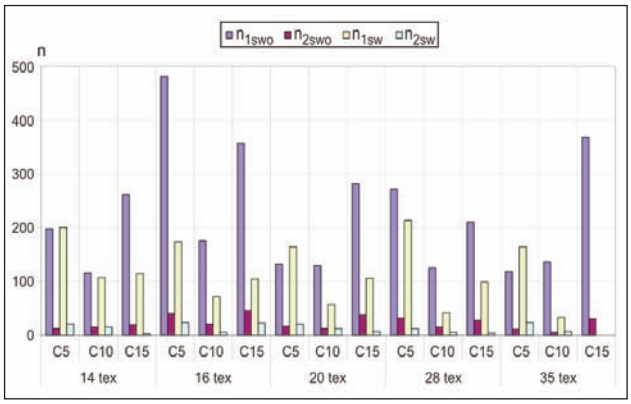

Fig. 4. Yarn hairiness of the yarn after sizing over the lengths of 2 mm (n_1) and 4 mm (n_2) (table 7): n_{1swo}, n_{2swo} – number of protruding fibers on the sized yarn without prewetting, n_{1sw}, n_{2sw} – number of protruding fibers on the sized yarn with prewetting

An increase in yarn abrasion resistance by sizing is mostly higher in a yarns sized with prewetting ($k_2 > k_1$). It is more significant in a finer yarn (14 tex and 16 tex).

Yarn hairiness

Yarn hairiness greatly affects the number of yarn breakages during the weaving process. Appearance of protruding fibers results in grip threads, removal or accumulation on the contact points between threads and weaving machine parts and thus to pinning and to breakage. The accumulation of short fibers in heddles and the reed has the effect of drawing the accumulated fibers into the shed and also into the final woven fabric, resulting in thickenings in the fabric. The aim of sizing is to reduce yarn hairiness and according to the obtained results (figure 4, table 7) that is achieved.

The frequency of protruding fibers was reduced, especially in the yarn sized with prewetting, which was expected because the yarn is smoothed during prewetting and in this state it enters the size box where the fibers are even more clung to the yarn body. An exception is 35 tex yarn having a greater number of longer protruding fibers after sizing with

Table 7

YARN HAIRINESS												
T_t (tex)	Unsized yarn				C (%)	Sized yarn without prewetting				Sized yarn with prewetting			
	n_{1u}	n_{2u}	n_{3u}	n_{4u}		n_{1swo}	n_{2swo}	n_{3swo}	n_{4swo}	n_{1sw}	n_{2sw}	n_{3sw}	n_{4sw}
14	1307.6	323.6	38.6	5.4	5	198	13	4	3	201	21	2	2
					10	116	16	1	1	107	16	1	2
					15	262	20	2	3	114	3	3	7
16	1023.0	203.4	19.0	1.6	5	481	40	7	5	174	23	1	1
					10	176	21	0	5	73	6	1	1
					15	356	46	9	17	105	22	2	8
20	1254.8	258.8	28.2	6.2	5	132	17	6	3	164	21	0	1
					10	129	12	2	0	57	12	1	3
					15	281	38	1	21	106	7	3	5
28	1347.8	266.0	26.4	3.6	5	272	32	6	1	213	12	2	2
					10	126	16	3	6	42	5	2	2
					15	210	28	14	5	99	4	11	9
35	1547.4	331.2	47.0	3.4	5	118	11	1	0	165	24	1	6
					10	137	5	0	0	34	7	3	2
					15	368	30	7	6	42	0	2	5

5 % size concentration and with prewetting process then the yarn sized without prewetting. This occurrence can be related to the assumption that a lower size concentration achieves a lower efficiency of clinging shorter fibers to a wet and rougher yarn.
The shortest length of protruding fibers (2 mm) is the most numerous before and after sizing, but that length of protruding fibers does not affect quality features of the yarn. The longer the protruding fibers, the greater is the possibility to cause a more frequent standstill of the weaving machine and lower quality fabric.

CONCLUSIONS

By sizing the warp threads are protected from destruction which might occur during the weaving process. That is particularly important in order to protect the weak spots that are actually potential points of breakage. Yarn unevenness affects the frequency of thick and thin places and despite the similar twist factors it varies from parts of the yarn. Thick places have fewer twist and size more easily penetrate into the interior of the yarn over the thin places. Finding the amount of size pick-up that will be optimal, requires long and complex analysis of the sizing and weaving processes. By the obtained results it can be concluded that the size pick-up changes as well as physical-mechanical properties of the yarn by different counts and sizing processes (with and without prewetting) despite similar twist factors of the yarns. The reason for different amounts of size pick-up is in the distribution and binding of size in the yarn. Prewetting allows filling the interspaces of the yarn with water. During the immersion of such wet yarn in size leads to diffusion of water (retained in the yarn) with size and very rapid mutual bonding, allowing quicker and easier penetration of size into the yarn. However, the concentration of size inside the yarn is lower, because the retained water dilutes it. Therefore the amount of size pick-up is lower (than on the yarn sized without prewetting process), but still sufficient to protect the yarn from the dynamic forces and tears in the weaving process. Lower amount of size pick-up on the yarn also means a significant economic and ecologic advantage.
The following conclusions can be obtained after sizing yarns with similar twist factors, under the same sizing conditions:

- Yarn size pick-up rises by increasing size concentration and by reducing yarn fineness.
- Size pick-up on the yarns sized with prewetting process is mainly lower in relation to yarns sized without prewetting.
- By analyzing the obtained results, it can be concluded that there are limiting finenesses towards the rougher yarns whose tensile strength does not increase after sizing.
- An increase in tensile strength by sizing yarns occurs, especially in finer yarns up to 72 % while in rougher yarns only up to 37 %. Lower size pick-up on the yarn sized with prewetting at lower size concentrations reflected also in a lower increase in breaking force, while at higher concentrations the increase is mainly greater. This means that increasing the size concentration increases the tensile strength of the yarn sized with prewetting.
- By sizing, elongation at break decreases for all tested yarn counts and sizing conditions. By increasing the size concentration from 5 % to 15 %, elongation at break decreases for all yarns sized with prewetting, while this occurrence is not observable for the yarns sized without prewetting.

- Regardless of increase in breaking force due to sizing, a reduction of elongation at break substantially affected the reduction of work to rupture, especially in case of rougher yarns.
- Yarn abrasion resistance increases by sizing. Rougher yarns sized with a 10 % size concentration have the highest yarn abrasion resistance for both sizing processes, regardless of the fact that size pick-up is higher when sizing with 15% size concentration. An increase of yarn abrasion resistance due to sizing is usually greater for the yarn sized with prewetting and it is more distinct for finer yarns.
- The frequency of protruding fibers is reduced by sizing, especially for the yarns sized with prewetting. The reason for this is that already during prewetting in water the threads are smoothed and by immersing in the size and squeezing an excessive size amount the protruding fibres cling to the thread even more.

The yarns sized with prewetting process have advantages in ecological and economical terms since the same or better properties are achieved with a lower size pick-up. Likewise, under the same sizing conditions the yarn sized with prewetting has greater yarn abrasion resistance and lower frequency of protruding fibers. By exceeding certain limiting values of size concentration and yarn count, tensile strength and elongation at break of sized yarn start changing nonlinearly.

BIBLIOGRAPHY

[1] Kovačević, S. *Determining Size Coat in Yarn on the Basis of Substance Content*, Ph.D. thesis, Faculty of Textile Technology, University of Zagreb, 2000.

[2] Gudlin Schwarz, I. Technological *Justification and Optimization of Pre-Wet Sizing*, Ph.D. thesis, Faculty of Textile Technology, University of Zagreb, 2012.

[3] Perković, V. *Impact of Yarn count of the Same Twist Coefficient on Size Pick-up*, Bs.C. thesis, Faculty of Textile Technology, University of Zagreb, 2010.

[4] Kovačević, S. et al. *Optimising Size Layer As Related to Input Humidity*, In: Tekstil, 49 (2000) 12, pp. 689–697.

[5] Behera, B.K.; Hari, P.K. *Woven textile structure*, Published by Woodhead Publishing Limited in association with The Textile Institute Woodhead Publishing Limited, Campridge, UK, 2010. www.woodheadpublishing.com

[6] Kovačević, S.; Grancarić, A. M., Stipančić, M. *Determination of the Size Coat*, In: Fibres & textiles in Eastern Europe, 10 (2002) 3, pp. 63–67.

[7] Kovačević, S.; Dimitrovski, K.; Orešković, V. *Optimization of Size Pick-up on Yarn*, 2nd International Textile, Clothing & Design Conference, Magic World of Textiles , October 03rd to 06th 2004, Dubrovnik, Croatia.

[8] Gudlin Schwarz, I.; Kovacevic, S.; Dimitrovski, K.: *Comparative Analysis of the Standard Sizing Process and the Pre-wet Sizing Process*, In: Fibres & Textiles in Eastern Europe, 19 (2011) 4 (87), pp. 135–141.

[9] Gudlin Schwarz, I.; Kovačević, S.; Dimitrovski, K.: *Analysis Of Changes In Mechanical And Deformation Yarn Properties by Sizing*, In: Textile Research Journal, 81 (2011) 5, pp. 545–555.

[10] Kovačević, S.; Dimitrovski, K.; Hađina, J. *The processes of weaving, University handbook*, Faculty of Textile Technology, University of Zagreb, Zagreb, 2008.

[11]Kovačević, S.: *Priprema pređe*, Faculty of Textile Technology, University of Zagreb, Zagreb 2002.

[12] Kovačević, S.; Gordoš, D.: *Impact of the Level of Yarn Twist on Sized Yarn Properties*, In: Fibres & Textiles in Eastern Europe, 17 (2009) 6, pp. 44–49.

[13] Hađina, J.; Kovačević, S. *Influence of Yarn Twist on the Texture of Fabric*, In: Tekstil, 47 (1998) 9, pp. 447–452.

[14] Reumann, R.D.: *Prüfen von Textilien*, VEB Fachbuchverlag Leipzig, 1984.

Authors:

Chief of works Prof. dr. STANA KOVAČEVIĆ

Dr. IVANA GUDLIN SCHWARZ

Prof. dr. ZENUN SKENDERI

University of Zagreb

Faculty of Textile Technology, Department of Textile Design and Management

Prilaz baruna Filipovica 28a, 10000 Zagreb, Croatia

e-mail: stana.kovacevic@ttf.hr, ivana.schwarz@ttf.hr, zenzn.skenderi@ttf.hr

Effect of knitted parameters on wicking behaviours

NESMA SAOUSSEN ACHOUR
AYDA BAFFOUN
MOHAMED HAMDAOUI
SASSI BEN NASRALLAH

REZUMAT – ABSTRACT

Efectul parametrilor de tricotare asupra capacităţii de absorbție a apei

În acest articol au fost propuse modele teoretice pentru a estima capacitatea de absorbție verticală a apei în funcție de compoziția, tipul de fire și parametrii țesăturii. Se utilizează un dispozitiv experimental care efectuează suspendarea verticală a suprafeței țesătură-lichid și care permite pătrunderea moleculelor de apă prin mostrele testate. Valorile experimentale ale absorbției verticale au fost măsurate gravimetric cu ajutorul unei microbalanțe electronice și studiate teoretic, folosind un model dublu exponenţial (DEM). Rezultatele au arătat că DEM se potrivește bine datelor experimentale cu valori medii semnificative ale coeficientului de determinare. O simplificare a modelului DEM este efectuată pentru a dezvolta un model liniar care descrie ascensiunea capilară în structurile tricotate. De asemenea, este demonstrat faptul că cinetica de absorbție este influențată de caracteristicile tricoturilor, cum ar fi compoziția, structura tricotului, tipul de fir și înălţimea ochiurilor.

Cuvinte-cheie: model dublu exponențial, ascensiune capilară, tricoturi, modelare lineară, cinetica de absorbție a apei

Effect of knitted parameters on wicking behaviours

Theoretical models have been proposed in this article to predict the vertical wicking behaviour of fabrics depending upon composition, yarns and fabric parameters. An experimental device performing the vertical suspension of fabric-liquid surface and permitting the penetration of water molecules through these tested samples is used. Experimental values of vertical wicking were gravimetrically measured using an electronic microbalance and theoretically studied using the double-exponential model (DEM). The results showed that the DEM fit well the experimental data with significant average determination coefficient values. A simplification of the DEM model is carried out to develop a linear one describing the capillary rise into knitted structures. It is also demonstrated that wicking kinetics is influenced by knitted fabric features, such as composition, knit structure, type of yarn and of couliering depth value.

Keywords: double-exponential model, capillary rise, knitted fabrics, linear modelling, water sorption kinetics

INTRODUCTION

In recent years, influence of various factors and prediction of transport of water through textiles and moisture transmission behaviour of the clothing has been recognized as a favorite research. In fact, liquid sorption behavior of fabrics plays an important role in maintaining thermo-physiological clothing comfort, especially in sweating conditions, in dyeing and finishing of fabrics, in liquid filtration, and so forth [1, 2]. In addition, textiles processing can require several dozen gallons of water for each pound of clothing, especially during the dyeing process. All additional products for dyeing are applied to fib mainly water as vehicle. Most fabric preparation steps, including desizing, scouring, bleaching and mercerizing, require the use of water. Thus, it is necessary to optimize its consumption and control its sorption kinetics in textile materials. Also, business competition between industrial leaders is based on minimizing consumption of natural resources, notably water.

To study the liquid-textile contact and to model this problem, optimization of various processes involving liquid-fibre contact, penetration of liquids into capillaries and textiles, and kinetic sorption of water onto textile fabric have been studied for many years [3–9; 10–13]. Among the extensive research in the field of liquid transport and capillary rise, the fluid flow through porous media is modelled by the well-known Lucas and Washburn equation which allows determining the diffusion coefficient [4, 5, 14, 15].

Among the extensive researches in the field of liquid transport, capillary flow through textile materials and liquid adsorption into textile fabrics, many techniques were used and developed to study experimentally this phenomenon. Many researchers developed an electrical method based on resistivity measurements [6, 7]. Others used a method based on the analysis of CCD images of a coloured liquid [14].

The kinetics of the capillary rise in textiles is investigated, for short time spans when the effects of gravity are neglected and the extent of the liquid flow in the fabric is significantly less than the maximum equilibrium height, by fitting the experimental data to the well-known Washburn equation. For long time, it has been shown that equations derived from Washburn law lead to erroneous results. One other approach proposed by Hamdaoui *and al.,* in order to interpret the sorption kinetics of the vertical capillary rise of water in woven fabrics. This approach, which has a double exponential form, is valid for short and long

time. It is found that the parallel double exponential kinetics model (DEM) fit well the experimental data [10, 11].
In this paper, attempts have been made to develop and validate mathematical models based on the double-exponential function for predicting the complete profile of the water sorption kinetics onto knitted fabrics and the linear logarithmic function for determining the water kinetic parameter, respectively.

EXPERIMENTAL PART

Materials and Method

The fabric samples used in this study were knitted using the same machine. The samples were knitted by changing fabric structural parameters, such as the kind of yarn, the composition and the knit structure. Table 1 gives the knitting parameters and physical properties of each sample used in this study.
The dimension of the dry sample used in experiments was 20 cm x 30 cm. We used the distilled water which is used frequently in textile industry. To remove the natural wax and paraffin oil that has been applied to yarns prior to knitting, a chemical treatment was used. The fabric was treated for 20 minutes at 65°C with a solution containing 2 mL/L of caustic soda and 2.5 mL/L of wetting agent (Lavotan TBU).
Figure 1 shows a sketch of the experimental system. It is composed of a device permitting the vertical suspension of the fabric-surface on the liquid and a lighting system. In order to measure the mass of liquid raised, the fabric is attached to a sensitive electronic balance with the accuracy of 0.001 g. The balance has the capability of recording the weight of the absorbed water (g) versus time (s) with its special software [4–7].

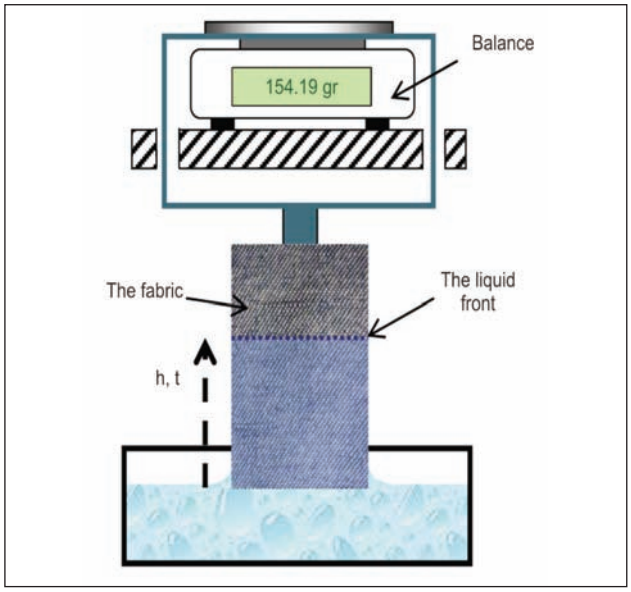

Fig. 1. Experimental device

RESULTS AND DISCUSSION

Experimental data

The knit fabric is maintained vertically in the warp direction. Then, the lab jack is used to hoist the liquid reservoir containing the distilled water. The mass of water absorbed by the textile is automatically determined every 20 seconds. The results of the experimental data are reported in figure 2, which shows the evolution of the water mass absorbed by the textile versus the time.
Figure 2 also shows that the experimental curve of the capillary rise onto the knit fabric has a positive slope which decreases with time and attains zero at full saturation. In this case, the uptake process of the distilled water capillary rise onto knitted fabric could

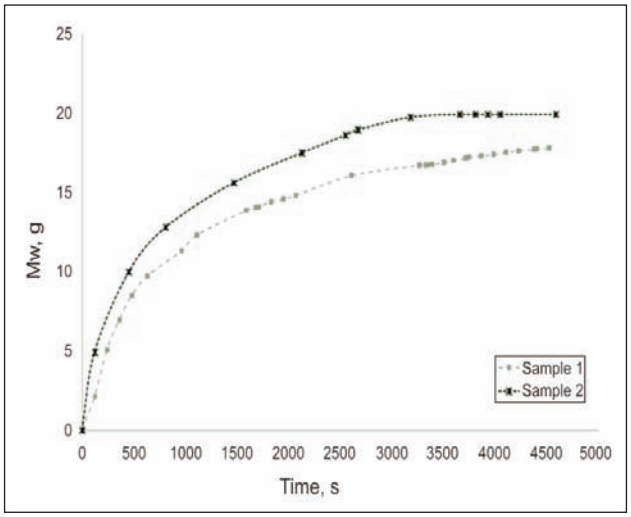

Fig. 1. Experimental data of water mass absorbed by the sample 1 and 2 versus time

Table 1

CHARACTERISTICS OF USED KNITTED FABRICS

Sample	Composition	Knit structure	Yarn spinning	Couliering depth	Thikness (10^{-3}m)	Weight (g/m^2)	Porosity
1	100% Cotton	Jersey	Carded	14	1.99	359.5	0.883
2	80% Cotton - 20% PES	Jersey	Carded	14	2.13	378.1	0.879
3	100% Cotton	Rib 1&1	Carded	14	2.85	419.2	0.869
4	100% Cotton	Jersey	Open-end	14	2.03	461.1	0.895
5	100% Cotton	Jersey	Carded	12	2.33	349.0	0.888

be divided into two phases: the rapid phase and the slow phase, respectively.

Kinetic sorption study

Mathematical models

In order to interpret sorption kinetic data of water molecules in cotton fabric, the experimental values of the mass of water absorbed by fabric at each time were curve fitted using MatLab to a double-exponential function [10, 11, 16]. The double exponential form used in this study is given by the following equation:

$$m_t = m_e - m_1 \exp(-K_1 t) - m_2 \exp(-K_2 t) \quad (1)$$

As mentioned above, the uptake process of water sorption on knitted fabrics could be divided into two steps. The first one is the rapid phase and the second one is the slow phase.

So, in equation (1): K_1 (min^{-1}) and K_2 (min^{-1}) are the diffusion parameters of the rapid step and the slow step, respectively; m_e is the quantity of water absorbed at equilibrium (saturation of fabric).

As shown in figure 3, the DEM curve presented by the solid line fits well the experimental data with higher determination coefficient (R^2 = 0.9957). The best fit model parameters (m_e, m_1, m_2, K_1, and K_2) corresponding to the higher determination coefficient (R^2) were given automatically by the MatLab software.

Figure 3 displays the water mass absorbed onto the sample 2 curve fitted using MatLab, it can be seen that the mass of water absorbed at equilibrium (m_e) was equal to 14.51 g, the diffusion parameters K_1 (s^{-1}) and K_2 (s^{-1}) were equal to 0.9770 min^{-1} and 0.00170 min^{-1}, respectively. We observe that K_1 was very larger than K_2, which means that the first and rapid process can be assumed to be negligible on the overall vertical capillary kinetics into knitted fabrics [11]. Then, the DEM equation can be simplified to be as:

$$m_t = m_e - C \exp(-Kt) \quad (2)$$

Where, "C" is a constant and "K" is the kinetic parameter of the capillary rise of water in knitted fabrics.

Equation (2) can be rearranged to linear form:

$$\mathrm{Ln}(m_e - m_t) = \mathrm{Ln}\ C - K^*t \quad (3)$$

K and C can be determined by plotting of $\mathrm{Ln}(m_e - m_t)$ against "t".

Influence of fabric structural parameters

The results of the linear fitting curves of experimental data of capillary rise in five different knitted fabrics are listed in table 2.

Because of its hydrophobic character and so it has a less absorbency ability, the water does not penetrate into the polyester fibre pore and the capillary kinetic of the distilled water in the cotton/polyester knit fabric (sample 2) is higher than in the 100% cotton knit fabric (sample 1).

We observe also that the value of the capillary diffusion parameter "K" in the 100% cotton rib fabric (sample 3) is higher than in the 100% cotton jersey fabric (sample 1). In fact, the rib fabrics contain more quantities of cotton materials per centimetre than the jersey fabric.

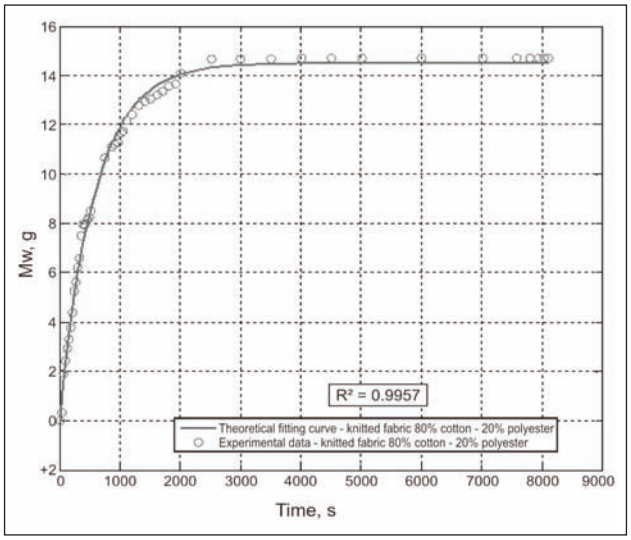

Fig. 3. Water mass absorbed by sample 2 over time with DEM fitting

Table 2

INFLUENCE OF FABRIC STRUCTURAL CHARACTERISTICS ON THE LINEAR MODEL

Sample N°	m_e	K (min^{-1})	C	R^2
1	18.81	0.0006	16.6182	0.9474
2	14.66	0.0013	12.1667	0.9661
3	31.04	0.0008	36.8332	0.9338
4	19.88	0.0288	25.3937	0.9232
5	20.75	0.0292	28.1009	0.9579

As the couliering depth value increasers and the stitches number per centimetre are more important, the capillary kinetic coefficient "K" increases. As a consequence, the quantity of water absorbed by the knit fabric and the capillary rise kinetic parameter are found to be greater for samples 4 and 5 than for sample 1.

On the other hand, the carded yarn is more regular and the cohesion between fibers is greater than the open-end yarn which is characterized by non regular organisation of fibres at the section. This explains the difference of the absorbed water quantity at equilibrium between sample 1 and 4.

Moreover, we note that the linear model equation has the same form of the pseudo-first-order equation of Lagergren whose equation is [17]:

$$\mathrm{Ln}(q_e - q_t) = \mathrm{Ln}\ q_e - \frac{k_1}{2.303} t \quad (4)$$

In the study of Yalçin *and al.*, q_e and q_t are the amounts of the absorbed dye at an instant 't' and at the equilibrium and k_1 is the rate constant of the pseudo-first-order sorption process. Plots of $\mathrm{Ln}(q_e - q_t)$ versus "t" can gives a straight line for pseudo-first-order kinetics, which allows computation of the sorption rate constant k_1, and equilibrium capacity q_e.

CONCLUSION

From the present work, mathematical models were established and have been demonstrated to be satisfactory describing the kinetic of water sorption through various knitted fabrics. In fact, the experimental data have been interpreted using double-exponential model (DEM) and the simulation curves showed good fits with the experimental data. Then, the DEM was simplified to be linear to make easy the determination of the kinetic coefficient of the capillary rise of the distilled water in knitted fabric.

Along this study, we conclude that the kinetic of water sorption is influenced by a large number of parameters like the construction parameters (the knit structure and the couliering depth values) and the composition of fabrics materials (100% natural fiber or a blend of natural and synthetic fiber).

BIBLIOGRAPHY

[1] Kerry A., Martin T. *Effect of textile hygroscopicity on stratum corneum hydration, skin erythema and skin temperature during exercise in the presence of wind and no wind,* In: J. Exerc. Sci. Fit., 2011, vol. 9, pp. 100–108

[2] Youngmin J., Chung H. P., Tae J. K. *Effect of heat and moisture transfer properties on microclimate and subjective thermal comfort of caps,* In: Text Res J, 2010, vol. 80, Issue 20, pp. 2195–2203

[3] Saîhi D., El-Achari A., Ghenaim A., Caze C. *Wettability of grafted poly (ethylene terephthalate) fibers*, In: Polymer Test, 2002, vol. 21, Issue 6, pp. 615–618

[4] Hamdaoui M., Fayala F., Ben Nasrallah S. *Experimental apparatus and mathematical model for determination of parameters of capillary rise in fabrics*, In. J of Porous media, 2006, vol. 9, Issue 4, pp. 381–392.

[5] Hamdaoui M., Fayala F., Ben Nasrallah S. *Dynamics of capillary rise in yarns: Influence of fiber and liquid characteristics,* In: J of Appl. Polym. Sci., 2007, vol. 104, pp. 3050–3056.

[6] Fayala F., Hamdaoui M., Ben Nasrallah S., Perré P. *Study of liquid distribution during capillary rise in fabrics using an electrical resistivity technique: Influence of structure and composition*, In: J of porous Media, 2008, vol. 11, Issue 3, pp. 231–240.

[7] Hamdaoui M., Fayala F., Perré P., Ben Nasrallah S. *Experimental study of capillary rise in fabrics using an electrical resistance technique,* In: AUTEX Research Journal, 2008, vol. 8, Issue 2, pp. 44–48

[8] Marmur A. *The radial capillary*, In. J. Colloid and interface sci., 1988, vol. 124, Issue 1, pp. 301–308

[9] Dullien F. A. L., El-Sayed M. S., Batra V. K. *Rate of capillary rise in porous media with non uniform pores,* In: J. Colloid and interface sci., 1977, vol. 60, Issue 3, pp. 497–506

[10] Hamdaoui M., Achour N. S., Ben Nasrallah S. *The influence of woven fabric structure on kinetics of water sorption,* In: J Eng Fibers and Fabrics, 2014, vol. 9, Issue 1, pp. 101–106

[11] Hamdaoui M., Ben Nasrallah S. *Capillary rise kinetics on woven fabrics – Experimental and theoretical studies,* In: Indian J Fibre Text Res, 2015, vol. 40, Issue 2

[12] Li Y., Luo Z. *An improved mathematical simulation of the coupled diffusion of moisture and heat in wool fabric,* In: Text. Res. J., 1999, vol. 69, Issue 10, pp. 760–768

[13] Wehner J., Miller B., Rebenfeld L. *Dynamics of water vapour transmission through fabric barriers,* In: Text. Res. J., 1988, vol. 58, Issue 10, pp. 581–592

[14] Perwuelz A., Mondon P., Cazé C. *Experimental study of capillary flow in yarns,* In: Textile Res. J., 2000, vol. 70, Issue 4, pp. 333–339

[15] Perwuelz A., Casetta M., Cazé C. *Liquid organisation during capillary rise in yarns – influence of yarn torsion*, In: Polymer Testing, 2001, vol. 20, Issue 5, pp. 553–561

[16] Hamdaoui M., Lanouar A. *A new kinetic model for cotton reactive dyeing at different temperatures*, In: Indian J Fibre Text Res, 2014, vol. 39, pp. 310-313

[17] Yalçin M., Gürses A., Doğar Ç., Sözbilir M. *The Adsorption Kinetics of Cethyltrimethylammonium Bromide (CTAB) onto Powdered Active Carbon*, In: Adsorption, 2004, vol. 10, pp. 339–348

Authors:

Nesma Sawssen ACHOUR[1,2]
Ayda BAFFOUN[1,2]
Mohamed HAMDAOUI[1,2]
Sassi Ben NASRALLAH[1]

Monastir University
[1]National School of Engineers, Department of Textile Engineering
[2]Laboratoire d'Etudes des Systèmes Thermiques et Energétiques (LESTE Laboratory)

Avenue Ibn Eljazzar-5019
Monastir-TUNISIA

Corresponding author:

M. HAMDAOUI
hamdaouimohamed@yahoo.fr

Impact of surface profile of polyester knitted rib structure on its thermal properties

ASIF MANGAT
VLADIMIR BAJZIK
LUBOS HES
FUNDA BUYUK

REZUMAT – ABSTRACT

Impactul aspectului de suprafață al structurii de tricot patent din poliester asupra proprietăților termice

Scopul acestui studiu este de a evidenţia efectul aspectului de suprafață al structurii unui tricot patent asupra conductivității, rezistenței și absorbției termice în condiții uscate. Epruvetele de tricot patent au fost realizate utilizând fire de poliester 100%, având mase și grosimi distincte. În plus, a existat o mare varietate a aspectului de suprafață a tricotului glat. Acest lucru a fost realizat prin utilizarea de reglaje diferite ale acelor la mașina de tricotat. Parametrii termici au fost testați utilizând un aparat de tip Alambeta. Epruvetele au fost păstrate în mod corespunzător într-un mediu controlat timp de 24 ore. Rezultatele demonstrează că aspectul de suprafață al tricotului patent are un efect important asupra parametrilor termici. Pe măsură ce scade distanța de contact, conductivitatea termică efectivă și absorbția termică scad, de asemenea, ceea ce este indicat pentru un confort termofiziologic mai bun. Acest studiu oferă o analiză precisă a aspectului de suprafață al parametrilor termici, care este extrem de valoros pentru designerii de lenjerie de corp.

Cuvinte-cheie: patent, conductivitate, absorbţie termică, parametri termici

Impact of surface profile of polyester knitted rib structure on its thermal properties

The reason for this venture is to recognize the effect of surface profile of knitted rib on thermal conductivity, thermal resistance and thermal absorptivity under dry condition. Knitted rib specimens were made utilizing 100% polyester yarn having distinctive planar weight and thickness. In addition, there was a huge variety in surface profile of the rib. This was accomplished utilizing distinctive settings of needles on knitting machine. We tested thermal parameters utilizing Alambeta. Specimens were properly kept in a controlled environment for 24 hours. Results demonstrate that surface profile of knitted rib has a noteworthy effect on thermal parameters. As the contact territory diminishes, effective thermal conductivity and thermal absorptivity diminishes as well, which is required for better thermo physiological comfort. This study gives a precise examination of surface profile of thermal parameters, which is highly valuable for internal articles of clothing designers.

Keywords: rib, conductivity, thermal absorptivity, thermal parameters

INTRODUCTION

Knitted rib is a thick fabric made up of coarse yarns. Its weight ranges from 200 to 400 grams for every square meter. In most of the cases, it is used to make undergarments. It provides better thermal comfort during cold weather and under wet conditions (sweating). Its surface profile is quite different as compared to the surface profile of normal knitted fabrics. Surface was made uneven using different knitting techniques, normally denoted by 1×1, 1×2, and 2×1 etc. Two types of knitting machines were used to make rib; the first was circular double knit machine and the second was flat double knit machine. In most of the cases, circular knitting machine is used to produce bulk quantity. Knitted rib made on circular knitting machine is used to make undergarments for example vests, underwears, and body warmers etc. Knitted rib, which is manufactured using flat knitting machines, is used to make waist and wrist bands and it is also attached with knitted shirts.

This study is an effort to analyse the impact of surface profile of knitted rib on thermal parameters (thermal conductivity, thermal resistance, and thermal absorptivity). For this purpose, we developed 18 samples of knitted rib using 100% polyester yarn and a flat knitting machine. There is no significant difference between the thicknesses of samples while major differences exist between their surface profile and planar weight. Surface of knitted rib is divided into two main categories (figure 1). Figure 1 shows that there

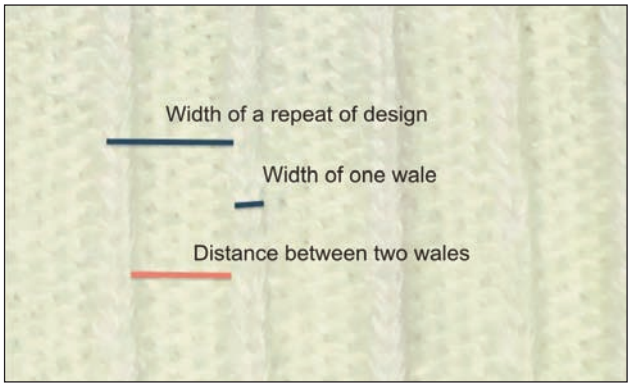

Fig. 1. Surface profile of knitted rib

are fins on the surface of knitted rib. These fins are called vertical stripes (columns), also called wales. Rest of the area is called base of knitted rib fabric. Vertical columns are separated by missed stitches. On other side of knitted rib, the same pattern is repeated but wales are alternatively arranged as compared to front side. Knitted rib has no face and back because both sides are similar and either side can be used.

Knitted rib and thermal parameters

Thermal parameters (conductivity, resistance, absorptivity) are very important for better thermal comfort. Thermal resistance is a vital property of material fabrics and it is a subject of various studies. It relies on the thermal conductivity of strands, thickness of material and course of action of yarn and filaments. Thermal conductivity shows the capacity of a material to transfer heat. Thermal conductivity is anisotropic in nature and to a great extent; it relies on the structure of the material. The thickness of a material prevents high temperature from passing through.

Thermal conductivity of knitted rib

Many studies have been conducted for various hypothetical examinations of heat transfer through fabrics [1–7]. Their outcomes demonstrate that the procedure of high temperature exchange through fabrics essentially happens by conduction, which is represented by:

$$q = \frac{\lambda \Delta T}{h} \quad (1)$$

Where q indicates heat flux [Wm^{-2}], T is temperature [K], λ shows thermal conductivity [$Wm^{-1}K^{-1}$] and h represents thickness [m]. This was also affirmed in a far-reaching exploratory investigation of high temperature exchange through woven and nonwoven fabrics, directed by Hes and Stanek, in which, the Grasshoff number (Gr) depicts the impact of free convection and it was found lower than 1,000 [8]. They further communicated that the extent of high temperature exchanged by radiation does not exceed 20% of the aggregate heat transfer. Heat transfer through radiation also depends upon the temperature. At low temperature, heat transfer through radiation is quite low because heat transfer through radiation depends upon the fourth power of temperature.

Thermal conductivity of dry fabrics needs to rely upon the structure and properties of the yarns or filaments. Crow explains that two components, which play a very critical role in this context, are thickness of the fabric and fibre arrangements [6]. Parallel strands bring about three times higher thermal resistance in connection to filaments, which are perpendicular to the fabric surface.

Thermal resistance

Thermal resistance R [m^2KW^{-1}] is calculated using the following equation:

$$R = \frac{h}{\lambda} \quad (2)$$

Where R speaks to the thermal resistance [m^2KW^{-1}], h is the fabric thickness [m], and λ is its thermal conductivity [$Wm^{-1}K^{-1}$]. Equation 2 demonstrates that thickness has a direct connection with thermal resistance. Any change in thickness can change the thermal resistance of a fabric. The estimation of fabric thickness is very delicate, especially because of the compressibility of the fabric. A minor change in weight will change the thickness of the fabric. Such change takes place because of high porosity and jutting strands on the surface of the fabric. Similarly, thick fabric having a smooth surface won't be essentially influenced by pressure.

Thermal absorptivity

Thermal absorptivity (b) of fabrics was acquainted by Hes, which provides warm feelings (heat transfer) through limited contact of human skin with the fabric surface [9]. Giving that the time of high temperature contact τ between the human skin and the material is shorter than a few seconds, the measured fabric can be disentangled into semi-unbounded homogenous mass ρc [Jm^{-3}] and starting temperature t_2. Unstable temperature field between the human skin (with steady temperature t_1) and fabric offers a relationship, which focuses the heat transfer q [Wm^{-2}] through the fabric:

$$q = \frac{b(t_1 - t_2)}{\pi \tau^{0.5}} \quad (3)$$

$$b = \sqrt{\lambda \rho c} \quad (4)$$

Where ρc [Jm^{-3}] is the thermal capacity of the fabric and the term b represents thermal absorptivity of fabrics. The higher the thermal absorptivity of the fabric, the cooler will be its inclination. In the material praxis, this parameter ranges from 20 $Ws^{0.5}m^{-2}K^{-1}$ (for fine nonwoven networks) to 600 $Ws^{1/2}m^{-2}K^{-1}$ (for wet fabrics).

Surface profile and thermal parameters

Xu et al. conducted a study to examine impact of supercritical-pressure fluid flows and heat transfer of methane in ribbed cooling tubes [10]. His study was focused on regenerative engine cooling. For this purpose, he examined turbulent fluid flows and heat transfer of cryogenic methane in ribbed cooling tubes at a supercritical pressure of 8 MPa. The conclusion of their study tells that a ribbed tube surface profile increases significantly during the heat transfer process. The study revealed another fact that height of rib should be suitable enough to facilitate heat transfer. Work of Xu et al. tells that the height of rib wales helps in increasing heat transfer. But at the same time, we cannot ignore the air trapped on the surface of rib.

In case of rib, which is commonly used to make clothing, fin height can increase surface area for more heat transfer. In this case, the purpose of making rib is not fulfilled. We use rib to increase thermal resistance and maintain the human body temperature. It is only possible if we enable rib to trap air, which helps

in increasing thermal resistance due to low thermal conductivity of air. If air is not trapped, surface area will increase, which will enhance heat flow from the human body.

Özdil et al. studied the impact of yarn properties on thermal comfort of knitted fabrics [11]. Özdil et al. developed 1×1 knitted rib and identified the thermal properties using various yarn varieties with distinct properties. They took yarn count, yarn twist and combing process as independent variables and thermal resistance, thermal absorptivity, thermal conductivity, and water vapour permeability of samples as dependent variables. They used Alambeta and Permetest devices developed by Sensora Czech Republic for testing. Their findings reveal that yarn count, yarn twist and combing process have significant impact on thermal absorptivity, thermal conductivity, and water vapour permeability of 1×1 knitted rib whereas yarn twist and yarn count decrease thermal resistance values and increase water vapour permeability values. Moreover, combing process has the same effect on the thermal properties. Study of Özdil et al. does not include the surface profile of the rib. We can deduct from this study that better combing and high twist have a significant impact on thermal parameters only due to smooth profile of knitted rib. Although, there is no significant impact of these parameters on the surface profile but still there is a substantial influence on thermal parameters, which shows that change in surface profile has a significant impact on thermal parameters.

Study of Taslim provides many new avenues of heat transfer and rib profile of any surface [12]. Taslim conducted a research to find out the fin effects on the overall heat transfer coefficient in a rib-roughened cooling channel. Rib structure is not only popular in fabric; it is also widely used in heat exchangers used in engines and hot bodies. The primary purpose is to increase the heat flow and keep the engine body at required temperature. But in textile, rib structure, which is quite similar to fins on the heat exchanger bodies, is not used to increase heat flow from human body to the environment. Rather rib structure is used to protect human body from heat loss and provide a layer of air to increase thermal resistance of the fabric. Taslim further describes the role of geometry of rib (fin) in heat transfer and calculation of heat transfer coefficient. In case of knitted rib, the geometry of the knitted rib is quite flexible and highly prone to changes due to any pressure and stretch. This change does not allow developing heat transfer coefficient. Moreover, the height of fin is more important. According to Taslim, height plays a crucial role. It contributes to increasing the area that regulates the amount of heat transferred in a certain unit of time. It is important to note that commonly used ribs have maximum 2.5 mm thickness and their fin height is normally in the range of 1–1.5 mm.

From the work of Taslim, it is quite important to deal with the question of air trapping in such a tiny gap between two rib wales. It may help transferring heat instead of trapping air to increase thermal resistance

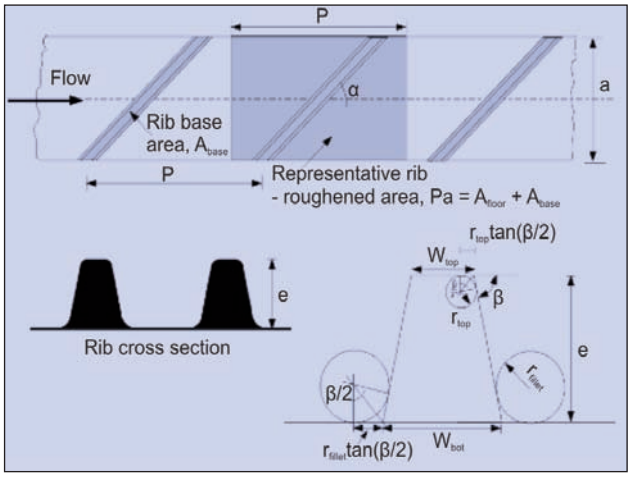

Fig. 2. Rib Geometry

of knitted rib. A researcher can infer from figure 2 that rib has three areas, base (space between two consecutive fins), area of fin (height*width) and top of the fin [12]. Moreover, when airflow will move on the surface of the rib, there are chances of angled view.

Taslim derived an equation to find out heat transfer coefficient. When it is applied on the base surface of the rib (projection surface), it will have the same thermal effects as that of the actual heat transfer coefficient applied on total exposed area of the rib. Taslim concludes that there is 20% possible error in calculating the heat transfer coefficient using geometry of the rib. All the above discussion reveals that fins are used to increase the heat flow not to trap the air to improve heat transfer area.

Another aspect of knitted rib is the number of contact points between the human body and surface of the fabric. Pac et al. conducted a study on the process of human hand touching the surface of a fabric while the skin had different temperature as compared to the fabric [13]. During this process, heat transfers between the hand and the fabric. The first feeling is warm-cool feeling. Pac et al. say that the significance of warm-cool feeling depends on the contact points between the skin and the fabric. Fabric surface profile has strong dependency on structural parameters of fabric, which include physical and chemical properties of fibre, knitting or weaving pattern, fabric thickness and porosity of the fabric. This study can be linked with the matter under discussion. Surface area of knitted rib largely differs from a fully knitted fabric. Contact area between human hand and knitted rib ranges from 20% to 80% depending upon the surface profile of the knitted rib. As proved by Pac et al. number of contact points provides a heat transfer channel. In case of rib, these contact points are quite a few. Based on this point, knitted rib is considered as a useful fabric for wearing as under garment to control the heat loss of human body [14].

Work of Tarhan and Sarisik does not have any direct link with contact points between the human hand and surface profile of the knitted rib [15]. It is about denim. Denim fabric produced from weaving machine has a rough surface. But during washing, surface is

smoothened, which increases the contact points. Higher contact points for trousers provide higher heat transfer, which is required during manual physical labour.

Thermal comfort depends upon the heat and moisture balance between human body and the environment through our clothing. Various aspects of fabric have a significant impact on thermal parameters. One of the most significant impacts is structure of the fabric [8, 16–20]. Knitted rib has a significant surface profile as compared to other plain fabrics. Considering this fact, it is obvious that knitted rib provides a different kind of thermal comfort.

Research by Hollies et al. on water transport mechanisms in textile materials reveals very unique results [21]. According to Hollies et al., the movement of water along fabrics depends on the laws of capillary action. They further say that water moves mainly in the capillaries formed by the fibres in individual yarns. Their ultimate conclusion is: the speed of travel of water in these capillaries significantly depends on arrangements of fibres rather than depending on the nature of fibres.

Bogaty et al. have elaborated that thermal parameters also depend upon the arrangements [22]. Rib has quite distinct fibre arrangements and as compared to a fully knit jersey fabric. This arrangement has a significant correlation with the thermal conductivity of the fabric. Keeping this factor in view, we can derive that the rib has a different thermal conductivity and changed thermal resistance, which a wearer needs.

All the above discussion depicts that arrangement of fibre and yarn has a significant impact on thermal parameters. As discussed in previous pages, there are two main issues linked with knitted rib and thermal parameters. First is surface profile of knitted rib, which does not have enough height of fins to trap air under even minor pressure to provide thermal resistance due to presence of air while in the second case, heat flow can be quite low due to the less number of contact points between human body and knitted rib.

EXPERIMENTAL PART

Sample description

Weft-knitted rib, knitted on a flat knitting machine, was used for this study in order to verify the impact of distinct rib structures on thermal parameters (thermal conductivity, thermal resistance, thermal absorptivity) in a dry state. Knitted rib consists of one type of yarn. It has similar surface profiles on both sides. It is commonly used to make collars, cuffs or waistbands. In some cases, undergarments are made using rib. Most common is vest, which provides better thermal feeling. Attires made up of rib are also called thermal dresses due to their capability to maintain body heat in cold climate. Most common materials for knitted rib are cotton, polyester and polypropylene in some cases. Eighteen types of knitted rib having diverse structures and surface profiles were used for testing purposes. See table 1.

Table 1

BASIC CHARACTERISTICS OF KNITTED RIB

Sample No.	Rib types	Planar weight (gm^2)
1	1.1	481
2	1.2	400
3	2.1	541
4	2.2	560
5	2.3	462
6	3.1	523
7	3.3	477
8	3.4	471
9	4.1	485
10	4.2	548
11	4.3	540
12	4.4	540
13	1.1	378
14	2.1	422
15	3.1	447
16	4.1	474
17	5.1	501
18	6.1	470

Testing procedure

The determination of thermal parameters (thermal conductivity, thermal resistance, thermal absorptivity) requires the use of a special testing instrument that enables a researcher to record a measurement. Many studies have used Alambeta (Sensora Czech Republic), which gives results in less than three minutes. The Alambeta is computer-controlled, semiautomatic, non-destructive thermal parameters testing device along with thickness tester for testing textile fabrics. The biggest advantage of the Alambeta testing is that the instrument immediately displays the thermal parameters along with the thickness levels of the tested fabrics. Selection of Alambeta is based on its efficient and effective use along with its application in many studies [3, 24–26].

All the samples were put openly in a flat position in the testing lab. In testing lab, the temperature ranged between 25–26°C and relative humidity was in the range of 20–22. It was done to give a uniform treatment to all the samples for more accurate results.

RESULTS AND DISCUSSION

The primary objective of this study is to find out the correlation among contact area, porosity, planar weight and thermal parameters.

Contact points and thermal parameters

Contact points of rib define the area which touches the human hand in the absence of pressure. It is calculated using the following equation:

$$C = \frac{F}{F + B} \times 100 \quad (5)$$

where C is the contact area (%), F – the area of fin on top (elevated courses) and B – the area between

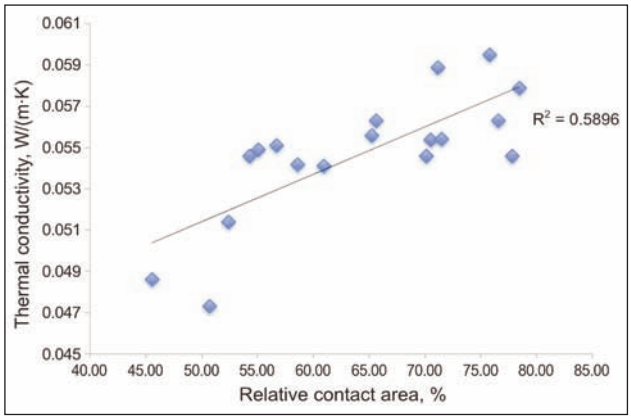

Fig. 3. Thermal conductivity and contact area

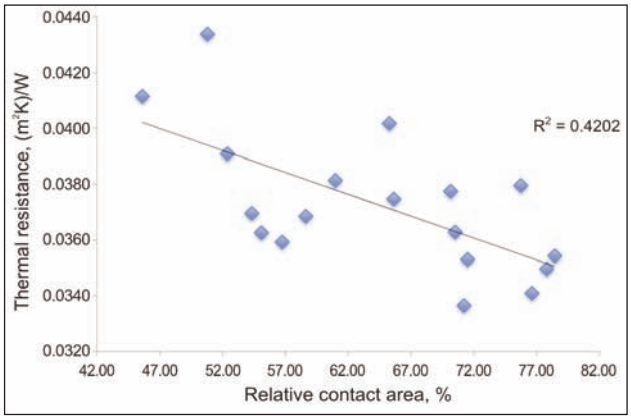

Fig. 4. Thermal resistance and contact area

two adjacent rows of courses. This area was calculated with the help of a computer-controlled camera. Area of contact (*C*) depends upon the type of rib structure. Normally, notations used for rib are 1×1, 1×2, and 2×1 etc. Figure 2 shows that on knitted rib, surface is divided into two portions; base and wale (or fin). Thickness of base is almost half of the thickness at the point of fin. When someone touches the knitted rib, only fin touches the skin. This is a technique to reduce the contact points between the human skin and the fabric.

Figure 3 tells that there is a significant correlation between thermal conductivity and contact area (R^2 0.58). It proves the observation of Tarhan and Sarisik [15]. Moreover, it shows that more contact points mean that there is less area for air between the human skin and knitted rib. Thermal conductivity of polyester is between 0.3–0.4 [$Wm^{-1}K^{-1}$] and thermal conductivity of air is 0.026 [$Wm^{-1}K^{-1}$] [27]. It also proves that less contact area shows that there is more space for air between human skin and knitted rib surface. From these results, we can conclude that less contact area will maintain human body temperature.

Figure 4 shows a weak relationship between thermal resistance and contact area (R^2 0.42). It may be due to the intervening variable, which is thickness. On Alambeta, we exert a pressure of 1000 Pa. It is required to make a solid contact between the plate and the fabric. Knitted rib is quite flexible and easy to compress. Due to this compressibility, error in measuring the exact thickness is possible.

Figure 5 depicts a strong correlation between thermal absorptivity and contact area (R^2 0.96). Thermal absorptivity indicates the warm-cool feeling. Figure 5 shows that as the contact point's increase, thermal absorptivity also increases or we can say that there is a direct relation between the number of contact points and thermal absorptivity. Its significance is obvious from R square value. Higher thermal absorptivity value is an indicator of coolness, which results in heat flow from human skin, whereas low thermal absorptivity values indicate a warm feeling.

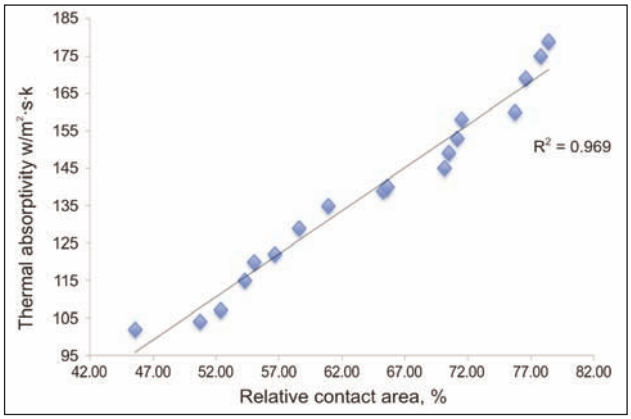

Fig. 5. Thermal absorptivity and contact area

CONCLUSION

Results demonstrate that there is a nonstop increment in thermal conductivity with the increment in contact focus. Contact focus is a point where human skin and fabric surface touches. Thermal conductivity of polyester is much higher than the thermal conductivity of air. Viable thermal conductivity of a fabric is not the same as thermal conductivity of polyester and air. It is not the aggregate of the individual thermal conductivity. Fabric contains polymer, dampness and air. Thermal conductivity of fabric is a consequence of consolidated impact of air, dampness and polymer. This is a vital result of the study, which will guide dress architects to plan internal apparels having least contact focuses to maintain the human body temperature. Second result of the study expresses a fact that there is limited connection between thermal safety and contact focus. It is essentially limited because thickness values vary in different varieties of the fabric and there was no variety in knitting machine set up. In any case, it is evident that there is a change in thermal safety because of progress in thermal conductivity. We additionally found out that there is a significant and noteworthy relationship between contact region and the thermal absorptivity. Higher thermal absorptivity allows skin to feel cool vibes. Rib structure gives less contact territory. It is primary reason of choice of knitted rib fabric for manufacturing undergarments.

ACKNOWLEDGEMENT

This research work is financially funded by project SGS 21098 Czech Republic.

BIBLIOGRAPHY

[1] Zhu, F., Li, K., *Determining effective thermal conductivity of fabrics by using fractal method*, In: Int Journal of Thermophysics, 2010, 31, pp. 612–619
[2] Yoshihiroa, Y., Hiroakia, Y. and Hajimeb, M., *Effective thermal conductivity of plain weave fabric and its composite*, In: Journal of Textile Engineering 2008; 54(4), 2008. 54(4): pp. 111–119
[3] Hes, L., Heat, *Moisture and air transfer properties of selected woven fabrics in wet state*, In: Journal of Fiber Bioengineering & Informatics 2008, pp. 968–976
[4] Özdil, N., Marmaralı, A., and Kretzschmar, S.D., *Effect of yarn properties on thermal comfort of knitted fabrics*, In: International Journal of Thermal Science, 2007, 46(12), pp. 1318–1322
[5] Militky, J., *Prediction of textile fabrics thermal conductivity, in thermal manikins and modelling*, J. Fan, Editor, 2006.
[6] Crow, R.M., *Heat and moisture transfer in clothing systems. Transfer through materials, a literature review*. Part 1. 1974, Ottawa: Ontario: Defence Research Establishment.
[7] Sugawara, A., and Yoshizawa, Y., *An investigation on the thermal conductivity of porous materials and its application to porous rock*, In: Australian Journal of Physics, 1961, 14, pp. 469–480.
[8] Hes, L., and Stanek, J., *Theoretical and experimental analysis of heat conductivity for nonwoven fabrics*, in NDA-TEC Transactions, Philadelphia, 1989
[9] Hes, L., *Non-destruction determination of comfort parameters during marketing of functional garment and Apparels*, In: Indian Journal of Fiber and Text. Research, 2008(33): pp. 239–245
[10] Xu, K., Tang, L., Meng, H., *Numerical study of supercritical-pressure fluid flows and heat transfer of methane in ribbed cooling tubes*, In: International Journal of Heat and Mass Transfer, 2015, 84, pp. 346–358
[11] Özdil, N., Marmaralı, A., Kretzschmar, S. D., *Effect of yarn properties on thermal comfort of knitted fabrics*, In: International Journal of Thermal Sciences, 2007, 46(12), pp. 1318–1322
[12] Taslim, M.E., *Rib fin effects on the overall equivalent heat transfer coefficient in a rib-roughened cooling channel*, In: International Journal of Heat Exchangers, 2005, VI, pp. 25–41
[13] Pac, M.J., Bueno, M., and Renner, M., *Warm-Cool Feeling Relative to Tribological Properties of Fabrics*, In: Textile Res. J., 2001, 71(9), pp. 806–812
[14] Tech, I.A., *HVAC Handbook – Thermal Comfort*, 2002, INNOVA Air Tech
[15] Tarhan, M., and Sarisik, M, *A comparison among performance characteristics of various denim fading processes*, In: Textile Research Journal, 79, pp. 301–309, 2009
[16] Hes, L., *Thermal properties of nonwovens*. Congress Index 87 Genf, 1987
[17] Hes, L., and Dolezal, I, *New method and equipment for measuring thermal properties of textiles,* In: J. Textile Mach. Soc. Jpn, 1989(71), pp. 806–812
[18] Hes, L., Martins, J. *Experimental Heat Transfer, Fluid mechanics, and thermodynamicsheld*, Third World Conference 1993, Honolulu
[19] Hes, L., Araujo, M.D., and Djulay, V.V., *Effect of mutual bonding of textile layers on thermal insulation and thermal contact properties of fabric assemblies*, In: Textile Research Journal, 1996, 66(4), pp. 245–250.
[20] Hes, L. *Fundaments of design of fabrics and garments with demanded thermophysiological comfort*, In: International Round Table «Clothing Comfort – Condition of Life Quality» 2009, Romania
[21] Hollies, N.R.S., Kaessinger, M. M., Watson, B. S., Bogaty. H., *Water transport mechanisms in textile materials. Part II: Capillary-type penetration in yarns and fabrics,* In: Textile Research Journal, January, 1957, 27(1), pp. 8–13
[22] Bogaty, H., Hollies, N.R.S., and Harris, M., *Some thermal properties of fabrics the effect of fiber arrangement*, In: Textile Research Journal (Abstract) 1957 27(6), pp. 445–449
[23] Plante, A.M., Holcombe, B.V., Stephens, L.G., *Fiber* Hygroscopicity and Perceptions of Dampness. *Part I: Subjective Trials*, In: Textile Research Journal 65, pp. 293–298, 1995
[24] Abbasi, A.M.R., Mangat. M. M., Baheti, V. K., and Militky, J., *Electrical and thermal properties of polypyrrole coated cotton fabric*, In: Journal of Fibres and Textile, 2012, 1, pp. 48–52.
[25] Karaca, E., Kahraman, N., Omeroglu, S., and Becerir, B., *Effects of fiber cross sectional shape and weave pattern on thermal comfort properties of polyester woven fabrics*, In: FIBRES & TEXTILES in Eastern Europe, 2012, 20(3(92)), pp. 67–72
[26] Schacher, L., Adolphe, D., and Drean, J.-Y., *Comparison between thermal insulation and thermal properties of classical and microfibres polyester fabrics*, In: International Journal of Clothing Science and Technology 2000, 12(2), pp. 84–95
[27] Wiley-VCH, ed. Ullmann's Fibers, vol. 1, 2008, Verlag GmbH & Co. KGaA, Weinheim

Authors:

ASIF ELAHI MANGAT[1]
LUBOS HES[1]
VLADIMIR BAZIKH[1]
FUNDA BUYUK[2]

Technical University of Liberec, Faculty of Textile Engineering,
[1]Department of Textile Evaluation,
[2]Department of Textile Clothing,
Studentska 2, Liberec, 461 17, Czech Republic

Corresponding author:

ASIF MANGAT
e-mail: asifmangat@gmail.com

Salt free neutral dyeing of cotton with anionic dyes using plasma and chitosan treatments

AMINODDIN HAJI SAYYED SADRODDIN QAVAMNIA FARHAD KHOSRAVI BIZHAEM

REZUMAT – ABSTRACT

Vopsirea fără săruri a bumbacului cu coloranţi anionici utilizând tratamentele cu plasmă şi chitosan

Modificarea ecologică a fibrelor de bumbac, în scopul îmbunătățirii capacității de vopsire cu coloranți anionici, a fost scopul principal al acestui studiu. Biopolimerul chitosan a fost selectat pentru introducerea radicalilor cationici în fibrele de bumbac. Tratamentul cu plasmă a fost utilizat pentru a produce zonele funcționale în scopul atașării chitosanului de suprafața fibrelor. În acest studiu, chitosanul a fost aplicat pe țesătura de bumbac folosind pre-tratamentul cu plasmă cu oxigen. Prezența chitosanului pe suprafața fibrelor de bumbac a fost evidențiată pe baza imaginilor SEM. Mostrele de bumbac netratate și tratate cu chitosan au fost vopsite cu coloranți acizi și direcți. Au fost studiate efectele sării (sulfatului de sodiu), timpului de vopsire și concentrației inițiale de colorant asupra rezistenței vopsirii probelor netratate și tratate cu chitosan.

Cuvinte-cheie: plasmă, chitosan, bumbac, fără conținut de sare

Salt free neutral dyeing of cotton with anionic dyes using plasma and chitosan treatments

Environmentally friendly modification of cotton fibers with the aim of improvement of its dyeability with anionic dyes was the main purpose of the current study. Chitosan biopolymer was selected for introduction of cationic moieties to cotton fibers. Plasma treatment was employed to produce the functional sites for attachment of the chitosan to the surface of the fibers. In this study, chitosan was applied on cotton fabric using oxygen plasma pre-treatment. The presence of chitosan on the surface of cotton fibers was approved by SEM images. Untreated and chitosan treated cotton samples were dyed with acid and direct dyes. The effects of salt (sodium sulfate), dyeing time, and initial dye concentration on the color strength of raw and chitosan treated samples were studied.

Keywords: plasma, chitosan, cotton, dyeing, salt free

INTRODUCTION

Cotton is the most used natural fiber in the textile industry globally because it is inexpensive, absorbent, breathable and soft. However, different chemical modifications have been studied for improvement of the wettability, dyeability, chemical affinity, crease recovery, hydrophilicity, and functional properties of cotton textiles. Cotton fibers can be dyed using anionic dyes easily, but usually the common processes of cotton dyeing require large amounts of salt and alkali which mostly remain in the dye bath after the dyeing and may harm the environment [1–2].

The reason for using the electrolytes in the dyeing process is to overcome the repulsion forces occurring between the negatively charged cotton fibers and the anionic dye molecules [2]. Improving the substantivity of cotton toward anionic dyes by surface modification techniques, it is possible to reduce the need for electrolyte in the dyebath, and increase the dyebath exhaustion [3].

Salt free dyeing of cotton has been an interesting subject for many researchers. In this regard, the most common method used in the literature has been the introduction of cationic moieties to cotton fiber (cationization) to interact with anionic dye molecules in the dyeing process and increase the dyeing color strength and improve the wash fastness [4–6].

Tutak and Ozdemir applied four different commercial quaternary ammonium salts on cotton using a simple pad-dry method. The untreated and cationized cotton samples were dyed with a reactive dye. Their results showed that in comparison with the untreated cotton dyed with traditional method, the exhaustion and fixation values of the cationized cotton fabrics were better having higher degree of wash fastness [2].

In another study, Patino et al investigated the single and combined effects of corona treatment and cationization of cotton using an epihalohydrin on reactive dyeing of the modified fibers. Cationization of cotton increased the color strength of the dyed sample by 80% while this increase was only 14% for the corona treated fabric. Plasma treatment previous to cationization caused no significant improvement in the color strength of the dyed sample [7].

Montazer et al studied the salt free dyeing of cationized cotton using three different reactive dyes. The cationization was performed using 2,3-epoxypropyltrimethylammonium chloride by a pad-batch method and the cationized cotton samples were dyed with monochloro triazine, dichloro triazine and vinyl sulphone reactive dyes. The dyeability of the cotton samples with all reactive dyes was significantly improved without using salt. The light fastness of the cationized samples was improved while the wash and rub fastness properties remained unchanged [8].

Cationization can improve the natural dyeing of cotton fibers as well. In a recently published study, it was found that the cationization of cotton fabrics by exhaustion method, significantly improved the dyeability and fastness properties of cotton fabrics dyed with the aqueous extract of *Vitis Vinifera L.* leaves [5]. Haddar et al investigated the salt free dyeing of cationized cotton fabrics with leaves of fennel (*Foeniculum vulgare*) and *Hibiscus mutabilis* (Gulzuba) as two sources of natural dyes and optimized the dyeing process using response surface methodology [9–10]. Application of other chemicals like dendrimers and hyperbranched polymers has enhanced the dyeability of cotton using direct and reactive dyes leading to salt free dyeing [4, 11–13]. Chitosan as a natural biopolymer can be applied on cotton by different techniques and enhance its dyeability with anionic dyes [14]. Coating of cotton fiber with chitosan can introduce amine groups to the fiber leading to the possibility to dye the cotton fibers with acid dyes [15]. Grafting of acrylic acid on cotton fibers using plasma pre-treatment improved the dyeability of the modified fabric with natural cationic dye, berberine [16]. Grafting of ethylenediamine and triethylenetetramine on cotton fibers pretreated with air and argon plasma enhanced the dyeability of cotton fabric with acid dyes [17].

In this paper, cotton fibers are first activated using oxygen plasma and then grafted with chitosan. The main objective is to explore the effects of plasma and chitosan treatments on the dyeability of modified cotton fabric without using salt and in neutral medium.

EXPERIMENTAL WORK

Materials and Methods

Plain weave 100% cotton fabric (100 g/m², yarn count Nm = 40) was obtained from Mazandaran Textile Co., Iran. Medium molecular weight chitosan (75-85% deacetylated), Triton X-100 (nonionic surfactant) and sodium sulfate were purchased from Sigma Aldrich (USA). C.I. Acid red 88 and C.I. Direct orange 26 dyes were obtained from Alvan Sabet Company, Hamedan, Iran. The chemical structures of the dyes are shown in figure 1.

Plasma treatment: Cotton samples were pretreated using radio frequency (13.56 MHz) low pressure plasma equipment (model: Junior plasma, Europlasma, Belgium) with oxygen gas. The sample chamber was evacuated to 100 mTor and maintained at this pressure during the treatment. Oxygen with a flow rate of 100 sccm (Standard Cubic Centimeters per Minute) was used in the plasma treatment process. Plasma was generated at 150 W for five minutes. Then, atmospheric air was introduced into the chamber and the plasma treated sample was removed.

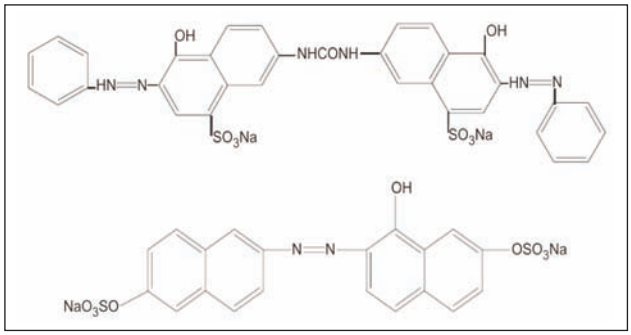

Fig. 1. The chemical structures of the C.I. Direct orange 26 (top) and C.I. Acid red 88 (bottom)

Chitosan treatment: Plasma treated samples were immediately impregnated in 0.5% w/v solution of chitosan containing 1% v/v acetic acid for 30 min. Then the samples were padded with 100% wet pick up and dried at 80 °C for 30 min. The dried samples were thoroughly washed with a solution containing 1% w/v Triton X-100 at 50 °C for 15 min to remove non-reacted chitosan from the surface of the fabric samples.

Dyeing: Dyeing of the raw and chitosan treated samples was performed using different amounts of direct and acid dyes (0.5–2 % owf) in the presence of varying amounts (0–10 % owf) of glauber's salt (L:G = 40:1) at the natural *p*H of the solution (around 7). The dyeing was started at 30°C and the temperature was raised to 50°C) at the rate of 2°C per minute. Then the samples remained in that condition with stirring for different times (30–120 min), and then rinsed and air dried.

Color strength measurements: The reflectance of dyed samples were measured on a Color-eye 7000A spectrophotometer using illuminant D65 and 10° standard observer. Color strength (K/S) of each dyed sample was calculated using kubelka-munk equation:

$$K/S = (1-R)^2 / 2R \quad (1)$$

Where R is the observed reflectance at wavelength of maximum absorbance, K – the absorption coefficient and S – the light scattering coefficient.

Color fastness test: Color fastness to washing was measured according to ISO 105-C01:1989(E) standard.

Scanning electron microscopy (SEM): Scanning electron micrographs were taken on an AIS2100 scanning electron microscope (Seron Technology, South Korea) to study the effect of plasma and chitosan treatments on the surface morphology of cotton fibers.

RESULTS AND DISCUSSION

SEM investigations

Figure 2 shows the SEM images of raw, plasma treated and chitosan coated cotton fibers respectively. Comparing the micrographs of raw and plasma treated fibers it is evident that serious etching has been done on the cotton fibers by oxygen plasma. Comparing these two samples with chitosan treated fibers, it can be seen easily that chitosan has been successfully grafted on cotton fibers.

Effect of dye concentration on color strength

To study the color build-up of both direct and acid dyes on raw and chitosan treated cotton fabrics, samples were dyed with four different concentrations of each dye. Figures 3 and 4 show the effect of concentration of direct and acid dyes on the color strength of raw and chitosan treated samples respectively. It can be seen that the concentration of

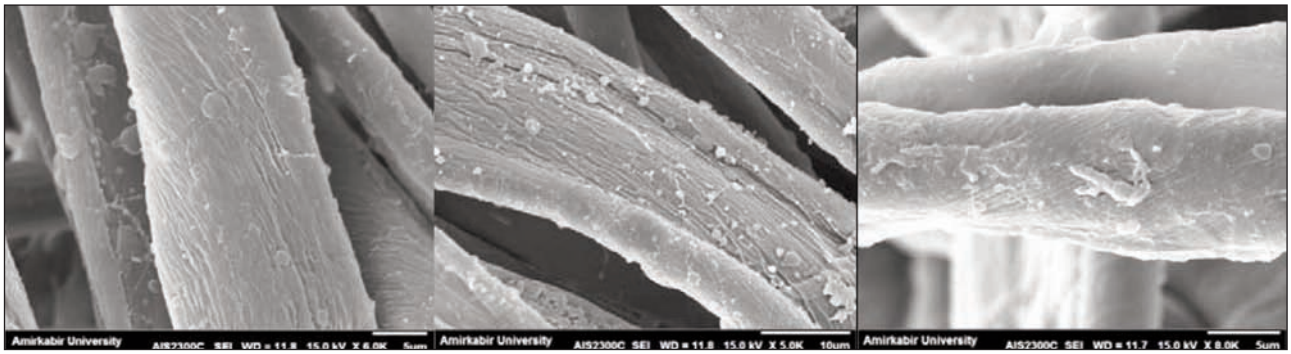

Fig. 2. SEM images of raw (left), plasma treated (middle) and chitosan coated (right) cotton fibers

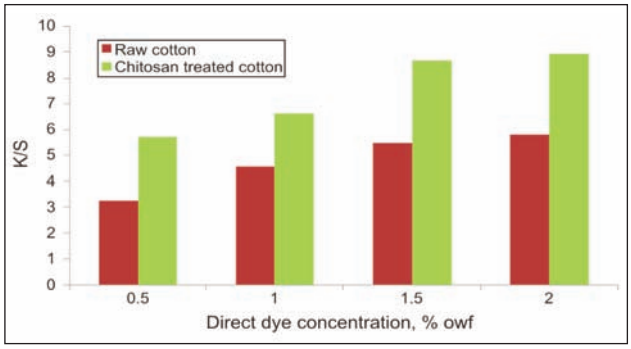

Fig. 3. The effect of direct dye concentration on color strength of raw and plasma treated samples (without salt, 30 min, 50 °C)

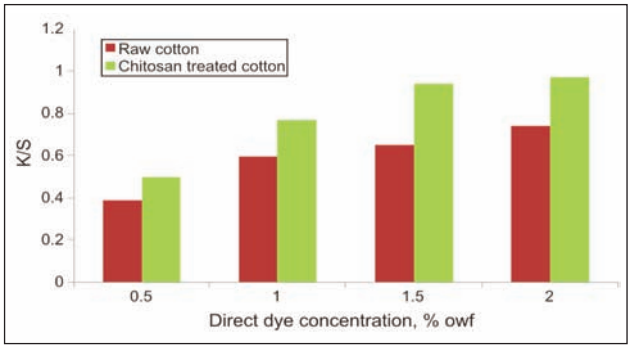

Fig. 4. The effect of acid dye concentration on color strength of raw and plasma treated samples (without salt, 30 min, 50 °C)

both dyes in the dyebath has an increasing effect on the color strength of the dyed samples. Using the same concentration of the dye in the dyebath, the samples dyed with the direct dye produced a much higher color strength comparing with the samples dyed with the acid dye.

The color strengths of chitosan treated samples are higher than the raw samples for both dyes and all concentrations. This improvement in dye absorption is due to the fact that chitosan treatment on cotton fabric provided more dye sites for absorption of the anionic dyes than the raw fabric. The application of chitosan improved the absorption of the dye molecules thanks to its cationic characteristic. Chitosan fixed on the surface of the cotton fibers makes the cotton cellulose positively charged. As a result, chitosan treated cotton is able to absorb anionic dyes through the ionic interaction between dye-anions and fiber-cations mechanism [18].

Effect of salt concentration on color strength

Figures 5 and 6 show the effect of salt concentration on the color strength of raw and chitosan treated samples dyed with direct and acid dyes respectively. As expected, the addition of salt increased the dye uptake for both raw and chitosan treated samples. However, the chitosan treated samples absorbed much higher amount of direct and acid dyes compared to raw fabrics. It is well-known that cellulose acquires negative charge when dipped in water and direct and acid dyes acquire anion in bath resulting repulsion between dye and cellulose. As a result, addition of electrolyte promotes dye uptake through reduction in zeta potential and promotes substantivity of dye. All direct dyes require salt at varying concentrations for better exhaustion on cellulosic fibers [19]. The presence of chitosan on the surface of the fibers makes the fiber's surface cationic and reduces the need for electrolyte in dyeing. For both dyes, addition of only 2% owf of salt in the dyebath of chitosan treated samples produced the same or higher color strength as the raw cotton dyed in the presence of 10% owf salt. So, it can be concluded that plasma and chitosan treatment can enable the cotton fabric to be dyed with direct and acid dyes without the need for electrolyte at low temperature.

Effect of dyeing time on color strength

Raw and chitosan treated samples were dyed with both dyes in the presence of 5% owf salt and without it. Figure 7 shows the effect of dyeing time on the color strength of raw and chitosan treated samples when dyed with the direct dye.

As expected, the color strength increased with prolonged time up to 90 min for all samples dyed with the direct dye. It seems that the optimum time for dyeing with C.I. Direct Orange 26 is 90 min and more contact with water molecules may cause the hydrolysis of the dye molecules resulting in reduced dye absorption.

As shown in figure 8, the optimum time for dyeing of both raw and chitosan treated cotton fabrics with the acid dye is 30 min. In this case, increasing the dyeing time caused considerable decrease in the color strength of the dyed samples. However this sensitivity is more pronounced for the raw samples and the

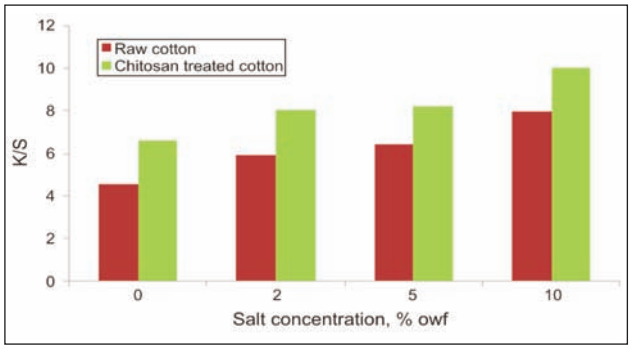

Fig. 5. The effect of salt on the color strength of raw and chitosan treated samples dyed with direct dye (1% owf dye, 30 min, 50 °C)

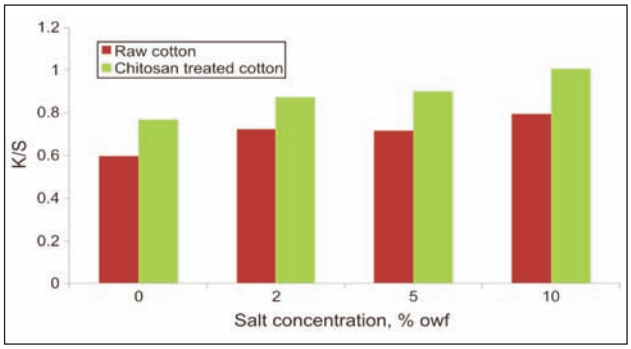

Fig. 6. The effect of salt on the color strength of raw and chitosan treated samples dyed with acid dye (1% owf dye, 30 min, 50 °C)

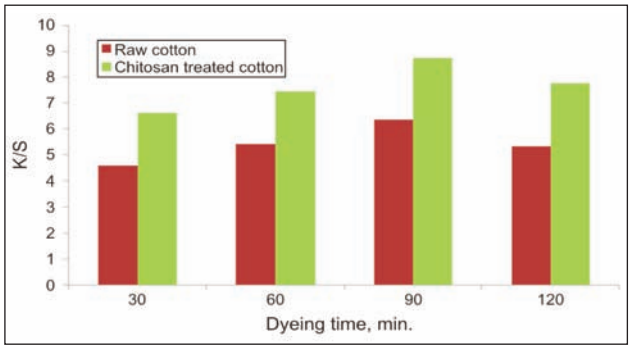

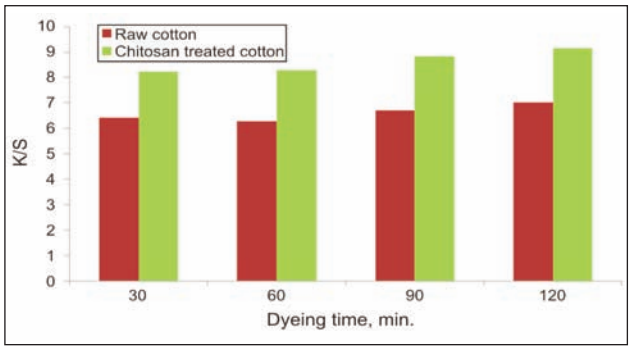

Fig. 7. The effect of dyeing time on the color strength of raw and chitosan treated samples dyed with the direct dye without (top) and with 5% owf salt (bottom)

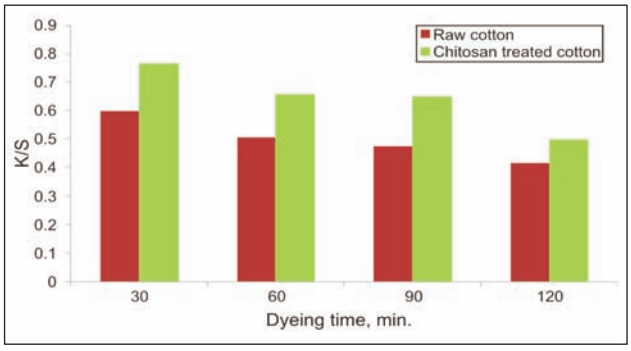

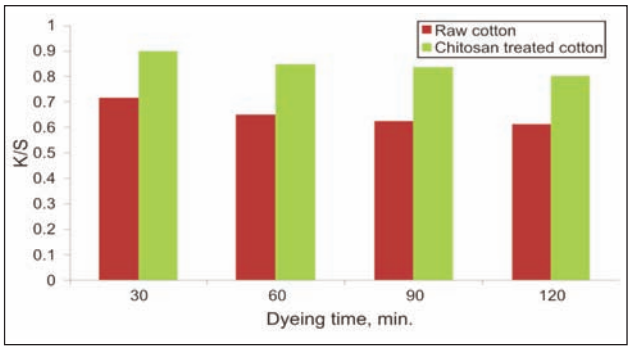

Fig. 8. The effect of dyeing time on the color strength of raw and chitosan treated samples dyed with the acid dye without (top) and with 5% owf salt (bottom)

chitosan treated samples were dyed with higher color strength at longer dyeing times when the direct dye was applied.

Washing fastness

Since the most important problem associated with the application of direct dyes on cellulosic fabrics is the poor wash fastness, the possibility to increase the wash fastness of the selected dyes was one of the goals of this study. Table 1 shows the wash fastness properties of different dyed samples. The fastness to washing was increased for both dyes when chitosan was applied on cotton samples. The ionic attraction between the cationic chitosan coated cotton and the anionic dye molecule increased the fastness of the color for this samples in comparison with the raw cotton samples which possess negative charge in contact with water causing the repulsion of the dye molecules and low wash fastness.

Table 1

WASH FASTNESS OF RAW AND CHITOSAN TREATED SAMPLES DYED WITH 1% OWF DIRECT AND ACID DYES (WITHOUT SALT, 30 MIN, 50 °C)

Sample	Wash fastness	
	Direct dye	Acid dye
Raw cotton	3	2–3
Chitosan treated cotton	4	4

CONCLUSION

Cotton fabric was successfully coated with chitosan using oxygen plasma as a pretreatment. The chitosan treated samples showed better dyeability besides good build up with direct and acid dyes used in this study. The application of chitosan on cotton fabric reduced the need for electrolyte in the dyebath markedly. The optimum dyeing time for the direct and

acid dye was 90 and 30 min respectively. The wash fastness of both dyes was significantly higher in case of chitosan treated samples. The method used in this study, can increase the dye uptake and wash fastness of direct and acid dyes on cotton fabric without the use of salt, alkali or acid. Plasma treatment is an environmentally friendly process and chitosan is a biodegradable and safe biopolymer with antibacterial activity. So this method can be considered as an environmentally friendly process for modification of cotton fabrics to enhance their dyeing, fastness and functional properties.

BIBLIOGRAPHY

[1] Zhang, F., Chen, Y., Lin, H., Wang, H., Zhao, B., *HBP-NH2 grafted cotton fiber: Preparation and salt-free dyeing properties*. In: *Carbohydrate Polymers,* 2008, vol. 74, issue 2, pp. 250–256

[2] Tutak, M., Oktay Özdemir, A., *Reactive dyeing of cationized cotton: Effects on the dyeing yield and the fastness properties*. In: *Journal of Applied Polymer Science,* 2011, vol. 119, issue 1, pp. 500–504

[3] El-Shishtawy, R. M., Youssef, Y. A., Ahmed, N. S. E., Mousa, A. A., *Acid dyeing isotherms of cotton fabrics pretreated with mixtures of reactive cationic agents*. In: *Coloration Technology,* 2004, vol. 120, issue 4, pp. 195–200

[4] Salimpour Abkenar, S., Malek, R., Mazaheri, F., *Salt-free dyeing isotherms of cotton fabric grafted with PPI dendrimers*. In: *Cellulose,* 2015, vol. 22, issue 1, pp. 897–910

[5] Rym, M., Farouk, M., Bechir, E. M., *Dyeing properties of cationized and non-cationized cotton fabrics dyed with Vitis vinifera L. leaves extract*. In: *The Journal of The Textile Institute,* 2015, In Press, DOI: 10.1080/00405000.2015.1046289

[6] Kamel, M., Kamel, M. M., Youssef, B. M., Shokry, G. M., *Dyeing of cationised cotton with acid dyes*. In: *Journal of the Society of Dyers and Colourists,* 1998, vol. 114, issue 3, pp. 101–104

[7] Patiño, A., Canal, C., Rodríguez, C., Caballero, G., Navarro, A., Canal, J., *Surface and bulk cotton fibre modifications: plasma and cationization. Influence on dyeing with reactive dye*. In: *Cellulose,* 2011, vol. 18, issue 4, pp. 1073–1083

[8] Montazer, M., Malek, R., Rahimi, A., *Salt free reactive dyeing of cationized cotton*. In: *Fibers and Polymers,* 2007, vol. 8, issue 6, pp. 608–612

[9] Haddar, W., Ben Ticha, M., Guesmi, A., Khoffi, F., Durand, B., *A novel approach for a natural dyeing process of cotton fabric with Hibiscus mutabilis (Gulzuba): process development and optimization using statistical analysis*. In: *Journal of Cleaner Production,* 2014, vol. 68, issue, pp. 114–120

[10] Haddar, W., Elksibi, I., Meksi, N., Mhenni, M. F., *Valorization of the leaves of fennel (Foeniculum vulgare) as natural dyes fixed on modified cotton: A dyeing process optimization based on a response surface methodology*. In: *Industrial Crops and Products,* 2014, vol. 52, issue 0, pp. 588–596

[11] Bafrooei, F. K., Malek, R. M. A., Mazaheri, F., *The effect of dendrimer on cotton dyeability with direct dyes*. In: *Chemical Industry and Chemical Engineering Quarterly,* 2014, vol. 20, issue 3, p. 379−385

[12] Burkinshaw, S. M., Mignanelli, M., Froehling, P. E., Bide, M. J., *The use of dendrimers to modify the dyeing behaviour of reactive dyes on cotton*. In: *Dyes and Pigments,* 2000, vol. 47, issue 3, pp. 259–267

[13] Zhang, F., Chen, Y., Lin, H., Lu, Y., *Synthesis of an amino-terminated hyperbranched polymer and its application in reactive dyeing on cotton as a salt-free dyeing auxiliary*. In: *Coloration Technology,* 2007, vol. 123, issue 6, pp. 351–357

[14] Jabli, M., Baouab, M. H. V., Roudesli, M. S., Bartegi, A., *Adsorption of acid dyes from aqueous solution on a chitosan-cotton composite material prepared by a New Pad-dry Process*. In: *Journal of Engineered Fibers and Fabrics,* 2011, vol. 6, issue 3, pp. 1–12

[15] Kaliyamoorthi, K., Thangavelu, R., *Union dyeing of cotton/nylon blended fabric by plasma-nano chitosan treatment*. In: *Fashion and Textiles,* 2015, vol. 2, issue 1, pp. 1–10

[16] Haji, A., *Eco-friendly dyeing and antibacterial treatment of cotton*. In: *Cellulose Chemistry and Technology,* 2013, vol. 47, issue 3-4, pp. 303–308

[17] Karahan, H. A., Özdo011Fan, E., Demir, A., Ayhan, H., Seventekin, N., *Effects of atmospheric plasma treatment on the dyeability of cotton fabrics by acid dyes*. In: *Coloration Technology,* 2008, vol. 124, issue 2, pp. 106–110

[18] Kampeerapappun, P., Phattararittigul, T., Jittrong, S., Kullachod, D., *Effect of chitosan and mordants on dyeability of cotton fabrics with Ruellia tuberosa Linn.* In: *Chiang Mai Journal of Science,* 2010, vol. 38, issue 1, pp. 95–104

[19] Chakraborty, J. N., *Fundamentals and practices in colouration of textiles*, Woodhead Publishing India Pvt. Ltd. New Delhi, India, 2010

Author:

AMINODDIN HAJI[1]
SAYYED SADRODDIN QAVAMNIA[1]
FARHAD KHOSRAVI BIZHAEM[2]

[1]Department of Textile Engineering, Birjand Branch, Islamic Azad University
[2]Department of Art, Birjand Branch, Islamic Azad University
Birjand, IRAN
e-mail: ahaji@iaubir.ac.ir, qavamnia@gmail.com, farhadkhosravi121@yahoo.com

Corresponding author:

AMINODDIN HAJI
ahaji@iaubir.ac.ir

Dyeing of enzymatically modified polyamide fabrics with natural dyes

M. İBRAHIM BAHTIYARI HÜSEYIN BENLI

REZUMAT – ABSTRACT

Vopsirea țesăturilor din poliamidă modificate enzimatic cu coloranți naturali

Fibrele sintetice au o cerere tot mai ridicată, determinată de creşterea populaţiei la nivel global. Datorită acestui fapt, studiile referitoare la fibrele sintetice au devenit populare. Aceste studii abordează în special modificarea fibrelor sintetice pentru a obține proprietăți asemănătoare fibrelor naturale și pentru a îmbunătăți capacitatea de vopsire a fibrelor. Scopul acestui studiu a fost de a investiga oportunitățile de modificare a fibrelor de poliamidă cu enzime de tip pepsină și tripsină și a capacităţii de vopsire cu surse naturale de vopsire. În prezent, există multe metode diferite de a modifica fibrele de poliamidă, cu toate acestea, modificarea enzimatică a fost examinată în acest studiu. Este binecunoscut faptul că procesele enzimatice sunt, în general, ecologice, ceea ce a determinat ca la finisarea ţesăturilor de poliamidă să se utilizeze în operaţia de vopsire tot surse naturale. Având în vedere aceste argumente, în acest studiu au fost folosite diferite enzime de protează pentru modificarea mostrelor de poliamidă. Țesăturile modificate au fost vopsite cu diferiți coloranți naturali pentru a investiga modificarea capacității de vopsire. În acest scop au fost analizate eficiența vopsirii și valorile CIE L*a*b*. Mai mult, modificarea suprafeței și modificările structurale au fost, de asemenea, investigate cu ajutorul SEM şi FTIR. S-a constatat că enzimele testate nu au afectat semnificativ capacitatea de vopsire a probelor de poliamidă cu surse naturale de vopsire, totuşi aceste surse de vopsire naturale reprezintă o alternativă pentru vopsirea probelor de poliamidă deoarece, cu excepția rezistenței la lumină, celelalte tipuri de rezistență s-au dovedit a fi satisfăcătoare.

Cuvinte-cheie: poliamidă, enzimă, protează, coloranți naturali, eficiența vopsirii

Dyeing of enzymatically modified polyamide fabrics with natural dyes

Synthetic fibers are in increasing demand because of the increasing world population. As a result of this, studies on synthetic fibers have become popular. These studies are especially focused on the modification of synthetic fibers to gain natural fiber like properties and to improve the dyeability of the fibers. The aim of this paper was to investigate the modification opportunities of polyamide fibers with pepsin and trypsin enzymes and the dyeability with natural dye sources. At present there are many different methods to modify the polyamide fibers, however enzymatic modification was examined in this study. As well known, enzymatic processes are generally environmentally friendly so it was planned to complete the finishing of polyamide fabrics by dyeing them via natural dye sources. In the light of these arguments different protease enzymes were used for the modification of polyamide samples in this study. The modified fabrics were dyed with different natural dyes to investigate the change in dyeability. For this aim color efficiencies and CIE L*a*b* color values were analyzed. Moreover, the surface modification and structural changes were also investigated by the help of SEM and FTIR. It was found that the tested enzymes did not significantly affect the dyeability of the polyamide samples with selected natural dye sources however these natural dye sources was found as an alternative for the coloration of polyamide samples and except light fastnesses, the fastnesses of the dyed fabrics were found sufficient.

Keywords: Polyamide, enzyme, protease, natural dyes, color efficiency

INTRODUCTION

Polyamides are polymers which contain recurring amide groups as integral parts of the main polymer chain [1]. The most common synthetic polyamides are polyamide 6 (Nylon 6) and polyamide 66 (Nylon 66). The annual world production of polyamide is 4 million tons [2]. Nylons are fairly resistant to chemical attack. They are attacked by acids, bases, and by reducing and oxidizing agents only under extreme conditions. They are unaffected by biological agents, but at elevated temperatures or in the presence of sunlight they will undergo oxidative degradation with yellowing and loss of strength [3]. Nylon fibers are widely used in apparel such as hosiery, blouses, dresses, foundation garments, lingerie, underwear, raincoats, ski apparel, windbreakers, swimwear, and cycle wear. They have also been used for house furnishings such as bedspreads, carpets, curtains, and upholstery [4]. They should be scoured with mild agitation at a moderate temperature of 50–60 °C to remove any impurities containing certain oils and greases. Nylon is a white fiber as produced by the manufacturer and so seldom requires bleaching [1].

A great disadvantage of some synthetic fibers is their low surface energy. This causes poor wettability and dyeability so different surface modification techniques have been studied [5]. Among these surface modification techniques, enzymatic modification of polyamide fibers has also been studied scientifically. For example, Silva et al. (2007) studied the modification ability of cutinase and protease enzymes. They also tested the effect of mechanical agitation. They reported that protease enzymes as well as cutinase

enzymes have the capacity to modify polyamide fabrics [6]. In another study, the usability of cutinase enzyme was introduced for polyethylene terephthalate and polyamide 6,6 fibers [7]. El-Bendary et al. (2012) studied the enzymatic surface hydrolysis of polyamide fabric by using protease enzymes. Firstly, they isolated different bacillus strains to produce protease enzymes. They then showed that by enzymatic modification of polyamide the hydrophilicity and cationic dye affinity can be improved [8]. The modification of polyamide 6.6 fabrics by a mixture of proteolytic and lipolytic enzymes was also studied and the efficiency of lipase and protease enzymes was also reported [9]. Differently, in this study, we tried to combine the enzymatic modification of polyamide fabrics with natural dyeing. Growing awareness of the organic value of eco-friendly products has increased interest in the use of textiles dyed with eco-friendly natural dyes [10]. In this study, it was planned to introduce an environmentally friendly process for the modification and dyeing of polyamide fabrics. For this aim two different natural dye sources, namely pomegranate peels and walnut barks, were used. Pomegranate is native to Western Asia, and is more commonly grown in Iran, Northeastern Turkey and the region of the South Caspian Sea. It has been cultivated science early antiquity [11]. The major coloring component in pomegranate is tannin and ellagic acid which are extracted from the fresh and dried peels [12]. The walnut is one of the oldest cultivated fruits in the world. It was brought to Europe in the 16th century and to America in the 17th century. Walnut belongs to the Juglandaceae family, juglans variety Juglans regia L. [13]. Extracts of walnut leaves and the dried shells of green walnut can be used for dyeing textiles such as wool, silk, nylon, and polyester and cellulose fibers [14].

EXPERIMENTAL

Materials

In this study, 100% polyamide 6.6 fabrics with a weight of 150 g/m^2 were used for the experiments. For the modification of the polyamide samples trypsin (Mp Biomedicals) from *Porcine Pancreas* and pepsin (Merck) from *Porcine Gastric Mucosa* were used. As natural dye sources *Pomegranate peels and walnut barks* which were cultivated in the Anatolian region were used. The walnuts' fresh green barks and pomegranate peels were collected and dried in the shade, then these barks were ground and used directly in the dyeing of polyamide as a natural dye.

Methods

The polyamide samples were firstly washed with a nonionic washing agent at 60 °C for 30 minutes prior to the enzymatic modification. In this way it was planned to clean the fabrics and prepare them for the application of the enzymes.

Enzymatic Modification: The modification of polyamide samples was managed with the use of two different protease enzymes (trypsin and pepsin) in different concentrations (0-1-3-5%). The duration of the modification was set to 60 or 120 minutes. The details of the modification process are given in figure 1. For the selected samples, the FTIR analysis with Perkin Elmer Spectrum 400 and scanning electron microscopy (SEM) analysis with LEO 440 instrument have been conducted to see the effect of the protease enzymes on polyamide samples. Moreover, the samples modified with the same enzyme for the same duration and the unmodified (blank) one were dyed with natural dye sources in the same bath.

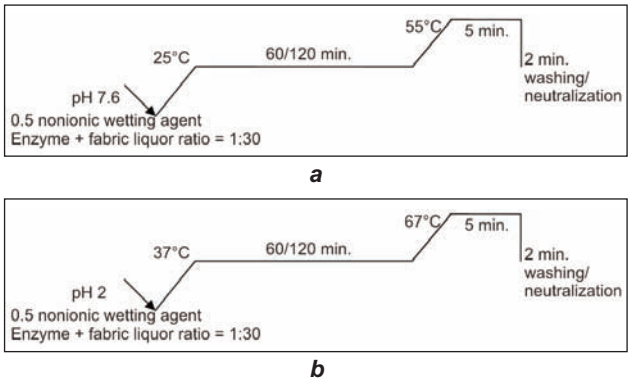

Fig. 1. Enzymatic modification process for: (a) trypsin and (b) pepsin

Natural Dyeing procedure: The modified and unmodified (blank) fabrics were dyed with two different natural dye sources. During the study, dried and ground pomegranate peels and the green barks of walnuts were used as natural dye sources. For the dyeing of polyamides, the concentration of natural dye sources (pomegranate peels and walnut barks) to the fabric was set to 100% (w/w) in the dye bath. Dyeing was managed by using these natural dye source powders without any mordanting process. First, the fabrics modified with the same enzyme for the same duration and the blank sample (treated in the same conditions but without enzymes) were soaked in the same dye bath at *p*H 6 with the dye plants. Then the samples were heated in a dye bath ratio of 1:30 to 100 °C and at this temperature the process was carried out for 60 minutes. After dyeing, the bath has been cooled and the fabrics were rinsed and washed. Subsequently, the natural dyed polyamide samples were dried at room temperature. The dyed fabrics were evaluated in terms of color efficiencies (K/S) and CIE *L*a*b** color space values by using a Konica Minolta 3600d spectrophotometer (D65/10°). The color efficiencies of the modified fabrics were then converted to relative color strength to see the change simply by equation 1.

$$\text{Relative Color Strength (K/S\%)} = \text{K/S}_{\text{modified}} * 100 \,/\, \text{K/S}_{\text{unmodified (blank)}} \quad (1)$$

The dyed samples were also investigated in terms of color differences. For this aim color differences (DE) between the enzymatically modified and blank processed fabrics have been investigated by the use of equation 2.

$$\text{Delta E (DE)} = \left[(\text{Delta L})^2 + (\text{Delta a})^2 + (\text{Delta b})^2\right]^{0,5} \quad (2)$$

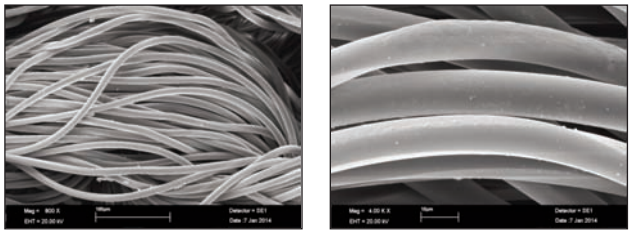

Mag. = 800X
Mag.= 4.00KX

Untreated Fabric

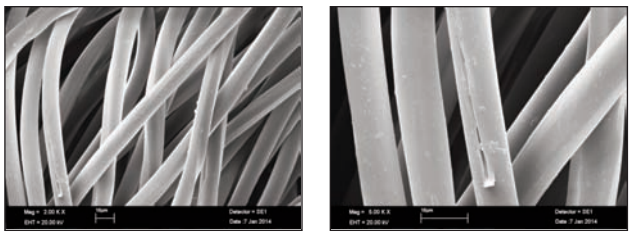

Mag. = 2.00KX
Mag. = 5.00KX

Fabric treated with 5% Pepsin

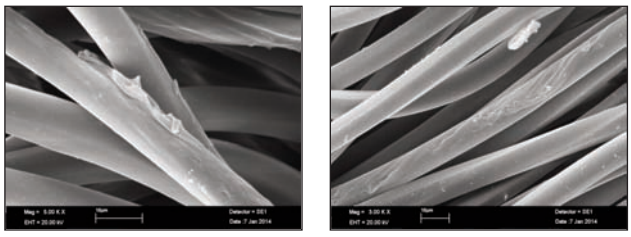

Mag. = 5.00KX
Mag. = 3.00KX

Fabric treated with 5% Trypsin

Fig. 2. SEM photographs of untreated and enzymatically modified fabrics

Moreover, the washing fastness (ISO 105-C10 test condition of Test A (1), 2006) and light fastness (ISO 105-B02, 1994) of the dyed samples were also tested [15, 16].

RESULTS AND DISCUSSION

Effect of Enzymes on Polyamide Fibers

In the first step of the study the effect of enzymes on polyamide fibers was tested. For this purpose the SEM photographs and FTIRs of the modified fabrics were compared with the untreated fabric.

Figure 2 shows the SEM views of the untreated and enzymatically treated fabrics. It was observed that no significant surface modification is present due to the protease enzymes; however, a somewhat peeling abrasion resulted from the enzymatic modification. In addition to this limited surface modification in order to see the chemical structure changes the FTIRs of the same samples were also collected (figure 3).

In general the FTIRs of the tested samples were seen to be similar and no significant differences, except for the band at 1635 cm^{-1}, were observed. On the other hand in terms of the enzymatic modification by proteases it is expected that the peptide bonds will be hydrolyzed and accordingly the amide bands will be changed. It was reported that the presence of the amide carbonyl group (Amide-I band) and N-H bending vibration (Amide-II band) are indicated by a strong band in the region of 1675–1620 cm^{-1} and the band at 1560–1520 cm^{-1} respectively [17]. In this respect it was found that T% at 1635 cm^{-1}, which is thought to be related with Amide-I, was increased after enzymatic modification. It was thought that this change could be related with the hydrolyzing of the peptide bands by the enzymes. As a result of this hydrolysis, free amino groups which are responsible for the dyeability of polyamide, especially with acid dyes, can be come out. To see the effect of this change on the dyeability of the polyamide fibers with natural dyes, the fabrics were dyed with walnut barks

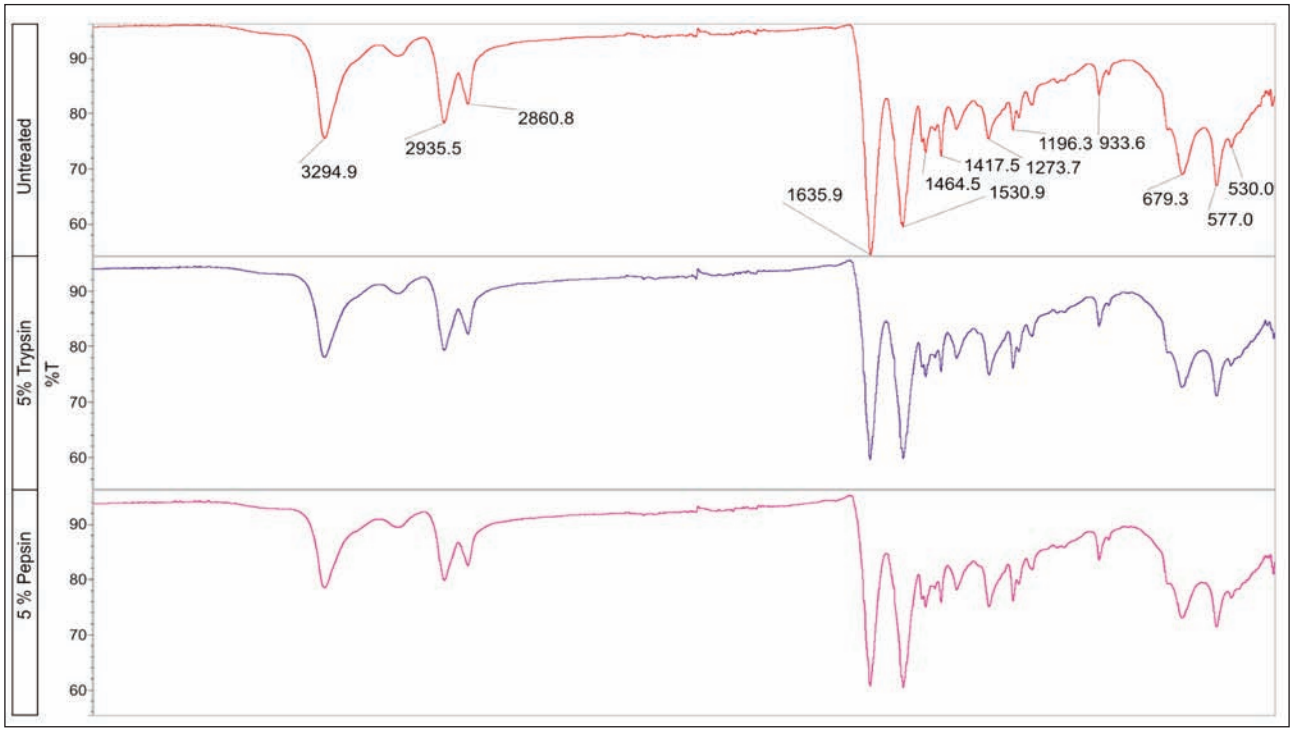

Fig. 3. FTIRs of untreated and enzymatically modified fabrics

Table 1

	PICTURES OF THE FABRICS DYED WITH WALNUT BARKS							
	Pepsin				***Trypsin***			
	0%	1%	3%	5%	0%	1%	3%	5%
60 min	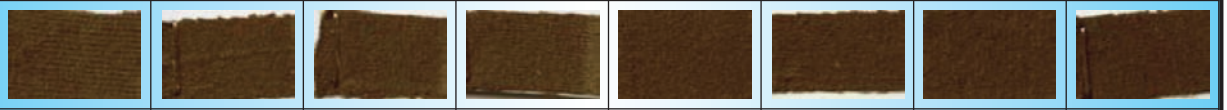							
120 min								

and pomegranate peels. As a result it can be said that enzymes can modify the polyamide fibers somewhat as has been previously reported by different authors.

Effect of enzymes on dyeability of polyamide fabrics with natural dyes

- **Dyeing with walnut barks**

In this part of the study the fabrics modified with different enzymes at different concentrations and durations were dyed directly with dried and ground walnut barks at *p*H 6. It was observed that polyamide samples can be colored with walnut barks and very dark desaturated orange colors and brown shades can be obtained (table 1).

Table 1 also shows the extent to which the color shades were changed depending on the enzymatic process conditions. To see these changes the CIE L*a*b* color values of the samples were also collected and given in table 2.

Table 2

CIE L*a*b* COLOR VALUES OF FABRICS DYED WITH WALNUT BARK								
Pepsin					**Trypsin**			
	60 min					**60 min**		
	0%	**1%**	**3%**	**5%**		**0%**	**1%**	**3%**	**5%**
L*	36.89	36.53	36.33	37.73	**L***	36.19	36.15	35.83	34.93
a*	8.65	8.56	8.61	8.72	**a***	8.24	8.28	8.22	8.07
b*	18.07	17.61	17.87	18.33	**b***	16.85	17.14	16.79	16.53
C*	20.03	19.58	19.84	20.3	**C***	18.76	19.03	18.7	18.4
h°	64.44	64.08	64.28	64.56	**h°**	63.95	64.24	63.91	63.99
DE	0.00	0.59	0.60	0.88	**DE**	0.00	0.30	0.37	1.31
	120 min					**120 min**		
	0%	**1%**	**3%**	**5%**		**0%**	**1%**	**3%**	**5%**
L*	36.95	36.48	36.83	36.76	**L***	36.18	36.32	35.99	34.38
a*	8.86	8.78	8.72	8.57	**a***	8.29	8.32	8.26	8.14
b*	18.33	18.19	18.2	17.72	**b***	16.89	17.01	16.98	16.54
C*	20.36	20.2	20.19	19.68	**C***	18.82	18.94	18.89	18.43
h°	64.21	64.24	64.4	64.19	**h°**	63.87	63.92	64.06	63.8
DE	0.00	0.50	0.23	0.70	**DE**	0.00	0.19	0.21	1.84

Table 2 shows that depending on the enzymatic process conditions the color values can be changed but this change was found to be limited. In other words, the main colors obtained were the same but the shade can be altered by the enzymes. One of the most significant color shade changes was observed in the fabrics modified for 60 minutes with 5% pepsin enzyme. The color difference (Delta E) according to the blank process (60 minutes modified with 0% pepsin enzyme) was found to be 0.88. In modification with trypsin enzymes the most significant color shade difference was observed in the fabrics modified for 120 minutes with 5% trypsin. In that case the color difference according to the blank process (120 minutes modified with 0% trypsin enzyme) was found to be 1.84.

Additions to the color values of the dyed samples, the color efficiencies of the fabrics were also collected. The obtained color efficiencies were converted to the relative color efficiency as explained in equation 1. In other words, each dyed sample was compared with its blank condition (fabric modified in the same conditions but without the use of any enzyme) and in this way the relative color efficiency was obtained.

Figure 4 shows that pepsin based enzymatic modification of polyamide samples did not have a significant effect on the color efficiencies and in some cases the color efficiency of the dyed samples was lower when compared with their blank counterparts. On the other hand, with the use of trypsin enzyme the color efficiencies were increased when compared

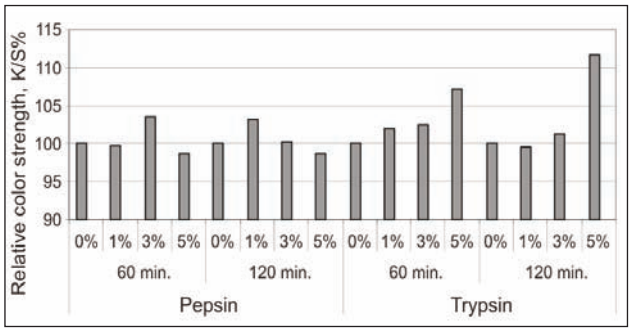

Fig. 4. Relative color strength (K/S%) of the fabrics dyed with walnut barks

Table 3

FASTNESSES OF THE FABRICS DYED WITH WALNUT BARKS

			Washing fastness		Light fastness
			Sta.	Alt.	
Pepsin	60 min	0%	5	5	2/3
		1%	5	5	2/3
		3%	5	5	2/3
		5%	5	5	2/3
	120 min	0%	5	5	2/3
		1%	5	5	2/3
		3%	5	5	2/3
		5%	5	5	2/3
Trypsin	60 min	0%	5	4/5	2/3
		1%	5	4/5	2/3
		3%	5	4/5	2/3
		5%	5	4/5	2/3
	120 min	0%	5	5	2/3
		1%	5	5	2/3
		3%	5	5	2/3
		5%	5	5	2/3

with their blank process. In particular, in the process that used 5% trypsin, the color efficiencies used increased nearly 10% compared to their blank process. For example if the fabric was modified with 5% trypsin for 120 min., the color efficiency was 11.6 % higher than that of the fabric dyed after the treatment with 0% trypsin for 120 minutes.

The other important parameter in the coloration of textile materials is the fastness properties of the colored fabrics. For this reason the fabrics colored with walnut barks were tested in terms of washing and light fastnesses.

The fastnesses of the fabrics dyed with walnut barks showed the usability of walnut barks in the coloration of polyamide samples. Dyeing with walnut barks exhibited excellent washing fastnesses but limited light fastnesses. Meanwhile, it was observed that the enzymatic processes prior to dyeing did not cause any change in the fastnesses of the fabrics.

- **Dyeing with pomegranate peels**

Pomegranate peels were also investigated for the coloration of the polyamide samples. It was observed that coloration of the polyamide samples could be achieved with the use of pomegranate peels. When using pomegranate peels slightly desaturated orange colors and yellow shades were obtained (table 4).

In addition to the dyeability of pomegranate peels, the effect of enzymes on the obtained colors was also tested by the use of CIE L*a*b* values.

It was observed that, depending on the enzymatic application, some differences according to the blank processed fabrics can occur. With the use of pepsin enzyme it was observed that the highest color difference (Delta E) according to the blank processed fabric was found to be 1.38. This difference was observed between the fabrics modified for 120 minutes with 0% pepsin enzyme and those modified for 120 minutes with 3% pepsin enzyme. On the other hand, with the use of trypsin enzyme the obtained colors were generally redder and the yellow shade was slightly reduced (table 5). As a result, the color differences (Delta E) according to the blank processes become dominant. For example, the fabrics modified with 5% trypsin for 60 and 120 minutes presented a 3.93 and 3.35 color difference according to their blank processed fabrics respectively.

The other important parameter for the evaluation of the colors was the color efficiencies after dyeing. It was found that pepsin based enzymatic modification did not cause a significant positive effect when the blank process for each enzymatic process was taken into account. In fact, in some cases, the use of pepsin enzyme also caused a reduction in color efficiencies. Likewise, the use of trypsin enzyme did not cause a significant improvement in the color efficiencies of the

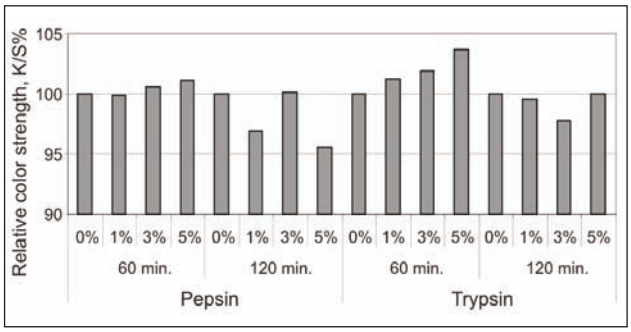

Fig. 5. Relative color strength (K/S%) of the fabrics dyed with pomegranate peels

Table 4

PICTURES OF THE FABRICS DYED WITH POMEGRANATE PEELS

	Pepsin				Trypsin			
	0%	1%	3%	5%	0%	1%	3%	5%
60 min								
120 min	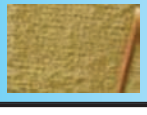							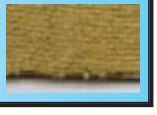

Table 5

CIE L*a*b* COLOR VALUES OF FABRICS DYED WITH POMEGRANATE PEELS

Pepsin					Trypsin				
	60 min					60 min			
	0%	1%	3%	5%		0%	1%	3%	5%
L*	67.00	67.07	67.11	67.69	L*	69.03	68.91	67.02	65.65
a*	2.10	2.01	2.03	1.93	a*	0.68	0.62	1.43	2.29
b*	26.77	26.69	26.90	27.33	b*	30.86	30.86	29.48	29.66
C*	26.85	26.77	26.97	27.39	C*	30.87	30.86	29.51	29.75
h°	85.53	85.70	85.69	85.96	h°	88.75	88.85	87.22	85.60
DE	0.00	0.14	0.18	0.90	DE	0.00	0.13	2.55	3.93
	120 min					120 min			
	0%	1%	3%	5%		0%	1%	3%	5%
L*	68.60	68.06	67.56	68.67	L*	68.24	68.42	66.24	65.54
a*	1.44	1.63	1.59	1.26	a*	0.96	0.90	1.89	2.40
b*	27.86	27.42	26.96	27.27	b*	30.44	30.16	28.56	29.08
C*	27.90	27.47	27.01	27.29	C*	30.46	30.17	28.62	29.18
h°	87.04	86.60	86.62	87.36	h°	88.20	88.29	86.22	85.30
DE	0.00	0.72	1.38	0.62	DE	0.00	0.34	2.90	3.35

Table 6

FASTNESSES OF THE FABRICS DYED WITH POMEGRANATE PEELS

			Washing fastness		Light fastness
			Sta.	Alt.	
Pepsin	60 min	0%	5	5	2
		1%	5	5	2
		3%	5	5	2
		5%	5	5	2
	120 min	0%	5	5	2
		1%	5	5	2
		3%	5	5	2
		5%	5	5	2
Trypsin	60 min	0%	4/5	5	2
		1%	4/5	5	2
		3%	4/5	5	2
		5%	4/5	5	2
	120 min	0%	5	5	2
		1%	5	5	2
		3%	5	5	2
		5%	5	5	2

fabrics. None of the process conditions ensured a 5% or higher improvement in color efficiencies according to the blank processes.

The fastnesses of the fabrics dyed with pomegranate peels were also tested and are shown in table 6. As in the dyeing with walnut barks, after dyeing with pomegranate peels the washing fastnesses of the fabrics were found to be excellent. No significant effect due to the enzymatic process was observed. On the other hand, the light fastnesses of the samples were found to be worse and, as in washing fastnesses, the enzymatic processes did not have any effect on the light fastnesses.

CONCLUSION

Man made fibers have become increasingly popular. This increase in the popularity of these fibers is of course related with the increase in population of the world. These fibers are generally clean, so no detailed pretreatment is necessary; however some modification prior to use can be applied for the improvement of their dyeability, comfort and functionality. There are a lot of studies on this issue. This study focused on the modification of polyamide fibers and their dyeability with natural dye sources.

There are studies on the modification of the polyamide with enzymes but information about dyeing after this modification with natural dyes is inadequate. Two different natural dye sources were selected because of widespread cultivation of them in Turkey. Walnut barks are typically alphanaphthoquinones based and can be considered as disperse dyes [10]. The dyeing principle in extracts from green walnut shells is 5-hydroxy-1,4-naphthoquinone [18]. The other tested natural dye source was the pomegranate peels which can be considered as a kind of direct dyes [10]. The major coloring component is tannin and ellagic acid [12]. It was observed that the selected natural dye sources could be used for the coloration of polyamide samples with low light fastnesses. Therefore in future studies, it will be interesting to determine if alternative natural dye sources can ensure higher light fastnesses. Moreover it was observed that protease enzymes can be used for the modification of polyamide fibers but this modification did not generally or significantly increase the dyeability of the polyamide samples with the selected natural dye sources because of their dyeing mechanism. So for the environmentally finishing of polyamide fabrics different natural dyes which behave like acid dyes can also be tested. Finally, it is hoped that the findings reported in the paper will be useful for the evaluation of alternative enzymatic processes and natural dyes in future studies.

ACKNOWLEDGMENT

This work was supported by the Research Fund of Erciyes University. Project Number: FBA-11-3777.

BIBLIOGRAPHY

[1] Cook, J. G., *Handbook of Textile Fibres: II. Man-Made Fibres,* Merrow Publishing Co. Ltd., 5th edn. repr., Durham England, 1993, pp. 194, 221–223.

[2] El-Ola, S. M. A, Moharam, M. E., Eladwi, M. M., El-Bendary, M. A., *Optimum conditions for polyamide fabric modification by protease enzyme produced by Bacillus sp*. In: Indian Journal of Fibre & Textile Research, 2014, vol. 39, no. 1, pp. 65–71.

[3] Needles, H.L., *Textile fibers, dyes, finishes, and processes*, Dyes Publications, New Jersey, USA, 1986, p. 75.

[4] Yang, H.H., *Polyamide Fibers*. In: Handbook of Fiber Chemistry, Edited by M. Lewin, 3rd ed., CRC Press, Taylor & Francis Group, Boca Raton, USA, 2007, pp. 124–125.

[5] Deshmukh, R. R. and Bhat, N. V., *Pretreatments of Textiles Prior to Dyeing: Plasma Processing*. In: Textile Dyeing, Edited by P.J. Hauser, InTech, Croatia. 2011, p. 33.

[6] Silva, C., Aráujo, R., Casal, M., Gübitz, G. M., Cavaco-Paulo, A., *Influence of mechanical agitation on cutinases and protease activity towards polyamide substrates*. In: Enzyme and Microbial Technology, 2007, vol. 40, no. 1, pp. 1678–1685.

[7] Araújo, R., Silva, C., O'Neill, A., Micaelo, N., Guebitz, G., Soares, C. M., Casal, M., Cavaco-Paulo, A., *Tailoring cutinase activity towards polyethylene terephthalate and polyamide 6,6 fibers*. In: Journal of Biotechnology, 2007, vol. 128, no. 4, pp. 849–857.

[8] El-Bendary, M. A., El-Ola, S. M. A., Moharam, M. E., *Enzymatic surface hydrolysis of polyamide fabric by protease enzyme and its production*. In: Indian Journal of Fibre & Textile Research, 2012, vol. 37, pp. 273–279.

[9] Gashti, M. P., Assefipour, R., Kiumarsi, A., Gashti, M. P., *Enzymatic Surface Hydrolysis of Polyamide 6,6 with Mixtures of Proteolytic and Lipolytic Enzymes*. In: Preparative Biochemistry & Biotechnology, 2013, vol. 43, pp. 798–814.

[10] Samanta, A. K. and Konar, A., *Dyeing of Textiles with Natural Dyes*, In: Natural dyes, edited by E.P. Akçakoca Kumbasar, InTech, Croatia, 2011, pp. 29–56 (ISBN 978-953-307-783-3).

[11] Bruni, S., Guglielmi, V., Pozzi, F., Mercuri, A.M., *Surface-enhanced Raman spectroscopy (SERS) on silver colloids for the identification of ancient textile dyes. Part II: pomegranate and sumac*. In: Journal of Raman Spectroscopy, 2011, vol. 42, pp. 465–473.

[12] Adeel, S., Ali, S., Bhatti, I.A., Zsila, F., *Dyeing of cotton fabric using pomegranate (punica granatum) aqueous extract*. In: Asian Journal of Chemistry, 2009, vol. 21, pp. 3493–3499.

[13] Çağlarırmak, N., *Biochemical and physical properties of some walnut genotypes (Juglans regia L.)*. In: Nahrung/Food, 2003, vol. 47, no. 1, pp. 28–32.

[14] Bechtold, T., *Natural Colorants – Quinoid, Naphthoquinoid and Anthraquinoid Dyes*. In: Hand Book of Natural Colorants, edited by T. Bechtold and R. Mussak, John Wiley and Sons, Ltd., United Kingdom, 2009, p. 157 (ISBN: 978-0-470-51199-2).

[15] ISO 105-C10:2006, Textiles–Tests for color fastness – Part C10: Color fastness to washing with soap or soap and soda, Test Condition: Test A (1), International Organization for Standardization, Geneva, Switzerland.

[16] ISO 105-B02:1994, Textiles–Tests for color fastness, Part B02: Color fastness to artificial light, International Organization for Standardization, Brussels, Belgium.

[17] Patel, H. S. Patel, K. C., *Synthesis and Properties of Novel Polycyanurates Derived from 2-(N-piperidino)-4,6-bis (naphthoxy-2-carbonyl chloride)-s-triazine*. In: International Journal of Polymeric Materials, 2006, vol. 55, no. 12, pp. 1043–1053.

[18] Bechtold, T., *Natural Colorants in Hair Dyeing*, In: Hand Book of Natural Colorants, edited by T. Bechtold and R. Mussak, John Wiley and Sons, Ltd., United Kingdom, 2009, p. 343 (ISBN: 978-0-470-51199-2).

Authors:

M. İbrahim Bahtiyari[1]
Hüseyin Benli[2]

[1]Erciyes University Textile Engineering Department, Kayseri, Turkey
[2]Erciyes University Mustafa Çıkrıkçıoğlu Vocational School, Kayseri, Turkey

e-mail: bahtiyari@erciyes.edu.tr, hbenli@erciyes.edu.tr

Corresponding author:

M. İbrahim Bahtiyari

bahtiyari@erciyes.edu.tr

Preparation and evaluation of the self-cleaning poly (lactic acid) (PLA) film blended with Titanium dioxide (TiO_2) nano particles

CHENGJIAO ZHANG XIN CAI FAMING WANG

REZUMAT – ABSTRACT

Prepararea și evaluarea peliculelor de acid poli (lactic) (PLA) cu funcție de autocurățare în amestec cu nanoparticule de dioxid de titan (TiO_2)

În această lucrare, un material fotocatalitic (nano dioxid de titan) a fost introdus în acid poli (lactic) (PLA) pentru a produce pelicule cu funcție de autocurățare. Prototipurile conținând 0, 5, 10, 15 şi 20 wt% nanomateriale au fost pregătite și corodate cu proteinază K pentru a depune nanoparticulele pe suprafață. Proprietățile termice ale matricei polimerice au fost evaluate prin calorimetrie cu scanare diferențială (DSC) și analiza termogravimetrică (TGA). Funcția de autocurățare a fost evaluată prin decolorarea albastrului de metilen (MB) în stare apoasă, prin intermediul unui spectrofotometru UV-VIS. S-a constatat că nanoparticulele au avut un efect minim asupra proprietății termice a matricii polimerice. Probele cu conținut de 15 wt% nanomaterial ar putea degrada în totalitate albastrul de metilen după iradierea cu UV timp de 24 de ore. Cercetările ar putea furniza recomandări utile în ceea ce privește dezvoltarea de textile cu funcție de autocurățare pe bază de nanoparticule de TiO_2.

Cuvinte-cheie: dioxid de titan (P25), acid poli (lactic) (PLA), suprafață cu funcție de autocurățare, fotocatalitic, corodare enzimatică, fotodegradarea albastrului de metilen

Preparation and evaluation of the self-cleaning poly (lactic acid) (PLA) film blended with Titanium dioxide (TiO_2) nano particles

In this study, a photocatalytic material (the nano-sized titanium dioxide) was introduced into poly (lactic acid) (PLA) to produce films with self-cleaning function. Prototypes containing 0, 5, 10, 15 and 20 wt% nano filler were prepared and then etched with proteinase K to expose the nano particles on the surface. Thermal properties of the polymer matrix were evaluated by the differential scanning calorimetry (DSC) and the thermogravimetric analysis (TGA). The self-cleaning function was assessed by the discoloration of methylene blue (MB) in aqueous condition via a UV-vis spectrophotometer. It was found that the nano particle had a minimal effect on the thermal property of the polymer matrix. The samples containing 15 wt% nano filler could totally degrade the methylene blue after 24h UV irradiation. The research findings might provide useful suggestions on the development of self-cleaning textiles based on TiO_2 nano particles.

Keywords: Titanium dioxide (P25), poly (lactic acid) (PLA), self-cleaning surface, photocatalytic, enzymatic etching, methylene blue photo-degradation

INTRODUCTION

Self-cleaning fabrics have gained extensive attention for its unique properties, having great potential on the hygienic, self-disinfecting and contamination free applications. In the textile field, two approaches could be used to produce self-cleaning surface, namely: hydrophobic and hydrophilic. The former approach is inspired by the Lotus effect, which mimics the microstructure of the surface of lotus leaf to get super hydrophobic surface. The later approach takes advantage of the photocatalytic effect, using photoactive materials such as titanium dioxide (TiO_2) to induce oxidation reactions on the surface, which could decompose organic dirt or contaminants attached on the surface [1]. However, the process used to produce hydrophobic surface has its drawbacks because the fluorocarbons used are harmful to the environment and human beings. Besides, the self-cleaning function disappears gradually over the number of laundering cycles and also the time [1]. Compared with the hydrophobic method, the hydrophilic approach provides a good alternative, as well as the self-cleaning function, it also imparts the textile surface with deodorizing, antimicrobial and UV protection functions.

Over the past few decades, the nano-sized TiO_2 has been widely investigated and used in the textile field as photocatalyst for self-cleaning applications [2, 3]. The mechanism of photoreaction induced by TiO_2 lies in: when TiO_2 surface is irradiated by the ultraviolet light (UV), with energy equal or higher than its band gap (> 3.0 eV), electrons on the surface will be excited and escaped from the valence band to the conduction band, resulting in the formation of negatively charged electrons in the conduction band as well as the positively charged holes in the valence band. The electron-hole pairs on the surface will react with the oxygen or water to form highly active oxygen species. The organic compounds will be finally oxidized by the active species to carbon dioxide

and water [3, 4].The sol-gel method is one of the most common methods to apply nano-sized TiO_2 particles onto textile substances, with the typical dip-pad-dry-cure process [5]. However, textile substances produced by this method tend to delaminate because of the relatively weak adhesion between the nano particles and its support fabrics, which limits the durability of the self-cleaning function [6]. In addition to functional coating, intrinsic self-cleaning textile substances could be produced by adding nano TiO_2 particles into the polymer matrix during the melt blending process [7]. Cho found that PET yarns containing low TiO_2 concentrations (no more than 1100 ppm) had no significant effects on the mechanical properties compared with that of the pure PET yarn [8]. By incorporating the nano-sized photocatalytic TiO_2 into textiles, it is possible to engineer textiles with a multifunctional antibacterial and self-cleaning surface [9]. In textile fields, both commercially available titanium dioxide nano powder (i.e., Degussa P25) and titanium dioxide particles synthesized from a precursor via the sol-gel method were applied to materials such as cellulose , cotton , wool , and synthesized materials [10, 11, 12, 13–15]. The poly (lactic acid) (PLA) is a low cost biodegradable material and the PLA fibres have good mechanical properties. The unique properties of PLA make it to have great potential to replace conventional fibres synthesized from the fossil fuel [16]. However, the PLA is a new emerged material and few studies have investigated the functional performance of the PLA fibre or film blended with the nano-sized TiO_2.

In this study, films with self-cleaning function were prepared by PLA with different concentration of TiO_2 via melt blending method. Enzymatic surface erosion was introduced to remove surface of the PLA polymer to expose nano filler to the environment. The effects of concentration of nano filler and the enzymatic surface erosion on the thermal properties of the films were investigated. The self-cleaning function was evaluated by the decolouration of Methylene blue in aqueous conditions.

METHODOLOGY

Materials

The PLA Polymer 6201D (NatureWorks, Blair, NE; melt flow index: 10–30 g/10min); P25 (the nano-sized Titanium (IV) oxide) (ALDEICH SIGMA, St. Louis, MO; diameter: 21 nm; surface area: 35–65 m^2/g); Proteinase K (P2308, SIGMA ALDEICH, St. Louis, MO) was applied to the enzymatic etching process, the protein content is > 90% and its specific activity is > 30 units/mg. In addition, the 30 mM Tris-HCl buffer was prepared by the following method: 3.634 g (i.e., 0.03 mol) Trizma base (Sigma) was first dissolved in the 800 ml MilliQ water, the *p*H value was adjusted to 8.6 with HCl, and finally 1 L MilliQ water was added.

Preparation of films

Five film batches, with contents of 0, 5, 10, 15, and 20 *wt%* nano filler were prepared via a two-step procedure:

1) preparation of the master batch containing 20 *wt%* nanofiller by mechanical mixing the nano powder with dried PLA pellet;
2) extrusion blending of the master batch and the pure PLA pellet according to the target nanofiller concentration and then extrusion with a 0.4 mm film spinneret.

The master batch was produced by Coperion compounder (ZSK 26K, Stuttgart, Germany), and the feeding of the PLA pellet and the nano filler was performed. The screw speed was 230 r/min. Before compounding, the titanium dioxide was dried at 100°C for 12 h and the PLA was dried at 80 °C for 12 h. After compounding, the master batch was cooled by water and chopped into granule by Scheer (Reduction Engineering GmbH, Korntal-Muenchingen, Germany).

The films were produced by a Micro 15 cc Twin Screw Compounder (DSM Research Netherlands) with a 0.4 mm film spinneret. Prior to production, the master batch and the pure PLA pellet were dried in a vacuum oven (MMM Einrichtungen GmbH, Planegg, Germany) at 80°C for 12 h. The screw speed was 100 r/min, the compounding temperature was controlled by three temperature zones on the compounder. The feeding temperature was 190°C, and the mixing temperature was 230°C. After the extrusion, the thickness of the obtained films was within the range of 100–400 μm. The films were named as Pure PLA, 5% TiO_2, 10% TiO_2, 15% TiO_2 and 20% TiO_2 respectively, according to the nano filler concentration.

Enzymatic surface erosion

During the enzymatic etching process, all experiments followed the method described by MacDonald et al. [17]. Four pieces of films, of the same batch (size: 1 cm × 3 cm) were placed in the conical flask containing 5 ml of the 30 mM Tris-HCl buffer, 1 mg proteinase K and 1 mg sodium azide. The flask was covered with a cotton ball and was put in water bath. The temperature of the water bath was maintained at 37°C and the flasks were shaken slowly at 80 r/min. throughout the whole incubating process. Before and after the incubation, samples were dried at an ambient temperature of 20°C. Different incubating time periods of 2, 4 and 6 h were introduced. The weight loss of per unit surface area was calculated according to eq. 1. Because the thickness of the film was between 100–400 μm, the surface area contributed by the thickness on the total surface area was minimal and thus could be neglected.

$$W_{loss}\,(mg/\mu m^2) = \frac{W_b - W_a}{S_{before}} \qquad (1)$$

where, W_b is the mean weight before erosion; W_a – the mean weight after erosion; S_{before} – the surface area before erosion.

Differential scanning calorimeter (DSC)

The DSC analysis was performed with a DSC Q1000 instrument (TA Instruments, New Castle, USA). Samples were heated to 200°C twice at a heating

rate of 10°C/min. In order to eliminate the previous heat history, the sample was held isothermally at 200°C for 2 min after the first heating process, and then was cooled down to –10°C at a cooling rate of 10°C/min before the second heating cycle. The cooling and second heating processes were used to evaluate the thermal property of the sample.

Thermogravimetric analysis (TGA)

The TGA experiments were performed with a TGA Q500 instrument (TA Instruments, New Castle, USA). Sample was heated to 600°C at a heating rate of 10°C/min, and was held at 600°C for 2 min. The platinum plate was cleaned by the alcohol burner before each test.

Degradation of methylene blue (MB)

The photocatalytic behaviour of the prototypes was determined by the decolouration of the methylene blue (MB) (GFS Chemicals, Powell, OH) in aqueous condition under the irradiation of two 6 W UV tubes (VL-206SLS) with the predominate wavelength of 365 nm. During the test, 2 pieces of films were put in a glass bottle containing 5 ml methylene blue solution and the bottle was then covered and placed under the UV tubes. The distance between the testing sample and UV tubes was 20 cm. The initial concentration of the methylene blue was 2 mg/l. The absorption spectrum was measured before UV irradiation, after 3, 7 and 24 h UV irradiation by a UV-Vis spectrophotometer (LIBRA S60, Cambridge, UK). By measuring changes in the absorption spectra and the absorbance at specific wavelengths, the degradation content of methylene blue could be calculated. The absorption spectra of the methylene blue solution without UV irradiation and the tap water was considered as the reference.

RESULTS AND DISCUSSION

Enzymatic surface erosion

The surface area of each sample film is 600 mm^2. The non-normalized mean weight loss after enzymatic surface erosion is displayed in table 1. The weight loss is caused by the hydrolysed PLA and released TiO_2 particles. After the 2 h enzymatic etching, the pure PLA showed the greatest per unit weight loss of 2.83 $\mu g/mm^2$, which is almost 1.8 $\mu g/mm^2$ higher than that of the 5% TiO_2. The per unit weight loss of 10% TiO_2, 15% TiO_2 and 20% TiO_2 was 1.75 $\mu g/mm^2$, 1.08 $\mu g/mm^2$ and 2.13 $\mu g/mm^2$, respectively. For those samples with 4 h enzymatic treatments, it was observed that the TiO_2-containing samples, compared with the pure PLA, had a more significant increase in the per unit weight loss. The 5% TiO_2, for example, lost 7.79 $\mu g/mm^2$ after 4 h surface erosion. If it is assumed that the 5% TiO_2 had the same weight loss during the first 2 h with that of the group had 2 h treatment, then, it had lost around 6.75 $\mu g/mm^2$ during the second 2 h. Similar trends were also found in other TiO_2-containing samples. This interesting finding might be attributed to the increase in activation of proteinase K or the deviation of pH which facilitated the PLA hydrolysis process. Another possibility was that for the TiO_2-containing samples, compared with the pure PLA, more enzyme molecules could be attached onto the PLA per unit area, and thus a higher etching speed was triggered. Besides, the release of nano TiO_2 may also contributed to the difference in weight loss.

After the 6 h treatment, the 20% TiO_2 lost more weight than the other samples, i.e., 9.79 $\mu g/mm^2$. It should be noticed that for TiO_2-containing samples, the weight loss after the 6 h treatment was almost equal to the sum of weight loss of samples after the 2 and 4 h treatments. For the pure PLA samples, the weight lost 8.13 $\mu g/mm^2$ after the 6 h treatment, which was approximately 1 $\mu g/mm^2$ smaller than that of TiO_2-containing samples. This finding was in line with the study of Fukuda and Tsuji [18], who also found the composite film of PLA/TiO_2 had a higher weight loss, compared to pure PLA, when treated with enzyme. This difference in weight loss might be due to the hydrophilic TiO_2 particle permitting facile permeation of the enzyme into interfaces, resulting in the enzymatic hydrolysis at interfaces as well as on the film surface. Such enzymatic hydrolysis at PLA and additive material interfaces has also been reported by other researcher [19].

Thermal properties

The typical DSC heating scans presented in figure 1, *a* showed that the nano titanium dioxide filler had limited effect on the thermal behaviour of the polymer matrix. For all samples, the introduction of the titanium dioxide did not affect the glass transition temperature (i.e., T_g = 62 °C), and the melting temperature (T_m = 165 °C). This indicated that the nano particles do not affect the mobility of the bulk polymer macromolecular chain. The introduction of TiO_2 in PLA did not result in noticeable change in T_g and T_m was also reported by Luo et al. [20]. However, nano particles affected the cold crystallization temperature.

Table 1

MEAN WEIGHT LOSS AFTER THE ENZYMATIC TREATMENT

Sample	Processing time (h)	Pure PLA	5% TiO_2	10% TiO_2	15% TiO_2	20% TiO_2
Per unit area weight loss ($\mu g/mm^2$)	2	2.83	1.04	1.75	1.08	2.13
	4	3.13	7.79	8.21	8.17	8.67
	6	8.13	9.25	9.54	9.04	9.79

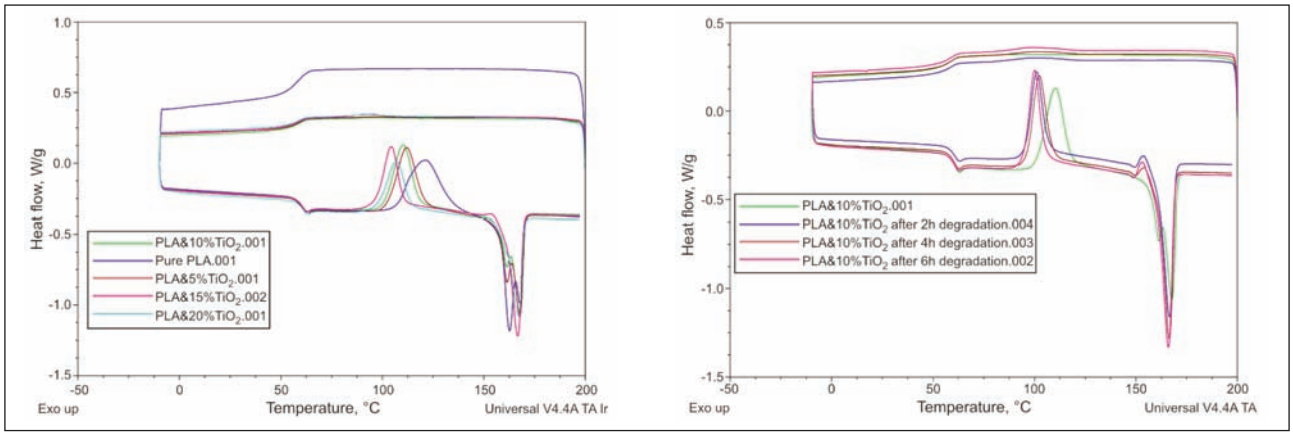

a *b*

Fig. 1. DSC curves of different prototypes:
a – prototypes without enzymatic treatment; *b* – samples with 10% TiO_2 before and after enzymatic treatment

Generally, compared to the pure PLA, the addition of TiO_2 in PLA led to a lower cold crystallization temperature, and the higher the TiO_2 filler, the lower the cold crystallization with the exception of 20% TiO_2. This was contrary to the finding of Luo et al. [20], who found no evident change in cold crystallization temperature of PLA matrix when the content of TiO_2 was 8 wt%. This difference might be caused by the variation in TiO_2 content.

Figure 1, *b* presents the typical effect of enzymatic treatment on the thermal property of the PLA containing 10% TiO_2. The enzymatic surface erosion had no significant impact on T_g and T_m. This was mainly because the enzymatic surface erosion only occurred on the surface and it had minor effect on the bulk property. However, enzymatic surface erosion affected the cold crystallization temperature, which decreased from 110°C to around 100°C. For all samples, it seemed that the processing time affected the cold crystallization temperature randomly.

Figure 2, *a* shows the thermal degradation of different samples in the TGA analysis. Generally, the introduction of the nano filler increased the thermal degradation temperature. The pure PLA started to degrade at about 300°C, approximately 20°C lower than that of the TiO_2-containing samples. It was evident that the added nano particles, instead of accelerating the thermal degradation of the PLA, made the polymer more thermal stabilized. The post-experiment weight percentage of the degraded samples was close to 0, 5, 10, 15 and 20%, which were the remaining TiO_2 particles.

Figure 2, *b* shows the effect of enzymatic treatment on the thermal degradation behaviour. Compared with samples without the enzymatic treatment, the enzymatic treated samples tended to degrade at a lower temperature. This might due to the degradation of the surface PLA during the enzymatic treatment.

Discoloration of methylene blue (MB)

In order to guarantee the maximum photocatalytic activity, samples with the maximum amount of the nano filler exposed onto the film surface (i.e., samples with greatest per unit area weight loss in each batch), were used to assess the degradation performance of methylene blue (MB). In order to examine whether the surface erosion was essential to make the film photocatalytic, the 20% TiO_2 without enzymatic treatment was used as a reference.

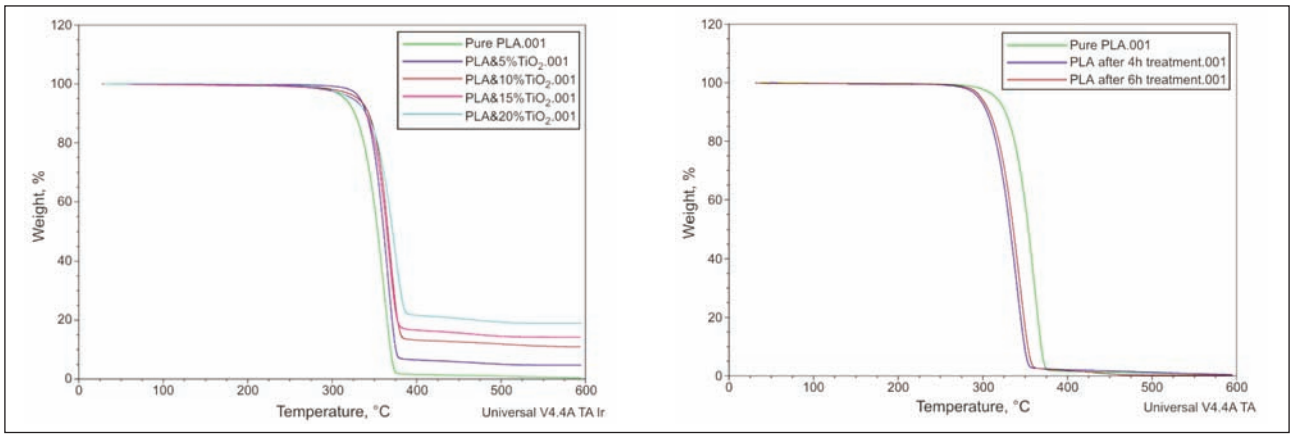

a *b*

Fig. 2. TGA curves of different prototypes:
a – samples without the enzymatic treatment; *b* – the pure PLA before and after the enzymatic treatment

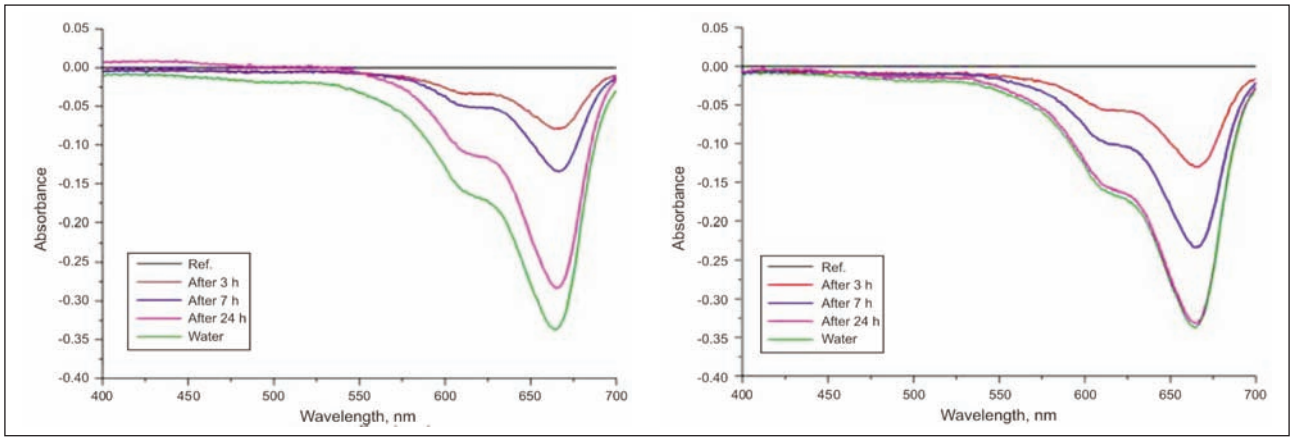

a *b*

Fig. 3. The absorbance character in MB solution:
a – the 5% TiO_2 samples after 6 h enzymatic treatment; *b* – the 10%TiO_2 samples after 6 h enzymatic treatment

Table 2

CHANGES IN THE ABSORBANCE OF SAMPLES AFTER 0, 3, 7 AND 24 H UV IRRADIATION

Irradiation time (h)	5%TiO_2	10%TiO_2	15%TiO_2	20%TiO_2	water
0	0	0	0	0	–0.337
3	–0.079	–0.130	–0.185	–0.110	
7	–0.133	–0.233	–0.264	–0.266	
24	–0.282	–0.331	–0.337	–0.305	
Degradation ratio of MB after 24 h irradiation (%)	83.7	98.2	100.0	90.5	100.0

Figure 3 shows the typical tendency in absorbance peak shift of the surface treated samples. With the increasing UV irradiation time, the absorption curves shifted towards to that of the water. After the 24 h irradiation, the absorbance curves were close to or overlapped with that of the water, which indicated the MB had almost or totally degraded. It was also found that for the 20% TiO_2 without enzymatic treatment, there was no change in the absorption spectra curve after 24 h UV irradiation, which indicated no photo-degradation of the methylene blue occurred. Hence it could be concluded that the enzymatic surface erosion was essential to make the sample photocatalytic.

During the experiment, it was found that all samples displayed significantly absorption changes at a wavelength of about 664 nm. Hence, the methylene blue solution had the maximum absorption at this wavelength. This was in good agreement with previous studies [21, 22]. Therefore, such a wavelength may be used as a sign to judge the MB concentration level. By measuring the absorbance changes at 664nm after UV irradiation and comparing that with the value of water, it is possible to quantitatively evaluate the degradation ratio of the methylene blue. It can be seen from table 2 that all samples had a degradation of over 84% MB after the 24 h UV irradiation. Among all samples, the 15% TiO_2 showed the same absorbance with that of the water, i.e., the methylene blue has totally degraded during the 24 h period, followed by the 10% TiO_2 with 98% methylene blue degradation. For the 20% TiO_2, the decrease in the discoloration performance may be an indication of unevenly dispersion of the nano filler in the polymer matrix. The registered decrement may also due to the aggregation of the inorganic nano filler occurred at such a high percentage of TiO_2 particles.

CONCLUSIONS

This study has demonstrated that it was possible to produce the photocatalytic film based on the nano-sized titanium dioxide and the poly (lactic acid) (PLA) via blending method. The enzymatic surface erosion was essential to make the product photocatalytic, and the proteinase K was capable of removing the surface PLA to expose the nano filler. The introduction of the nano filler and surface erosion process had minor effect on the thermal behaviour of the polymer matrix. All samples showed more than 84% degradation of MB after 24 h UV irradiation, and the film containing 15 wt% nano filler proved properties of oxygen and argon RF plasma-activated polyester fabrics loaded with TiO_2 nanoparticles. However, the dispersion of the nano filler in the polymer matrix was not addressed in this study. It is necessary to investigate this in further studies to find the most suitable approach to combine textile substances with nano TiO_2 particles.

Acknowledgements

The authors would like to express their appreciation for the support from the Swedish School of Textiles, University of Borås and the work was financially supported by 'The Open Foundation of Key Laboratory of Advanced Textile Materials and Manufacturing Technology (Zhejiang Sci-Tech University), Ministry of Education' (Project No: 2014002).

BIBLIOGRAPHY

[1] Tung W.S., Daoud W.A. *Photocatalytic self-cleaning keratins: A feasibility study*, In: ACTA Biomaterialia, 2009, vol. 5, no. 1, pp. 50–56
[2] Mejía M.I., Marín J.M., Restrepo G., Pulgarín C., Kiwi J. *Photocatalytic evaluation of TiO_2/nylon totally degraded the MB.* The research findings may provide useful suggestions on the preparation and optimization of self-cleaning textiles based on TiO_2 nano particles. However, the dispersion of the nano filler in the polymer matrix was not addressed in this study. It is necessary to investigate this in further studies to find the most suitable approach to combine textile substances with nano TiO_2 particles.
[3] Daoud W. *Self-clean only*, In: Materials World, 2008, vol. 16, no. 12, pp. 42–44
[4] Dastjerdi R., Montazer M. *A review on the application of inorganic nano-structured materials in the modification of textiles: Focus on anti-microbial properties*, In: Colloids and Surfaces B: Biointerfaces, 2010, vol. 79, no. 1, pp. 5–18
[5] Yuranova T., Laub D., Kiwi J. *Synthesis, activity and characterization of textiles showing self-cleaning activity under day-light irradiation*, In: Catalysis Today, 2007, vol. 122, issue 1–2, pp. 109–117
[6] Chen X., Mao S.S. *Titanium Dioxide Nanomaterials: Synthesis, Properties, Modifications, and Applications*, In: Chemical Reviews, 2007, vol. 107, no.7, pp. 2891–2959
[7] Daoud W.A., Xin J.H. *Low Temperature Sol-Gel Processed PhotocatalyticTitania Coating*, In: Journal of Sol-Gel Science and Technology, 2004, vol. 29, issue 1, pp. 25–29
[8] Böttcher H., Mahltig B., Sarsour J., Stegmaier T. *Qualitative investigations of the photocatalytic dye destruction by TiO_2-coated polyester fabrics*, In: Journal of Sol-Gel Science and Technology, 2010, vol. 55, issue 2, pp. 177–185
[9] Hao L., Konagaya S., Yamada T., Tada K., Takemasa J., Katsuya I. *Dispersion of Nano TiO_2 in Ethylene Glycol and Poly(ethylene terephthalate)*, In: Composite. Interfaces, 2010, vol. 17, issue 5-7, pp. 559–570
[10] Cho D.H. *Experimental Study on Dyeing Technical PET Yarns Having Different TiO_2 Contents*, In: Fibers and Polymers, 2004, vol. 5, issue 4, pp. 321–326
[11] Hashimoto K., Irie H., Fujishiha A. *TiO_2 Photocatalysis: A Historical Overview and Future Prospects*, In: Japanese Journal of Applied Physics, Part 1, 2005, vol. 44, no. 12, pp. 8269–8285
[12] Moafi H.F., Shojaie A.F., Zanjanchi M.A. *Flame-retardancy and photocatalytic properties of cellulosic fabric coated by nano-sized titanium dioxide*, In: Journal of Thermal Analysis and Calorimetry, 2011, vol.104, issue 2, pp. 717–724
[13] Mihailović D., Šaponjić Z., Molina R., Puač N., Jovančić P., Nedeljković J., Radetić M. *Imsystems prepared at different impregnation times*, In: Catalysis Today, 2011, vol. 161, issue 1, pp. 15–22
[14] Karbownik I., Kowalczyk D., Malinowska G., Paruch B. *Antibacterial Properties of Polyester Fibres' Materials with Titanium Dioxide Deposited on Their Surface*, In: Acta Physica Polonica A, 2009, vol. 116, pp. 169–171
[15] Bozzi A., Yuranova T., Kiwi J. *Self-cleaning of wool-polyamide and polyester textiles by TiO_2-rutile modification under day-light irradiation at ambient temperature*, In: Journal of Photochemistry A: Chemistry, 2005, vol. 172, issue 1, pp. 27–34
[16] Lee S.H., Song W.S. *Modification of polylactic acid fabric by two lipolytic enzyme hydrolysis*, In: Textile Research Journal, 2013, vol. 83, no. 3, pp. 229–237
[17] MacDonald R.T., McCarthy S.P., Gross R.A. *Enzymatic Degradability of Poly(lactide): Effects of Chain Stereochemistry and Material Crystallinity*, In: Macromolecules, 1996, vol. 29, no. 23, pp. 7356–7361
[18] Fukuda N., Tsuji H. *Physical Properties and Enzymatic Hydrolysis of Poly(L-lactide)–TiO_2 Composites,* In: Journal of Applied Polymer Science, 2005, vol. 96, pp.190–199
[19] Fukuda N., Tsuji H., Ohnishi Y. *Physical properties and enzymatic hydrolysis of poly(L-lactid $CaCO_3$ composites*, In: Polymer Degradation and Stability, 2002, vol. 78, no.1, pp. 119–127
[20] Luo Y., Li W., Wang X., Xu D., Wang Y. Preparation and properties of nanocomposites based on poly(lactic acid) and functionalized TiO_2, In: Acta Materialia, 2009, vol. 57, pp. 3182–3191
[21] Yao J., Wang C. *Decolorization of Methylene Blue with TiO_2 Sol via UV Irradiation Photocatalytic Degradation*, In: International Journal of Photoenergy, 2010, vol. 2010, pp. 1–6
[22] Lak A, Simchi A and Nemati Z A. *Photocatalytic activity of TiO_2-capped ZnO nanoparticles,* In: Journal of Materials Science: Materials in Electronics, 2012, vol. 23, issue 2, pp. 361–369

Authors:

CHENGJIAO ZHANG[1, 2]
XIN CAI[3]
FAMING WANG[1]

[1] Laboratory for Clothing Physiology and Ergonomics (LCPE), the National Engineering Laboratory for Modern Silk, Soochow University, Suzhou 215123, China
[2] The Swedish School of Textiles, University of Borås, Borås 50190, Sweden
[3] Key laboratory of Advanced Textile Material and Manufacturing Technology of Ministry of Education, College of Materials and Textiles, Zhejiang Sci-Tech University, Hangzhou 30018, China

e-mail: chengjiaozhang@gmail.com, 507054163@qq.com, dr.famingwang@gmail.com

Corresponding author:

FAMING WANG
dr.famingwang@gmail.com

Interlaminar shear strength properties of multistitched preform nano composites

KADIR BILISIK HUSEYIN OZDEMIR GAYE YOLACAN KAYA

REZUMAT – ABSTRACT

Proprietățile de rezistență la forfecare interlaminară a nanocompozitelor cu cusături multiple

Au fost studiate proprietățile de rezistență la forfecare interlaminară în direcția urzelii și bătăturii ale nanocompozitelor țesute bidimensionale din E-glass/poliester multistratificate cu cusături multiple. Când conţinutul de nanomaterial din dioxid de siliciu din structura compozitului fără cusătură E-glass/poliester crește, forțele de forfecare interlaminară direcționale specifice ale nanostructurilor fără cusătură cresc. Pe de altă parte, forțele de forfecare interlaminară direcționale specifice ale structurilor fără cusătură au fost mai mici decât cele ale nanostructurilor cu cusături multiple. Toate structurile compozite au înregistrat o scădere a forței de forfecare interlaminară între straturi, în secțiunile transversale. Dar, scăderea forței de forfecare interlaminară în nanostructurile cu cusături multiple nu s-a propagat în zone mai mari. Direcția de coasere, densitatea de coasere, firul de cusut, tipul de cusătură și cantitatea de nanomateriale din structurile compozite au fost identificate ca parametri importanți.

Cuvinte-cheie: țesătură preformată cu multiple cusături, rezistență la forfecare interlaminară urzeală-bătătură, insuficiența forței de forfecare interlaminară, nanocompozit, delaminare

Interlaminar shear strength properties of multistitched preform nano composites

Warp and weft directional interlaminar shear strength properties of the developed two dimensional multistitched multilayer E-glass/polyester woven nano composites were studied. When the nano silica material in the unstitched E-glass/polyester composite structure increased, the directional specific interlaminar shear strengths of the unstitched/nano structures increased. On the other hand, the directional specific interlaminar shear strengths of unstitched structures were lower than those of the multistitched/nano structures. All composite structures had interlaminar shear failure between layers in their cross-sections. But, the interlaminar shear failure in multistitched and multistitched/nano structures did not propagate to the large areas. The stitching direction, stitching density, stitching yarn, stitching type and the amount of nano materials in the composite structures were identified as important parameters.

Keywords: multistitched woven preform, warp-weft interlaminar shear strength, interlaminar shear failure, nano composite, delamination

INTRODUCTION

Textile structural composites have been used in various industrial, ballistic and medical areas due to their high stiffness to weight ratio, delamination free and damage tolerance properties [1]. Stitching in layered two dimensional (2D) woven preform improved the tensile and flexural properties of the composite through the distribution of the stress among the layers by stitching yarn [2]. It was reported that stitching fiber base composites in the out-of-plane direction enhanced the Mode-I and Mode-II interlaminar fracture toughness which was experimentally determined by using double cantilever beam and an end notched flexure test, respectively [3–6]. The delamination crack propagation was suppressed when the 2D stitched woven composites were under repeated impact loading at an energy level close to the delamination threshold. It was also claimed that high linear density stitching yarns offered a better delamination resistance [7]. Another study showed that three dimensional (3D) orthogonal woven composite had the greatest resistance to penetration under low velocity impact and dissipated more total energy than 2D plain woven composites. This is due to the Z-fiber in the structure [8]. Absorbed energy for the dense stitch spacing composite was high compared to the loose stitch spacing composite and the dense stitch composite showed less damage size compared to the loose stitch composite [9–11].

The mechanical properties of carbon fiber/phenolic multi-walled carbon nanotube (MWCNT) composites are better compared to carbon fiber/phenolic composites [12]. In addition, it was reported that the carbon nanotubes enhanced the interface properties of composite structure through a toughening effect, fiber-bridging mechanism and the direct reinforcement of the matrix [13, 14]. Carbon nanotubes (CNT)-modified composites had an increase in glass transition temperature, coefficient of thermal expansion and fracture toughness due to the modification of the interfacial properties and the increased matrix rigidity [15, 16]. It was reported that grafting of CNT onto a carbon fiber surface caused a three dimensional

network around the carbon fibers [17, 18]. The fiber was coated using the CNTS in order to enhance the fiber/matrix interfacial properties. It was claimed that CNTS coated fiber/matrix composite showed the better interfacial shear strength due to tougher and stiffer interfacial regions [19, 20]. Another study was also claimed that 2D woven composite aligned with CNTs to the out-of-plane direction provided improvements on Mode-I interlaminar fracture toughness due to the pull-out of nanotubes which was occurred between fiber and epoxy via bridging [21–23].

It was reported that the silane functionalized MWCNTs in the composites generally enhances their mechanical, thermal and electrical conductivity properties compared to the untreated CNTs composites [24–28]. Another study showed that the flexural and fracture properties of basalt fiber/epoxy silane-treated CNTs composites were improved partly due to the decreased agglomeration and partly interfacial bonding between the CNTs and epoxy resin, and supported the homogeneous load transfer capacity of basalt fibers [29, 30]. It was also stated that the fluorine functionalized carbon nanotubes (f-CNTs) in the fiber reinforced epoxy composite increased the interlaminar shear fracture toughness [31].

Recently, it was shown that the interlaminar shear failure in multistitched and multistitched/nano structures did not propagate to the large areas. The specific interlaminar shear strengths of the unstitched/nano structures increased by increasing the nano silica material [32, 33]. As seen in literature, there is a little study on stitched and nano composite structures. Therefore, the objective of this study was to experimentally understand the interlaminar shear strength properties of the developed 2D multistitched E-glass/polyester nano structures.

EXPERIMENTAL PART

2D unstitched and multistitched woven E-glass/polyester preform and composite

E-glass woven fabric (Cam Elyaf A.S., Turkey) was used to make unstitched and multistitched multilayer woven structures. The fiber (Cam Elyaf Inc., TR), matrix (Crystic 703PA, Scott Bader, UK) and nano material (nano sphere, Sigma-Aldrich, Germany) specifications are presented in table 1. Fabric specifications are presented in table 2. Four types of E-glass preform structures were mainly developed: unstitched (U1-U3), unstitched/nano (N1-N4), multistitched (M1-M12) and multistitched/nano (NM). Figure 1 shows the schematic top views of one directional stitching (a1), two directional stitching (a2), four directional stitching (a3), and schematic cross sectional views of multistitching at 0°–90°, ±45° directions (a4, a5). Figure 2 shows actual multistitched woven E-glass/polyester nano composite structures.

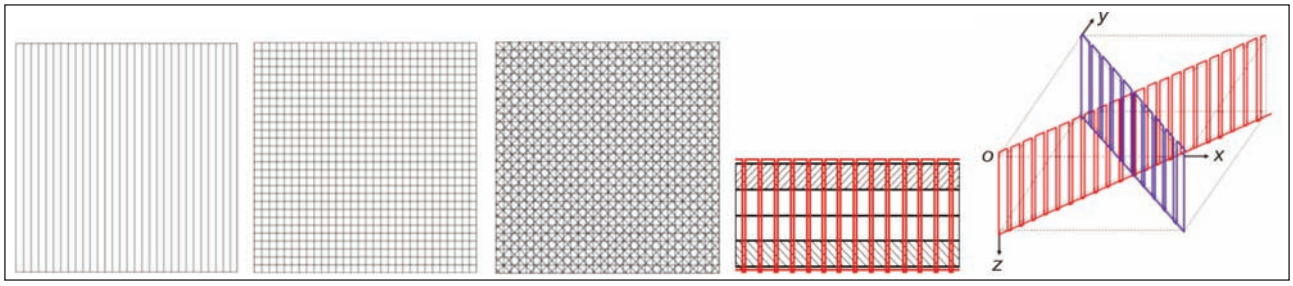

Fig. 1. Schematic views of stitching directions of E-glass preforms:
(a1) top view of one direction; (a2) top view of two direction; (a3) top view of four direction stitching;
(a4, a5) cross-sectional view of multistitching at 0° and 90°, and at ±45° [32]

Table 1

SPECIFICATIONS OF FIBER, MATRIX AND NANO USED FOR MAKING COMPOSITE

	E-glass fiber	Polyester Resin	Nano Silica (SiO_2)	Nano Carbon (C)
Fiber diameter (μ)	17	-	-	-
Density (g/cm^3)	2.56	1.20	2.2-2.6	2.1-2.3
Tensile strength (GPa)	3.5	0.05	0.11	0.2
Tensile modulus (GPa)	76	2.8	73	1000
Elongation at break (%)	4.8	2.1	-	-
Melting point (C°)	841	-	>1600	3550
Measured average particle size (nm)	-	-	30.80±8.6	40.71±7.4
Molecular weight (g/mol)	-	-	60.1	12.01
Purity (%)	-	-	99.5	>99
Surface area (m^2/g)	-	-	140-180	>100

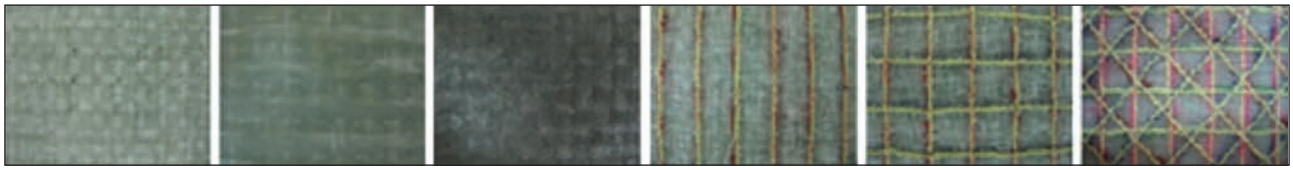

Fig. 2. Multistitched woven E-glass/polyester nano composite structures for short beam test [32]:
(a) unstitched (U1), (b) unstitched/nano (N1, N4); (c) multistitched (M10, M11); (d) multistitched/nano (NM)

Table 2

SPECIFICATIONS OF E-GLASS WOVEN FABRIC USED FOR MAKING COMPOSITE		
		E-glass fabric (Cam Elyaf Inc., TR)
Weave type		Plain
Yarn linear density (tex)	**warp**	2400
	weft	2400
Density (per 10 cm)	**warp**	16
	weft	18
Weight (g/m^2)		800
Crimp (%)	**warp**	1.24
	weft	1.20
Thickness (mm)		1.01

The developed unstitched performs included a layered fabric [(0°/90°)]4 (U1) and oriented layered fabrics as [0°/90°/±45°/±45°/0°/90°] (U2), and [±45°/0°/90°/0°/90°/±45°] (U3). The developed unstitched preforms included a layered fabric [(0°/90°)]4 having 2.5% nano silica (N1), 5% nano silica (N2), 7.5% nano silica (N3) and 5% nano carbon (N4). The developed multistitched preforms were divided into three subgroups. The first was a layered fabric [(0°/90°)]4 one-directionally lightly Nylon 6.6 (M1), Kevlar 129 (M7) and densely Nylon 6.6 (M4), Kevlar 129 (M10) stitched in the warp (0°) direction. The second was a layered fabric [(0°/90°)]4 two-directionally lightly Nylon 6.6 (M2), Kevlar 129 (M8) and densely Nylon 6.6 (M5), Kevlar 129 (M11) stitched in the warp (0°) and weft (90°) directions. The third was a layered fabric [(0°/90°)]4 four-directionally lightly Nylon 6.6 (M3), Kevlar 129 (M9) and densely Nylon 6.6 (M6), Kevlar 129 (M12) stitched in the warp (0°), weft (90°) and ±bias directions in where these preform structures were called “multistiched structure”. Although, the previosly conducted studies on these structures were only one-dimensional stitched or only two-dimensional stitched at 0°/90° or ±45°, the currently developed structure was four-directional stitched at 0°/90° or ±45° all together. In stitching, lock stitching was used and the stitching density was varied at 2 step/cm (light stitching) and 6 step/cm (dense stitching). The distance between the adjacent stitching lines was 1 cm. The stitching yarns were also varied using fully nylon 6.6 (bobbin and needle yarn) and, Kevlar® 129 (DuPont, USA) as the bobbin stitching yarn and nylon 6.6 as the needle stitching yarn. The tensile strength and modulus of Kevlar® and Nylon 6.6 were 3400 and 600 MPa; 99 and 2.46 GPa, respectively. The breaking elongation of Kevlar® 129 and Nylon 6.6 were 3.3 and 41%, respectively. The yarn linear density of Kevlar® 129 and Nylon 6.6 were 110 tex and 44 tex, respectively. The stitching machine was made by Brother Industries Ltd. DB2-B736-3TR, Japan.

2D unstitched and multistitched multilayer woven E-glass/polyester preforms were consolidated to make composites by using vacuum assisted resin transfer molding (VaRTM) technique. Dicyclopentadiene based unsaturated polyester resin (Crystic 703PA, Scott Bader, UK) was used. Methyl ethyl ketone peroxide (MEKP) was used as hardener, 2% by weight of resin to produce neat E-glass/polyester composites. The polyester resin and hardener were mixed homogenously and applied to the preforms under vacuum at 20°C. However, catalyst (Cobalt Naftalat-CoNAP) was also used to produce nano composite structures. Amounts of MEKP and CoNAP by weight of resin and mixing conditions are given in table 3.

Table 3

MIXING CONDITIONS OF NANO MATERIALS IN POLYESTER RESIN FOR VARTM [32, 33]						
Nano materials	**Amount of nano materials (% wt.)**	**Hardener (MEKP) (%)**	**Catalyzer (CoNAP) (%)**	**Mixing conditions**		**Gelling time (min)**
				Mechanical mixing (min, rpm)	**Ultrasonic mixing (min, °C)**	
Silica (SiO_2) (nano sphere)	%2.5	%4	%0.3	2 min. 20.000 rpm	5 min. 25°C	40 min.
	%5					60 min.
	%7.5					90 min.
Carbon (C) (nano sphere)	%5	%4	%0.3	2 min. 20.000 rpm	5 min. 25°C	40 min

Nano materials were mixed first by a mechanical stirrer (IKA-T25 Digital Ultra Turrax, IKA® Werke GmbH & Co. KG) in which mixing was gradually carried out starting from 3000 rpm to 20000 rpm, stayed for 2 min, then from 20000 rpm to 3000 rpm. Later on, mixing was continued in ultrasonic bath, for 5 min at 25°C, to get homogeneous distribution of nano particles in polyester resin. After that, matrix was vacuumed to get rid of the air bubble, and finally hardener and catalyst were added. This matrix was applied to the preforms under vacuum at 20°C. The density of the composite was determined by ASTM D792-91. The composite volume fraction and void content were determined by ASTM D3171-99 and ASTM D2734-91, respectively. Before the short beam test, the stitching area of the composite sample was examined by a scanning electron microscope-SEM (LEO 440® model, UK).

Short beam test

The short beam test of the composite structures was performed on a Shimadzu AG-XD 50 (Japan) tester equipped with Trapezium® software based on ASTM D2344-00. The short beam testing speed was 1.0 mm/min. The test dimensions were considered as 25 (width) × 20 (length) mm. The L/d (support span length/thickness) ratio was 4/1. The short beam load applied to each sample was the warp (0˚) and weft (90º) directions, respectively. The cross section of the structures was examined by an optical microscope (Olympus SZ61, Japan). Based on this examination, the failure modes under the short beam load for each structure were identified.

RESULTS AND DISCUSSION

Density and fiber volume fraction results

The density and fiber volume fraction results of 2D unstitched, unstitiched/nano, multistitched and multistitched/nano multilayer E-glass/polyester composites are presented in table 4. As seen in table 4, the density, total fiber volume fraction and the void content results indicated that partly stitching and partly VaRTM process caused a local misalignment and uneven fiber-matrix-nano placement in the structure as shown in figure 3. The stitching caused a local misalignment and uneven fiber placement during needle piercing to the preform structure. In addition, when the stitching directions in the structure increased, the stitching yarn volume fraction (Vsfw) increased depending on the stitching density and yarn types. However, the total volume fraction (Vtfw) of the structures did not increase proportionally due to the stitching. It can be considered that the stitching parameters in the developed composite structures

Table 4

DENSITY AND FIBER VOLUME FRACTION RESULTS OF VARIOUS DEVELOPED COMPOSITE STRUCTURES [32, 33]

Label	Density (g/cm^3)	Total fiber volume fraction weight (volume) (%)	Fiber volume fraction weight (volume) (%)	Stitching yarn volume fraction weight (volume) (%)	Void content (%)
U1	1.99	78.7 (61.2)	78.6 (61.2)	-	3.34
U2	1.95	78.2 (59.4)	78.2 (59.4)	-	5.11
U3	2.01	78.3 (61.1)	78.1 (61.1)	-	2.60
N1	1.95	74.2 (56.2)	-	-	2.36
N2	1.81	74.7 (52.4)	-	-	10.27
N3	1.87	76.0 (55.3)	-	-	8.73
N4	1.91	77.5 (57.7)	-	-	7.30
M1	2.02	79.8 (62.7)	79.43 (62.4)	0.40 (0.31)	3.08
M2	1.98	79.0 (60.8)	78.2 (60.2)	0.78 (0.60)	3.84
M3	1.97	77.5 (59.6)	76.2 (58.6)	1.30 (1.00)	2.35
M4	2.00	79.8 (62.1)	79.1 (61.6)	0.63 (0.50)	3.62
M5	1.95	77.9 (59.1)	76.7 (58.2)	1.24 (0.94)	3.92
M6	1.95	76.8 (58.3)	74.8 (56.7)	2.05 (1.55)	2.28
M7	1.91	79.3 (59.1)	78.7 (58.5)	0.69 (0.52)	7.44
M8	1.92	78.2 (58.4)	76.9 (57.4)	1.34 (1.00)	5.63
M9	1.89	76.0 (56.0)	73.8 (54.3)	2.18 (1.61)	4.31
M10	1.92	77.7 (58.1)	76.7 (57.3)	1.09 (0.81)	5.29
M11	1.89	75.4 (55.3)	73.3 (53.8)	2.05 (1.51)	4.26
M12	1.87	77.3 (56.4)	73.9 (53.9)	3.46 (2.53)	5.30
NM	1.82	68.9 (48.3)	65.8 (47.2)	3.08 (1.02)	2.65

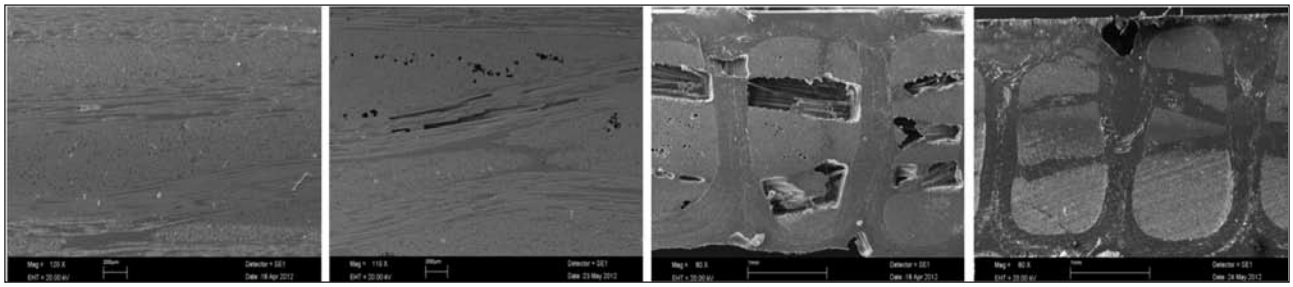

a b c d

Fig. 3. SEM photos of 2D woven E-glass/polyester composite structures at 0°(warp direction): (a) unstitched structure (U1); (b) unstitched/nano structure (N2); (c) multistitched structure (M12); (d) multistitched/nano structure (NM)

were stitching direction, stitching density and stitching yarn type.

Short beam results

Figure 4 shows the short beam strength and the specific short beam strength of 2D woven E-glass/polyester unstitched, unstitched/nano, multistitched/nano composite structures. Figure 5 shows the short beam strength and the specific short beam strength of 2D woven E-glass/polyester multistitched composite structures. As seen in figure 4, the warp and weft directional short beam strengths of the 2D unstitched (U1-U3) woven E-glass/polyester composite structures varied from 23.60 to 17.47 MPa and from 20.51 to 15.67 MPa, respectively. The warp and weft directional short beam strengths of the 2D unstitched/nano (N1-N4) woven E-glass/polyester composite structures varied from 23.05 to 16.94 MPa and from 20.05 to 15.59 MPa, respectively. The warp and weft directional short beam strengths of the 2D multistitched/nano (NM) woven E-glass/polyester composite structure was 23.21 MPa and 19.54 MPa, respectively. It was found that the specific short beam strengths of all unstitched, unstitched/nano and multistitched/nano structures were proportional to their warp and weft directional short beam strengths. The warp and weft directional specific short beam strengths of unstitched structures (U1-U3) were lower than those of the multistitched/nano structures (NM) but they were higher than those of unstitched/nano (N1-N4) except N3. In addition, the short beam strength of U1 was higher than those of U2 and U3. When the nano silica material in the unstitched E-glass/polyester composite structure increased from 2.5 wt. % to 7.5 wt. %, the warp and weft directional specific short beam strengths of the N1-N3 structures increased. Also, it was found that there was a slight difference between the warp and weft directional specific short beam strengths. Generally, the warp directional specific short beam strengths of the composite structures were higher than those of the weft.

As seen in figure 5, the warp and weft directional short beam strengths of the 2D multistitched (M1-M12) woven E-glass/polyester composite structures varied from 19.91 to 17.16 MPa and from 20.79 to 14.87 MPa, respectively. It was found that the specific short beam strengths of all multistitched structures were proportional to their warp and weft directional short beam strengths. In low modulus (stitching yarn Nylon 6.6) lightly and densely stitched structures, the warp and weft directional short beam strengths of the

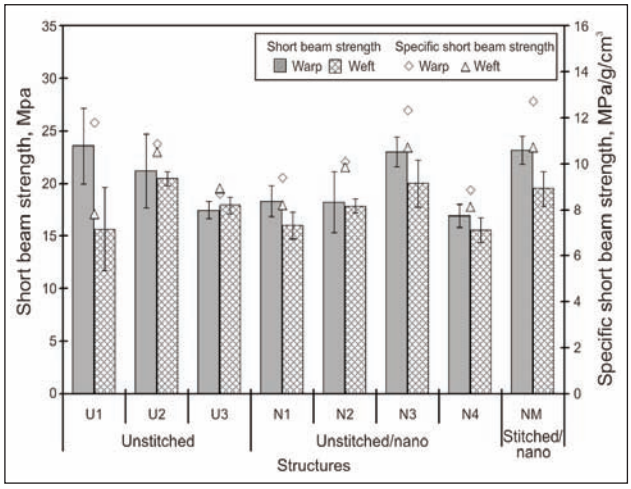

Fig. 4. Short beam strength and specific short beam strength of 2D woven E-glass/polyester unstitched, unstitched/nano and multistitched/nano composite structures

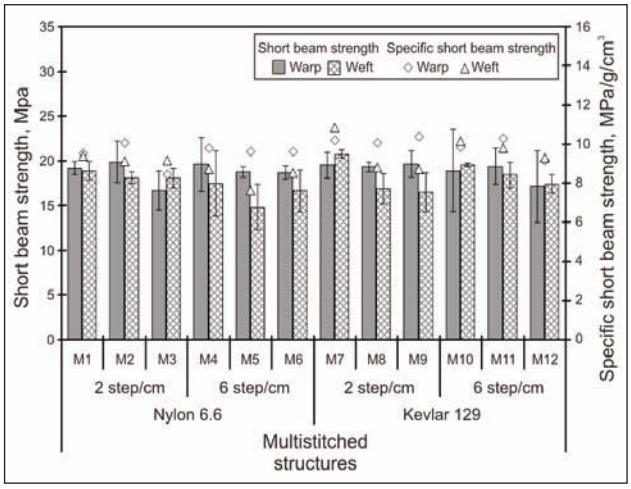

Fig. 5. Short beam strength and specific short beam strength of 2D woven E-glass/polyester multistitched composite structures

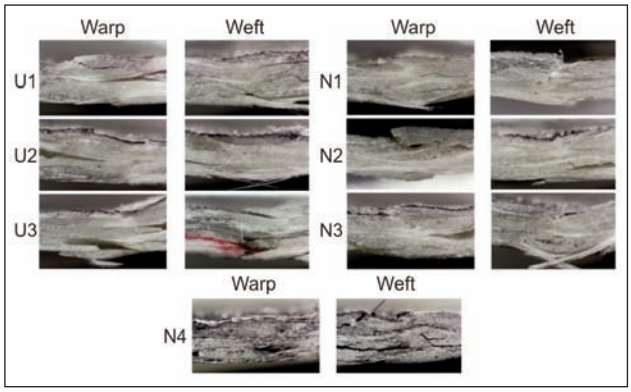

Fig. 6. Cross sectional (microscopic photos at ×6.7 magnification) views of unstitched and unstitched/nano 2D E-glass/polyester woven composites after short beam strength test at warp and weft directions

M4-M6 were slightly higher than those of the M1-M3. In high modulus (stitching yarn Kevlar® 129) lightly and densely stitched structures, the warp and weft directional short beam strengths of the M7-M9 were almost the same with those of the M10-M12. It was found that the warp and weft directional short beam strengths of densely stitched structures (M4-M6) were slightly higher than those of the lightly stitched structures (M1-M3). In addition, the warp and weft directional short beam strengths of high modulus (stitching yarn Kevlar® 129) lightly and densely stitched structures were slightly higher than those of the low modulus (stitching yarn Nylon 6.6) lightly and densely stitched structures. When the stitching directions increased, the warp and weft directional short beam strengths of low (stitching yarn Nylon 6.6) and high modulus (stitching yarn Kevlar® 129) lightly and densely stitched structures slightly decreased due to some filament breakages during stitching. Also, it was found that there was a slight difference between warp and weft directional short beam strengths.

Failure results after short beam test

Some of the failure results on various developed 2D woven E-glass/polyester unstitched, unstitched/nano, multistitched and multistitched/nano composite structures after warp and weft directional short beam test were investigated. Figure 6 shows the cross sectional views of unstitched and unstitched/nano 2D E-glass/polyester woven composites after warp and weft directional short beam load was applied. Figure 7 shows the cross sectional views of multi stitched and multistitched/nano 2D E-glass/polyester woven composites after warp and weft directional short beam load were applied. As seen in figure 6, the failures of warp and weft directional 2D unstitched (U1-U3) and unstitched/nano (N1-N4) woven E-glass/polyester composite structures were observed as a form of major matrix breakages, and partial or total fiber breakages on their top and bottom surfaces. The failures of warp and weft directional 2D unstitched/nano silica woven E-glass/polyester composite structures showed more brittle behavior compared to the unstitched structures. In addition, the

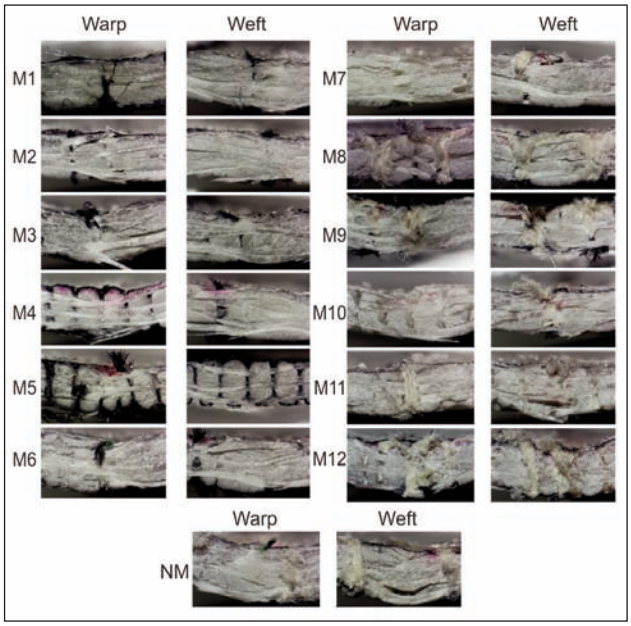

Fig. 7. Cross sectional (microscopic photos at ×6.7 magnification) views of multistitched and multi-stitched/nano 2D E-glass/polyester woven composites after short beam strength test at warp and weft directions

unstitched and unstitched/nano composites had interlaminar shear failure between layers in their cross-sections and the failure was propagated to the large areas. Also, it was observed that there was a flexure failure in the top surface of structure as a form of compression and in the bottom surface as a form of tension. As seen in figure 7, the failures of warp and weft directional 2D multistitched (M1-M12) and multistitched/nano (NM) woven E-glass/polyester composite structures were observed as a form of major matrix breakages, and partial and complete filaments and yarn (tow) breakages on their surfaces. In addition, the multistitched and multistitched/nano composites had interlaminar shear failure between layers in their cross-sections but the failure did not propagate to the large areas. The interlaminar shear failure occurred around the stitching yarn regions at a small area. Also, there was a flexure failure on the top surface of structure as a form of compression and at the bottom surface as a form of tension in where the intra-yarn openings were observed.

CONCLUSIONS

The warp and weft directional specific short beam strengths of unstitched structures were lower than those of the multistitched/nano structures. When the nano silica material in the unstitched E-glass/polyester composite structure increased, the warp and weft directional specific short beam strengths of the unstitched/nano structures increased. When the stitching directions increased, the warp and weft directional short beam strengths of low (stitching yarn Nylon 6.6) and high modulus (stitching yarn Kevlar® 129) lightly and densely multistitched structures slightly decreased due to stitching. In addition, the warp and weft directional short beam strengths of high modulus (stitching yarn Kevlar® 129) lightly and

densely multistitched structures were slightly higher than those of the low modulus (stitching yarn Nylon 6.6) lightly and densely multistitched structures. The results indicated that the stitching direction, stitching density, stitching yarn, stitching type and the amount of nano materials in the composite structures were important parameters.

The failures of warp and weft directional two dimensional unstitched, unstitched/nano and multistitched woven E-glass/polyester composite structures were observed as a form of major matrix breakages, and partial or total fiber breakages on their top and bottom surfaces. In addition, all composite structures had interlaminar shear failure between layers in their cross-sections. But, the interlaminar shear failure in multistitched and multistitched/nano structures did not propagate to the large areas.

ACKNOWLEDGEMENTS

This work was partly supported by Erciyes University Scientific Research Unit (EUBAP) under contract number EUBAPFBD-10-3383. The authors would like to thank the Scientific Research Department of Erciyes University for this invaluable support. The authors also would like to thank Erciyes University Technology Research and Application Center (TAUM) for the mechanical testing of the composite materials. In addition, the authors would like to thank Prof. Dr. Mustafa Guden for allowing the use of composite lab facilities in İzmir Institute of Technology (IYTE) for this project.

BIBLIOGRAPHY

[1] Bilisik, K., Yilmaz, B. *Multiaxis multilayered non-interlaced/non-Z E-Glass/Polyester preform and analysis of tensile properties of composite structures by statistical model*. In: Textile Research Journal, 2012, vol. 82, issue 4, p. 336

[2] Kang, T.J., Lee, S.H. *Effect of stitching on the mechanical and impact properties of woven laminate composite*. In: Journal of Composite Materials, 1994, vol. 28, issue 16, p. 1574

[3] Dransfield, K.A., Jain, L.K., Mai, Y.W. *On the effects of stitching in CFRPS-I: Mode I delamination toughness*, In: Composites Science and Technology, 1998, vol. 58, issue 6, p. 815

[4] Rosselli, F., Santare, M.H. *Comparison of the short beam shear (SBS) and interlaminar shear device (ISD) tests*, In: Composite Part A: Applied Science and Manufacturing, 1997, vol. 28A, issue 6, p. 587

[5] Li, M., Matsuyama, R., Sakai, M. *Interlaminar shear strength of C/C-composites: the dependence on test methods,* In: Carbon, 1999, vol. 37, issue 11, p. 1749

[6] Pahr, D.H., Rammerstorfer, F.G., Rosenkranz, P., Humer, K., Weber, H.W. *A study of short-beam-shear and double-lap-shear specimens of glass fabric/epoxy composites,* In: Composite Part B, 2002, vol. 33, issue 1, p. 125

[7] Wu, E., Wang, J. *Behavior of stitched laminates under in-plane tensile and transverse impact loading*, In: Journal of Composite Materials, 1995, vol. 29, issue 17, p. 2254

[8] Baucom, J.N., Zikry, M.A. *Low-velocity impact damage progression in woven E-glass composite systems*, In: Composites Part A: Applied Science and Manufacturing, 2005, vol. 36, issue 5, p. 658

[9] Hosur, M.V., Karim, M.R., Jeelani, S. *Studies on stitched woven S2 glass/epoxy laminates under low velocity and ballistic impact loading*, In: Journal of Reinforced Plastics and Composites, 2004, vol. 23, issue 12, p. 1313

[10] Hosur, M.V., Abraham, A., Jeelani, S., Vaidya, U.K. *Studies on the influence of through-the-thickness reinforcement on low velocity and high strain rate response of woven S2-glass/ vinyl ester composites*, In: Journal of Composite Materials, 2001, vol. 35, issue 12, p. 1111

[11] Wu, E., Liau, J. *Impact of unstitched and stitched laminates by line loading*, In: Journal of Composite Materials, 1994, vol. 28, issue 17, p. 1640

[12] Yeh MK, Tai NH, Lin YJ., *Mechanical properties of phenolic-based nanocomposites reinforced by multi-walled carbon nanotubes and carbon fibers*, In: Composite Part A: Applied Science and Manufacturing, 2008, vol. 39, issue 4, p. 677

[13] Garcia, E.J., Wardle, B.L., Hart, A.J. Joining prepreg composite interfaces with aligned carbon nanotubes, In: Composite Part A: Applied Science and Manufacturing, 2008, vol. 39, issue 6, p. 1065

[14] Zhu, J., Imam, A., Crane, R., Lozano, K., Khabashesku, V.N., Barrera, E.V. *Processing a glass fiber reinforced vinyl ester composite with nanotube enhancement of interlaminar shear strength*, In: Composite Science and Technology, 2007, vol. 67, issue (7-8), p. 1509

[15] Warrier, A., Godara, A., Rochez, O., Mezzo, L., Luizi, F., Gorbatikh, L., Lomov, S.V., VanVuure, A.W, Verpoest, I. *The effect of adding carbon nanotubes to glass/epoxy composites in the fibre sizing and/or the matrix*, In: Composite Part A: Applied Science and Manufacturing, 2010, vol. 41, issue 4, p. 532

[16] Shen, Z., Bateman, S., Wu, D.Y., McMahon, P., DellOlio, M., Gotama, J. *The effects ofcarbon nanotubes on mechanical and thermal properties of woven glass fibre reinforcedpolyamide-6 nanocomposites*, In: Composite Science and Technology, 2009, vol. 69, issue 2, p. 239

[17] Laachachi, A., Vivet, A., Nouet, G., Doudou, B.B., Poilâne, C., Chen, J., Bai, J.B., Ayachi, M. *A chemical method to graft carbon nanotubes onto a carbon fiber*, In: Material Letters, 2008, vol. 62,, issue 3, p. 394

[18] Cebeci, H., Villoria, R.G., Hart, A.J., Wardle, B.L. *Multifunctional properties of high volume fraction aligned carbon nanotube polymer composites with controlled morphology*, In: Composite Science and Technology, 2009, vol. 69, issue 15-16, p. 2649

[19] Godara, A., Gorbatikh, L., Kalinka, G., Warrier, A., Rochez, O., Mezzo, L., Luizi, F., Vuure, A.W., Lomov, S.V., Verpoest, I. *Interfacial shear strength of a glass fiber/epoxy bonding in composites modified with carbon nanotubes,* Composite Science and Technology, 2010, vol. 70, issue 9, p. 1346

[20] Sager, R.J., Klein, P.J., Lagoudas, D.C., Zhang, Q., Liu, J., Dai, L., Baur, J.W. *Effect of carbon nanotubes on the interfacial shear strength of T650 carbon fiber in an epoxy matrix*, In: Composite Science and Technology, 2009, vol. 69, issue 7-8, p. 898

[21] Wicks, S., Villoria, R.G., Wardle, B.L. *Interlaminar and intralaminar reinforcement of composite laminates with aligned carbon nanotubes*, In: Composite Science and Technology, 2010, vol. 70, issue 1, p. 20

[22] Askari, D., Nejhad, M.N.G. *Effects of vertically aligned carbon nanotubes on shear performance of laminated nanocomposite bonded joints*, Science and Technology of Advance Materials, 2012, vol. 13, issue 4, p. 1

[23] Fan, Z., Santare, M.H., Advani, S.G. *Interlaminar shear strength of glass fiber reinforced epoxy composites enhanced with multi-walled carbon nanotubes*, In: Composite Part A: Applied Science and Manufacturing, 2008, vol. 39, issue 3, p. 540

[24] John, N.A., Brown, J.R. *Flexural and interlaminar shear properties of glass–reinforced phenolic composites*, In: Composite Part A: Applied Science and Manufacturing, 1998, vol. 29A, p. 939

[25] Ma, P.C., Kim, J.K., Tang B.Z. *Functionalization of carbon nanotubes using a silane coupling agent*, In: Carbon 2006, vol. 44, p. 3232

[26] Ma, P.C., Kim, J.K., Tang, B.Z. *Effects of silane functionalization on the properties of carbon nanotube/epoxy nanocomposites*, In: Composite Science and Technology, 2007, vol. 67, p. 2965

[27] Shanmugharaj, A.M., Bae, J.H., Lee, K.Y., Noh, W.H., Lee, S.H., Ryu, S.H. *Physical and chemical characteristics of multiwalled carbon nanotubes functionalized with aminosilane and its influence on the properties of natural rubber composites*, In: Composite Science and Technology, 2007, vol. 67, p. 1813

[28] Chandrasekaran, V.C.S., Advani, S.G., Santare, M.H. *Role of processing on interlaminar shear strength enhancement of epoxy/glass fiber/multi-walled carbon nanotube hybrid composites*, In: Carbon, 2010, vol. 48, p. 3692

[29] Kim, M.T., Rhee, K.Y., Park, S.J., Hui, D. *Effects of silane-modified carbon nanotubes on flexural and fracture behaviors of carbon nanotube-modified epoxy/basalt composites*, In: Composite Part B, 2012, vol. 43, p. 2298

[30] Yu, B., Jiang, Z., Tang, X.Z., Yue, C.Y., Yang, J. *Enhanced interphase between epoxy matrix and carbon fiber with carbon nanotube-modified silane coating*, In: Composite Science and Technology, 2014, vol. 99, p. 131

[31] Davis, D.C., Whelan, B.D., *An experimental study of interlaminar shear fracture toughness of a nanotube reinforced composite*, In: Composite Part B, 2011, vol. 42, p. 105

[32] Bilisik, K., Yolacan, G. *Interlaminar shear strength properties of multistitched woven nano composites*, 1st Joint Turkey-Japan Workshop on Polymeric Composite Materials, Sabancı University, Istanbul, Turkey, 12-13 May 2014, p. 1

[33] Bilisik, K., Yolacan, G. *Short beam strength properties of multistitched biaxial woven E-glass/polyester nano composites*, In: Journal of Industrial Textiles, 2015, vol. 45, p. 199.

Authors:

KADIR BILISIK*[1]
HUSEYIN OZDEMIR[2]
GAYE YOLACAN KAYA[3]

[1]Department of Textile Engineering, Faculty of Engineering
Erciyes University
38039 Talas-Kayseri, Turkey

[2]Vocational School of Technical Sciences
Gaziantep University
27310 Sehitkamil-Gaziantep, Turkey

[3]Department of Textile Engineering, Faculty of Engineering and Architecture
Kahramanmaras Sutcu Imam University
46100 Kahramanmaras, Turkey

Corresponding author:

KADİR BİLİŞİK
e-mail: kadirbilisik@gmail.com; kbilisik@erciyes.edu.tr

Study regarding the use of a cotton fiber reinforced composite for obtaining protection helmets

VIRGIL TUDOSE
RADU FRANCISC COTERLICI
DANIELA TUDOSEGE

HORIA GHEORGHIU
STEFAN DAN PASTRAMA

REZUMAT – ABSTRACT

Studiu privind utilizarea unui compozit armat cu fibre de bumbac pentru obținerea căștilor de protecție

Scopul acestei lucrări este de a evalua proprietățile mecanice ale unei rășini poliesterice armate cu fibre de bumbac și de a prezenta o aplicație practică pentru acest material. Au fost efectuate încercări mecanice de încovoiere în trei puncte, în scopul determinării caracteristicilor mecanice ale materialului studiat. Valorile obținute au fost utilizate în analiza cu metoda 3D a elementelor finite. Rezultatele obținute în urma analizei numerice au evidențiat faptul că materialul studiat poate fi utilizat cu succes pentru realizarea căștilor de protecție. Studiul se poate extinde pentru alte tipuri de elemente de protecție utilizate în activități sportive sau industriale.

Cuvinte-cheie: biodegradabil, bumbac, element finit, analiză dinamică, teste mecanice

Study regarding the use of a cotton fiber reinforced composite for obtaining protection helmets

The objectives of this work are to evaluate the mechanical properties of an unsaturated polyesteric resin reinforced with cotton fibers and to present a practical application of this material. Three point bending tests have been performed in order to determine the mechanical characteristics of the studied material. The obtained values were further used in a 3D finite element analysis. The numerical results revealed the fact that the studied material can be successfully used for manufacturing protection helmets. The study may be extended to other types of protection elements used in sports or industrial activities.

Keywords: biodegradable, cotton, finite element, dynamic analysis, mechanical tests

INTRODUCTION

The current trend to use natural fibers as reinforcement material is explained by the fact that they present good mechanical properties compared to fiber glass, have a low density, a low cost and a high spreading degree [1–3]. Also, the natural reinforcement fibers confer to the composite materials with synthetic matrix a biodegradable character, which motivates the concerns in the field.

Cotton represents a type of reinforcement fibers, very often used in engineering. The mechanical strength of a composite increases with the percentage of cotton fibers if they are under the form of fabric [4–5]. Pamuk and Ceken studied the variation of tensile, compression and impact strength, of an epoxy resin reinforced with flax or cotton fibers as knitted preforms and showed that this type of materials have mechanical properties superior to resin [6]. This is explained by the fact that the natural fibers used for reinforcement have mechanical properties much better than the composite matrix [7]. Alomayri et al. studied the influence of the short cotton fiber percentage on the flexural and tensile strength in a composite and established that the optimum value for it is 2.1% [8]. They investigated the impact strength and fracture toughness of the same material with different cotton fiber percentages (3.6% up to 8.3%), examining also the fracture surface of the composite material using scanning electron microscopy, [9]. The authors showed that the higher the cotton fiber percentage, the higher the fracture toughness, due to the unique properties of cotton fibers in withstanding greater bending and fracture forces than the more brittle geopolymer. Wu et al., prepared composite materials having polypropylene matrix reinforced with cotton stalk bast fibers (CSBF) and tested their mechanical properties (flexural strength, tensile strength and impact strength) [10]. Properties of the same composite material were also investigated by Qu et al. [11]. Their results revealed that the incorporation of CSBF decreased the tensile and impact strength, while significantly enhanced the flexural strength, flexural modulus and tensile modulus. The influence of water content in CSBF during the explosion and fiber content on the mechanical properties was also studied, the authors concluding that biocomposites reinforced by fibers with 40 and 50 wt% water contents during the explosion had the best mechanical properties.

The properties of reinforced materials with natural fibers motivate the fact that their practical applications are numerous, from packages to car industry components [12–13]. This work presents a composite material obtained from polyester resin reinforced with cotton fabric with a mass percentage of 35%. Three point bending tests were performed to investigate the mechanical properties. A finite element

calculation model of a protection helmet was further realized, using the mechanical characteristics obtained following the bending tests. The calculation results showed that, from the point of view of the mechanical strength, this material can be used for manufacturing protection helmets, since the maximum dynamic stresses obtained from the numerical analysis are much smaller than the ultimate strength of the material.

Following the study presented herein, a subsequent research direction could involve the study of the influence of this material upon the helmet placed on the head, during the impact. Also, another important aspect is represented by the choice of appropriate interior jacketing (foams or other types of elastic elements). There are several studies in the literature which show the importance of the helmet material regarding its influence over the head during the impact and the effect of various types of internal jacketing [14–17].

The analysis of such composite materials can also be extended for other types of industrial protection elements.

EXPERIMENTAL WORK

Materials and method

For the experimental research, commercial cotton and an unsaturated polyester resin were purchased. The unsaturated polyester resin is a thermoset. Thermosetting polyesters are commonly used in fiber-reinforced plastics, epoxies being the main unsaturated polyester used in the current market for advanced composites resins. Initially, the viscosity of these resins is low; however, thermoset resins undergo chemical reactions that crosslink the polymer chains and thus connect the entire matrix together in a three-dimensional network. This process is called curing. Thermosets, because of their three-dimensional cross-linked structure, tend to have high dimensional stability, high-temperature resistance, and good resistance to solvents. It is usual to refer to unsaturated polyester resins as “polyester resins”, or simply as “polyesters”. On the other hand, saturated resins are thermoplastic. Unlike the curing process of thermosetting resins, the processing of thermoplastics

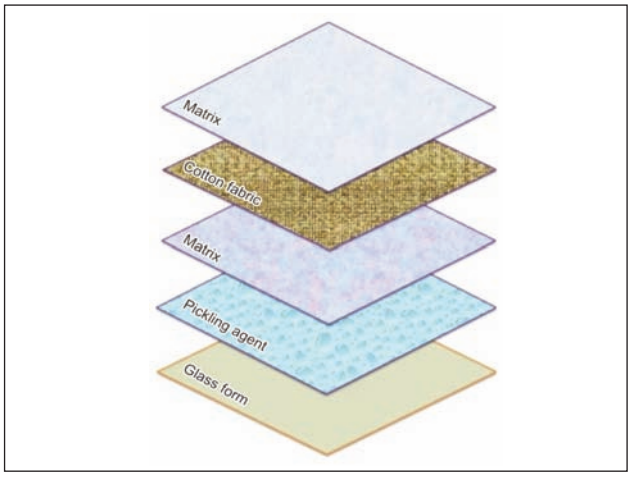

Fig. 1. Hand Lay-up method

is reversible, and, by simply reheating to the process temperature, the resin can be formed into another shape if desired. Thermoplastics, although generally inferior to thermosets in high-temperature strength and chemical stability, are more resistant to cracking and impact damage [18–19]. Due to the better chemical and thermal resistance, an unsaturated resin was chosen as matrix of the studied green composite material.

Figure 1 presents the Hand Lay-up method, applied to obtaining cotton fabric/unsaturated polyester resin composite plate with five layers.

For the composite matrix, Nestrapol 450-66 unsaturated polyester resin was used and, for reinforcement, a cotton fabric with a mass percentage of 35% was considered. By the hand lay-up process, resin was cast alternatively between five layers of cotton fabric, the total thickness being 2.75 mm. The material thus obtained was left seven days for hardening, at a temperature of 20ºC.

Three point bending test results

Five samples for three point bending were manufactured, according to SR EN ISO 14125, and presented in figure 2 [20]. The samples dimensions were: length – 80 mm, width – 15 mm and thickness – 2.5 mm.

The three point bending tests were performed with a LR5K Plus machine from Lloyd Instruments (figure 3)

Fig. 2. Composite samples

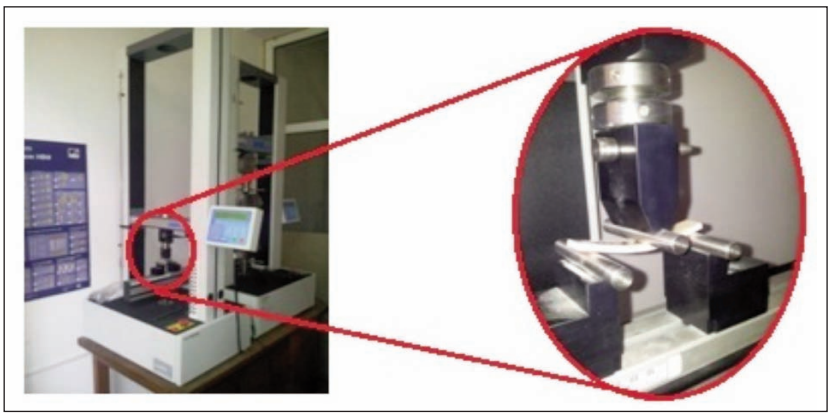

Fig. 3. LR5K Plus machine and three point bending test

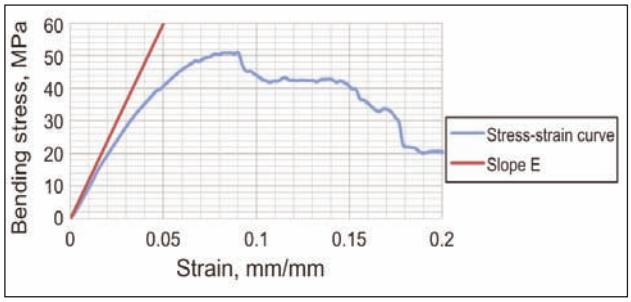

Fig. 4. Stress-strain curve of composite and initial slope of Young's modulus

at a temperature of 20 ºC. The loading rate was 5 mm/min. Figure 4 shows the characteristic curve of material, obtained by the average of the values resulted following the five sample tests and the line tangent to the curve in the origin, whose slope is the initial Young's modulus E. A value of 1200 MPa was obtained for this elastic constant.

We notice that the average tensile strength for this material is about 50 MPa. The failure is sudden because the cotton fabric takes the load after the polyester resin creeping. The percent elongation is about 20%, which is not relevant for this research. If one considers that the material has a linear behavior and Young's modulus is 1200 MPa, the characteristic curve would be represented by the red line in figure 4. We can notice that, for a certain specific deformation, the stress is always higher if the material behavior is considered as linear and thus, the analysis in this case is conservative.

NUMERICAL ANALYSIS

Numerical model

The numerical analysis, performed with the finite element software ANSYS LS-DYNA, simulated the impact on a protection helmet, using a 5 kg spherical body, left to fall free from one meter height, according to the standard EN 397 [21–22]. For the simplification of the numerical model, the helmet material was considered to be isotropic and linear. The obtained results confirm that this hypothesis is reasonable, since the maximum stresses obtained from the finite element analysis is less than 23 MPa, value up to which the differences between the real curve and the linear approximation are small. Thus, an analysis using the real curve is not justified in this case, saving computing time and resources.

The geometry of the protection helmet is shown in figure 5, *a*. The impacting body was modeled as a steel sphere, having a diameter of 107 mm. Figure 5, *b* presents the helmet's dimensional parameters.

Table 1 presents the characteristics of the materials of the two bodies and their dimensions. Figure 6 gives the mesh of the helmet, the imposed boundary conditions (movement constrained on the impact direction) and the mesh of the impactor.

The mesh was built using SHELL 163 elements, for the helmet mesh, and SOLID 164 elements, for the impacting body [21]. The thickness of the SHELL element was 4 mm, equal to the thickness of the material used in the manufacturing of the helmet. The imposed load was an acceleration of 9.81 mm/s^2 for

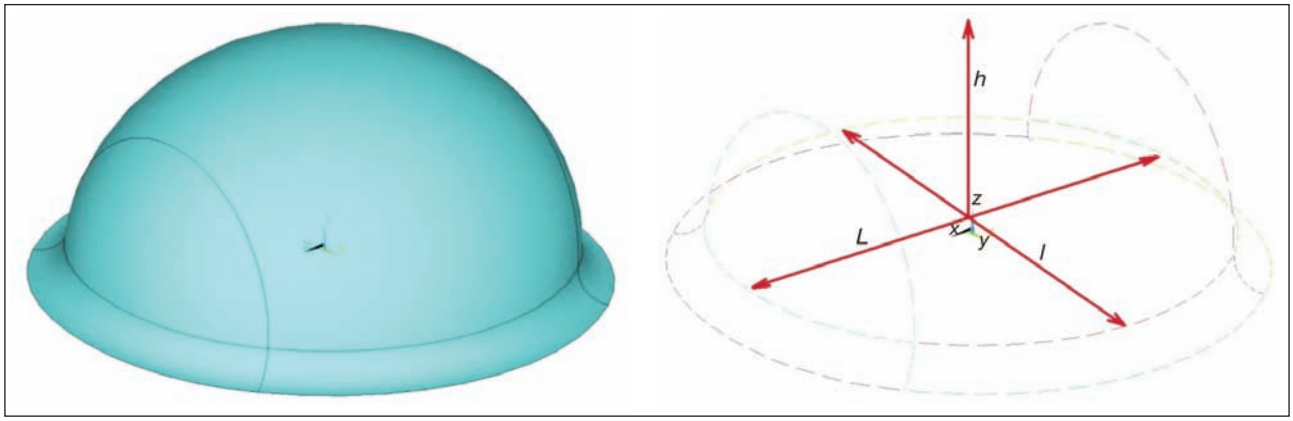

a b

Fig. 5. Geometry (a) and dimensions (b) of helmet

Table 1

Characteristics	Helmet	Sphere
Young's modulus [MPa]	1200	$21 \cdot 10^4$
Poisson ratio	0.28	0.3
Mass density [kg/m^3]	1500	7800
Dimensions [mm]	L = 230 L = 200 h = 110	Diameter = 107

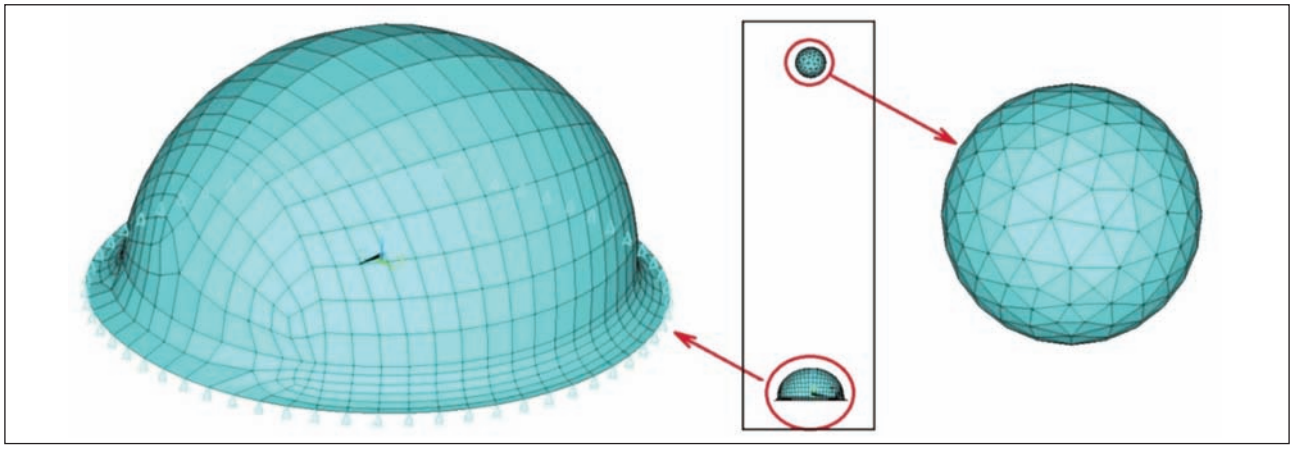

Fig. 6. Mesh structure and constraints of helmet

the sphere. The results were obtained following 50 integration steps.

RESULTS AND DISCUSSIONS

In order to verify the accuracy of the parameters introduced in the numerical calculation, the evolution in time of the impacting body velocity was plotted from the numerical results in figure 7. One can notice that the sphere falls free from a height of one meter in around 0.44 s and reaches, at the moment of impact, a velocity of (–4.32 m/s). After 0.02 s, the velocity decreases to zero (moment when the deformation of the helmet is maximum) and then rebound occurs in 0.02 s with a velocity of 2.2 m/s. Thus, a loss of energy of the impactor occurs, which should be recovered in the residual deformation of the helmet, presented further in this paper. The 4.32 m/s impact velocity obtained from the numerical analysis can be verified using the kinematics equations:

$$t = \sqrt{\frac{2h}{g}} = \sqrt{\frac{2 \times 1}{9.81}} = 0.452 \text{ s};$$

$$v = g \times t = -9.81 \times 0.452 = -4.43 \text{ m/s}.$$

The very small differences between the results (about 2.7%) show that the parameters were correctly

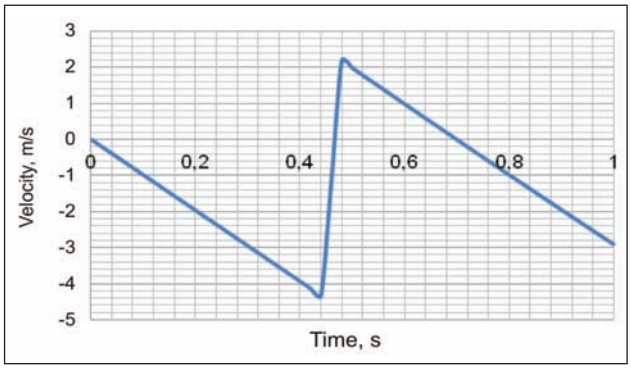

Fig. 7. Rate evolution in time of the impacted body velocity

introduced and can be diminished considerably if the number of integration steps increases.

Figure 8, *a* presents the equivalent von Mises stress at the moment t = 0.46 s, when the maximum stress value is recorded in the structure. This value was obtained in node 1393 (figure 8, *b*). Figure 9 presents the evolution in time of the equivalent von Mises stress in this node. One can notice the maximum of the obtained curve, corresponding to the impact moment and the range within which the stress decreases and is stabilized, corresponding to the

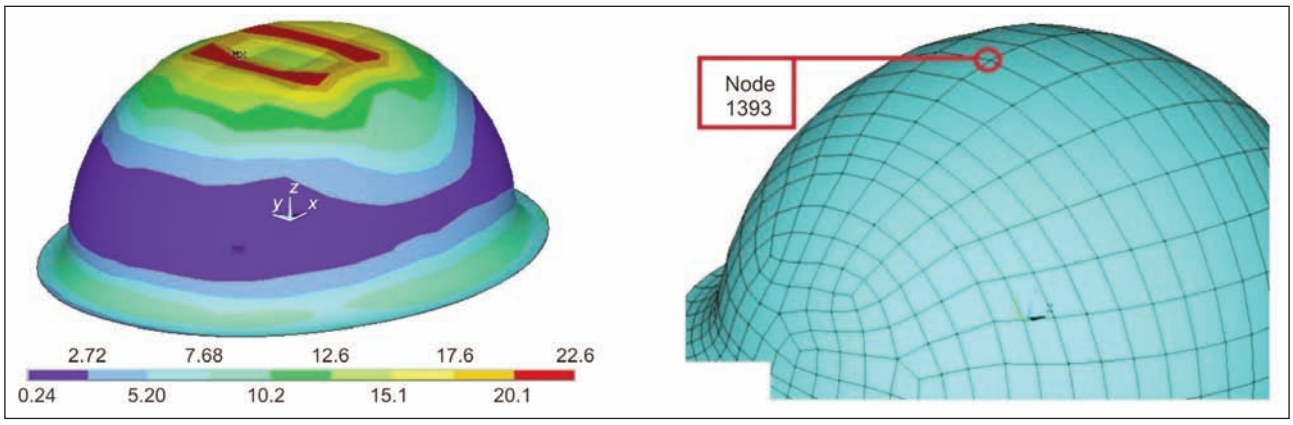

a b

Fig. 8. Von Mises stress field at t = 0.46 s (a) and node number 1393 position (b)

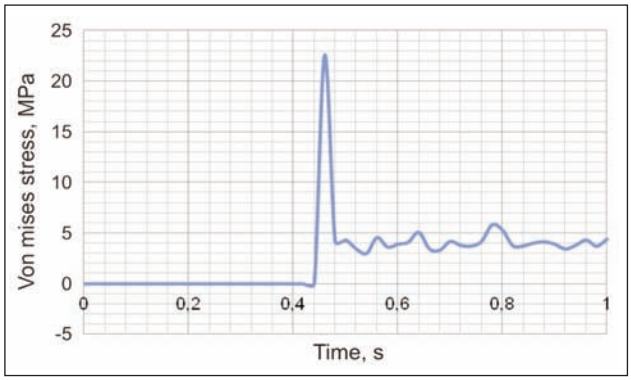

Fig. 9. Evolution in time of von Mises stress field for node 1393

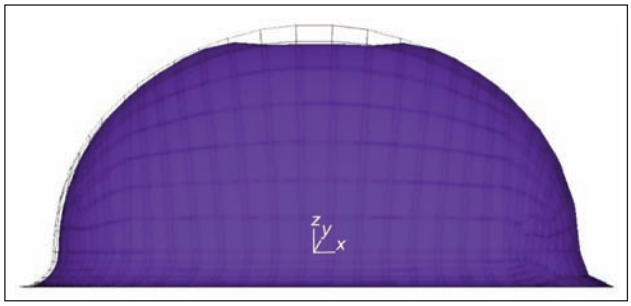

Fig. 10. Helmet deformed shape after impact moment

period after the rejection of the sphere. The stress does not reach the value zero after the impact, as it should happen for an elastic structure, because the helmet is deformed in such a manner as it cannot return to its initial form (is clogged) and remains strained, as one can see in figure 10, which reveals the structure deformation.

CONCLUSIONS

From the point of view of mechanical strength, the material proposed for manufacturing a protection helmet meets the requirements. From the numerical analysis, a maximum equivalent stress was obtained at the simulated impact test of the helmet, much below the material's ultimate strength.

In figure 4, we can notice that the von Mises stress obtained from the calculation is higher than the real ones, as, in the finite elements analysis, the material was considered to be linear elastic. Thus, the obtained results can be considered as conservative.

Since the mechanical properties obtained for the studied biocomposite material are comparable with those of composites reinforced with glass or carbon fibers, the cotton fiber reinforced material represents an ecological alternative in engineering applications of classic composites. In some practical applications, flexibility or a low stiffness may be required. In such cases, the low Young's modulus of this material is an argument for its practical use. The food industry is a field where the researches regarding the ecological and biodegradable materials are motivated not only by the mechanical characteristics, but also by the health norms imposed.

In a future study, the effects of the impact on the helmet placed on the head will be analyzed, for different elastic elements or foam jacketing used inside it. This aspect is important as the impact energy is absorbed in different ways, depending on the elements inside the helmet. A complex finite element model will be also developed, to take into account the anisotropic and non-linear character of the helmet material, as well as the internal elements of the helmet and its clamping on the head.

Acknowledgements

The work of Virgil Tudose has been funded by the Sectoral Operational Programme Human Resources Development 2007-2013 of the Ministry of European Funds through the Financial Agreement POSDRU/159/1.5/S/134398.

Radu Francisc Coterlici wishes to acknowledge the Structural Funds Project, Sectoral Operational Programme Human Resources Development (SOP HRD), ID137516 and the Structural Founds Project PRO-DD (POS-CCE, O.2.2.1., ID 123, SMIS 2637, ctr. No 11/2009) financed from the European Social Fund and by the Romanian Government respectively for providing the infrastructure used in this research work.

BIBLIOGRAPHY

[1] M. Ramesh, K. Palanikumar, K. Hemachandra Reddy, *Comparative evaluation on properties of hybrid glass fiber - sisal/jute reinforced epoxy composites*. In: Procedia Engineering, 2013, Vol. 51, pp. 745–750;

[2] F.A. Silva, R.D.T. Filho, J.A.M. Filho, E.M.R. Fairbairn, *Physical and mechanical properties of durable sisal fiber-cement composites*. In: Construction and Building Materials, 2010, Vol. 24, pp. 777–785;

[3] G. Koronis, A. Silva, M. Fontul, *Green composites: A review of adequate materials for automotive applications*. In: Composites: Part B, 2013, Vol. 44, pp. 120-127;

[4] T. Alomayri, F.U.A. Shaikh, I.M. Low, *Effect of fabric orientation on mechanical properties of cotton fabric reinforced geopolymer composites*. In: Materials and Design, 2014, Vol. 57, pp. 360–365;

[5] T. Alomayri, F.U.A. Shaikh, I.M. Low, *Synthesis and mechanical properties of cotton fabric reinforced geopolymer composites*. In: Composites: Part B, 2014, Vol. 60, pp. 36–42;

[6] G. Pamuk, F. Ceken, *Comparison of the mechanical behavior spacer knit cotton and flax fabric reinforced composites*. In: Industria Textilă, 2013, vol. 64, issue 1, pp. 3–7;

[7] A. Baltazar-Y-Jimenez, M. Sain, *Natural fibres for automotive applications – Handbook of natural fibres*, Vol. 2, Woodhead Publishing Limited, Ryszard M. Kozlowski, Cambridge, 2012, p. 225;

[8] T. Alomayri, F.U.A. Shaikh, I.M. Low, *Characterisation of cotton fibre-reinforced geopolymer composites*. In: Composites: Part B, 2013, Vol. 50, pp. 1–6;

[9] T. Alomayri, F.U.A. Shaikh, I.M. Low, *Synthesis and mechanical properties of cotton fabric reinforced geopolymer composites*, In: Composites: Part B, 2014, Vol. 60, pp. 36–42;

[10] Z. Wu, C. Wei, L. Lv, *Preparation and mechanical properties of cotton stalk bast fibers reinforced polypropylene composites*, In: Advanced Materials Research, 2012, Vol. 482–484, pp. 929–932.

[11] J.P. Qu, B. Tan, Y.H. Feng, S.X. Hu, *Mechanical properties of poly(butylene succinate) reinforced with continuously steam-exploded cotton stalk bast*, In: Polymer-Plastics Technology and Engineering, 2011, Vol. 50, nr. 14, pp. 1405–1411.

[12] A. K. Mohanty, M. Misra, L. T. Drzal, *Sustainable bio-composites from renewable resources: opportunities and challenges in the green materials world*, In: Journal of Polymers and the Environment, 2002, Vol. 10, pp. 19–26;

[13] D. Gon, K. Das, P. Paul, S. Maity, *Jute composites as wood substitute*. In: International Journal of Textile Science, 2012, Vol. 1, pp. 84–93;

[14] M. Aare, S. Kleiven, *Evaluation of head response to ballistic helmet impacts using the finite element method*. In: International Journal of Impact Engineering, 2007, Vol. 34, pp. 596–608;

[15] V. Kostopoulos, Y.P. Markopoulos, G. Giannopoulos, D.E. Vlachos, *Finite element analysis of impact damage response of composite motorcycle safety helmets*. In: Composites: Part B, Vol. 33, 2002, pp. 99–107;

[16] M.A. Forero Rueda, L. Cui, M.D. Gilchrist, *Optimisation of energy absorbing liner for equestrian helmets. Part I: Layered foam liner*. In: Materials and Design, Vol. 30, 2009, pp. 3405–3413;

[17] P.K. Pinnoji, P. Mahajan, N. Bourdet, C. Deck, R. Willinger, *Impact dynamics of metal foam shells for motorcycle helmets: Experiments & numerical modeling*. In: International Journal of Impact Engineering, Vol. 37, 2010, pp. 274–284;

[18] http://www.netcomposites.com/guide/polyester-resins/8

[19] https://www.princeton.edu/~ota/disk2/1988/8801/880106.PDF

[20] SR EN ISO 14125. *Clasa II. Materiale plastice armate cu „mat”-uri, continui și țesături, precum și formate mixte* (Class II. Plastic materials reinforced with continuous “matt’s and woven fibers and mixed formats), 2000 (in Romanian);

[21] http://148.204.81.206/Ansys/150/ANSYS%20Mechanical%20Users%20Guide.pdf (ANSYS Mechanical user guide, 2013);

[22] EN 397:2012, Industrial safety helmets, Section: Impact testing, 2012.

Authors:

VIRGIL TUDOSE
DANIELA TUDOSE
HORIA GHEORGHIU
STEFAN DAN PASTRAMA

University Politehnica of Bucharest
Faculty of Engineering and Management of Technological Systems
Splaiul Independentei nr. 313, Sector 6, 060042 Bucharest, Romania
e-mail: virgil.tudose@upb.ro, daniela.tudor@upb.ro,
hgheorghiu@yahoo.com, stefan.pastrama@upb.ro

RADU FRANCISC COTERLICI

Transilvania University, Department of Materials Science,
Bulevardul Eroilor nr. 29, 500036, Brasov, Romania
e-mail: coterliciradufrancisc@yahoo.com

Corresponding author:

STEFAN DAN PASTRAMA
stefan.pastrama@upb.ro

Construction of adapted garments for people with scoliosis using virtual prototyping and CASP method

ZORAN STJEPANOVIČ
ANDREJ CUPAR
SIMONA JEVŠNIK

TANJA KOCJAN STJEPANOVIČ
ANDREJA RUDOLF

REZUMAT – ABSTRACT

Construcția articolelor de îmbrăcăminte adaptate persoanelor cu scolioză utilizând prototiparea virtuală și metoda CASP

Obiectivul studiului prezentat în acest articol este de a explora o nouă modalitate de proiectare și realizare de prototipuri virtuale ale articolelor de îmbrăcăminte, adaptate persoanelor cu scolioză. Persoanele cu scolioză se confruntă cu probleme zilnice legate de achiziționarea și utilizarea de articole de îmbrăcăminte adecvate, ajustate pe corp și confortabile. Considerăm că putem îmbunătăți aspectul și ajustarea pe corp a îmbrăcămintei purtate de persoanele cu scolioză prin construirea unui model de îmbrăcăminte adaptat, ținând seama de zonele deformate ale corpului. Din acest motiv, s-au aplicat instrumente și metode virtuale avansate, cum ar fi CASP (Curbură, Accelerare, Simetrie, Proporționalitate), pentru construirea tiparului de îmbrăcăminte adaptat la modelul 3D al corpului deformat din cauza scoliozei. În acest fel, este posibil să se îmbunătățească aspectul optic al articolului de îmbrăcăminte și ajustarea acestuia pe corp. Cu un design adaptat al articolului de îmbrăcăminte, s-a proiectat o rochie cu un aspect mai bun al cusăturii pe partea din spate, precum și ajustarea în zona omoplaților. Rezultatele studiului au confirmat faptul că procesul de reconstrucție a modelului de bază al rochiei îmbunătățește aspectul și ajustarea acesteia pe un corp deformat.

Cuvinte-cheie: construcția articolului de îmbrăcăminte, modele adaptate, scolioză, metodă CASP, analiza suprafeței

Construction of adapted garments for people with scoliosis using virtual prototyping and CASP method

The goal of the study presented in this article is to explore the new way to design and produce virtual prototypes of garments, adapted for people with scoliosis. People with scoliosis are faced with everyday problem related to purchase and use of suitable, well-fitted and comfortable garments. Our assumption was that we can improve the appearance and fit of the garment to the person with scoliosis by constructing the adapted garment pattern design, taking into account the deformed areas of the body. For this reason we have applied advanced virtual tools and methods, such as CASP (Curvature, Acceleration, Symmetry, Proportionality), for constructing the garment pattern designs adapted to the 3D body model deformed as a consequence of scoliosis. In this way, it is possible to improve the optical appearance of the garment and its fit to the body. With adapted dress pattern design, we succeeded to design a dress with better appearance of the seams on the back as well as the fit in the area of shoulder blades. The results of the study confirmed that reconstruction process of the basic dress pattern design improves the appearance and fit of the dress to a deformed body.

Keywords: garment construction, adapted patterns, scoliosis, CASP method, surface analysis

INTRODUCTION

This article presents a study on design and construction of adapted patterns for people suffering from scoliosis. Scoliosis can be understood as a medical condition represented as a three-dimensional deviation of the spinal axis [1]. It is defined as a spinal curvature of more than 10 degrees to the right or left as the examiner faces the patient (in the coronal plane). Deformity may also exist to the front or back (in the sagittal plane) [2]. Within this study we have investigated the possibilities of virtual prototyping of garments and CASP (Curvature, Acceleration, Symmetry, Proportionality) methodology for evaluation of the shape of surfaces. The methodology proved to have a significant potential for construction of adapted pattern designs in order to produce garments for people suffering from scoliosis or other body deformations. CASP has been developed by a group of researchers at the University of Maribor and represents a new attempt to describe the shape of different surfaces using four classification properties [3]. The methodology is described in more details below

GARMENTS FOR PEOPLE SUFFERING FROM SCOLIOSIS

It is not easy to find appropriate, well-designed and well-fitted garments for people with scoliosis. They are often faced with a problem how to dress nicely and comfortable. Different advices can be found in literature and lately on specialized webpages or blogs, such as [4–6]. Approximately 4% of the population has scoliosis. Scoliosis can cause visible symptoms: uneven shoulders, head not centered, ribs different

Fig. 1. Scoliotic and a normal spine

heights, a shoulder blade that sticks out more than the other, uneven hips, one leg appearing shorter than the other, the body leaning to one side. More severe cases will present with more severe outward appearance of these symptoms [7–9]. Because scoliosis causes this asymmetry in the body, imperfectly-fitting clothing can become an everyday problem. The waist on pants or skirts may appear uneven or shirts and dresses may not fit or hang on the body properly. Dressing in a way that makes the individual feel best and secure with their scoliosis can become a challenge [4–5]. One of the easiest ways to mask scoliosis is avoid tightly fitting clothing. Individuals with scoliosis tend to be small framed, and long waisted, so their bones are very pronounced. Tight shirts can reveal the asymmetry more obviously. Not only can clothing like tight t-shirts and blouses emphasize scoliosis more, but because there is an asymmetry one side might feel much tighter than the other making these types of clothing uncomfortable [6]. A scoliotic and a normal spine are presented in figure 1 [10].

EXPERIMENTAL PART

3D body models

In our study, we focused on design and construction of garments, adapted for people with scoliosis. Our assumption was that we can improve the appearance and fitting of the garment on the person with scoliosis by constructing the adapted garment pattern design taking into account the deformed areas of the body. For this reason, we have prepared a synthetic 3D body model using Makehuman software, figure 2 [11]. As it can be seen from the figure, the gray model represents a normal body and the green one a model with scoliosis. The spine is curved, which causes the leaning of the body model in the area of the shoulder blade to the left. Consequently, left shoulder blade is protruding from the normal plane. 3D body model was finally improved using Blender software, figure 3 [12].

Idealized human body is symmetric. The producers of ready-made garments cannot consider the deformations of the body, caused by scoliosis, because

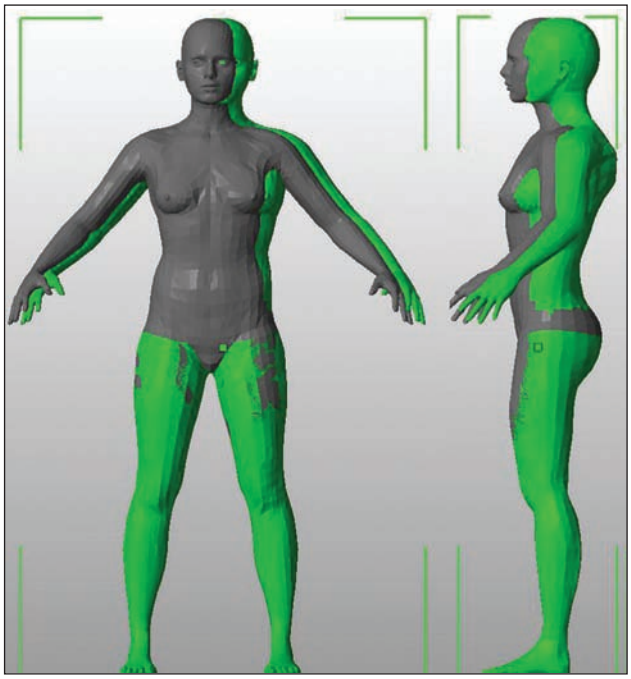

Fig. 2. Normal (gray) and scoliotic synthetic female body (green)

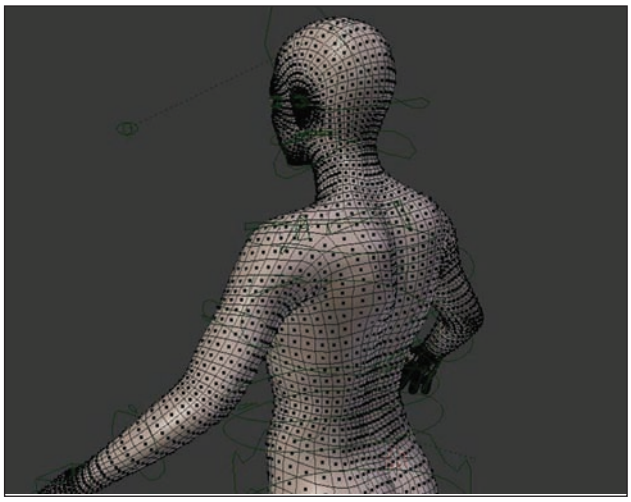

Fig. 3. Improvement of a 3D body model using Blender software

they are specific and differ from case to case. Therefore, the only solution to improve the appearance and fit of the garment seems to be an individual approach to this problem. This means that it is necessary to study the deformation areas of the body and construct adapted garment pattern designs for each case individually.

Introduction of CASP method

For the purpose of analysis of the deformed areas of a human's body, we have applied in this study a new method called CASP (Curvature, Acceleration, Symmetry, Proportionality). CASP was originally developed as a method for classification of perceptual surfaces and for analyzing digital geometry [3, 13–14]. Methodology of surface evaluation was developed to establish the meta-language in design

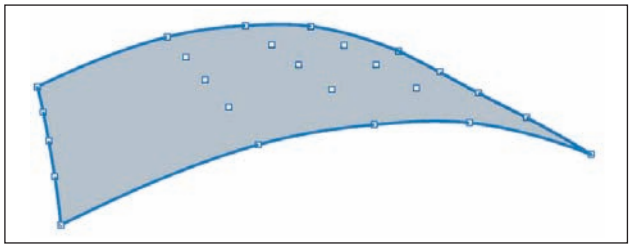

Fig. 4. Curvature

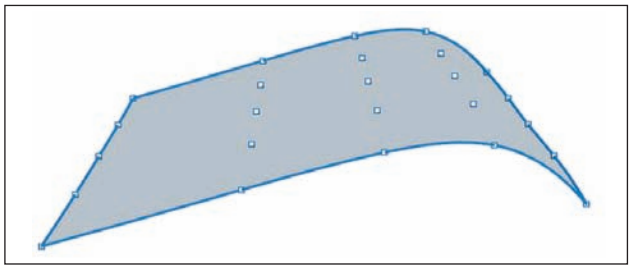

Fig. 5. Accelerated surface

communication, which was perceived as necessary part of styling. The first step was analysis of existing geometry and the second a synthesis of newly created geometry considering desired property. There are four properties, which characterize surfaces similar to colors in color space [15], where each color is represented as a mix of values L*, a* and b*.

The surface's geometrical space consists of these four properties:

- Curvature – C,
- Acceleration – A,
- Symmetry – S and
- Proportionality – P.

A surface is indicated as (C, A, S, P). Curvature goes from – to + sign. Zero determinates a neutral curvature and represents a plane. Negative values mean a concave surface and positive values are for convex surfaces, figure 4 [3, 13–14]. They are evaluated with sign and values of entities in $n \times n^{10}$ matrix. Value is calculated as arithmetic average of normalized $n \times n$ distances including a preposition sign. The $n \times n$ matrix follows natural directions and is not the same as in mathematical writing. It has swapped rows over middle row. Therefore, the matrix starts with entry (0,0) at bottom left corner as shown in expression (1).

$$\begin{bmatrix} a_{n-1,0} & \cdots & a_{n-1,n-1} \\ \vdots & & \vdots \\ a_{0,0} & \cdots & a_{0,n-1} \end{bmatrix} \quad (1)$$

Starting point marked with (0,0) is at the bottom left side on analyzed surface, same as in $n \times n$ matrix. This enables to locate position of same point in 3D space and in $n \times n$ matrix.

Acceleration is a characteristic of an elementary surface, which is observed in a longitudinal direction, figure 5 [3, 13–14]. Figures 4–7 have been originally created by the authors from the University of Maribor,

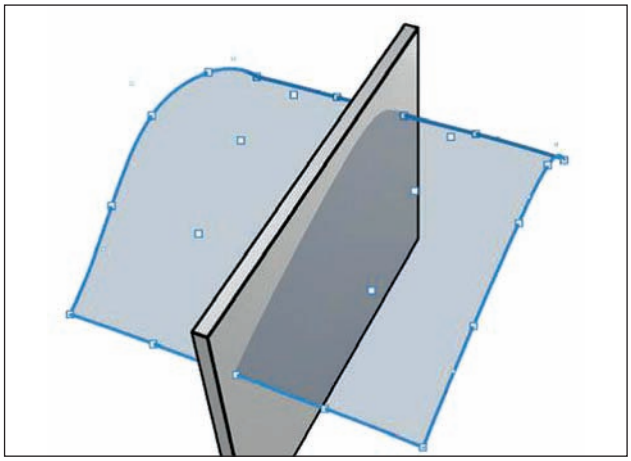

Fig. 6. Symmetry

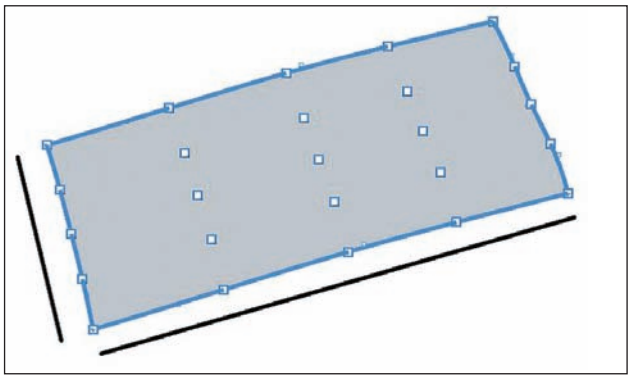

Fig. 7. Proportionality

Slovenia, within the research related to the CASP methodology development [3, 13–14].

Symmetry takes just positive values. Zero means perfect symmetry of a surface observed over middle column of $n \times n$ matrix, figure 6 [3, 13–14]. Symmetry can be detected as differences between entities pairs compared over the middle column. The first and last column are compared and second and the last but one. The middle one stays untouched in this case. Symmetry is calculated as arithmetical average of all entity pairs. Proportionality, figure 7, is the fourth property to indicate the size or width of the surface [3, 13–14]. It is calculated as a ratio between the length and width of the observed surface, projected on a triangular plane.

The whole $n \times n$ procedure is based on the use of a graphical algorithm Grasshopper® (GH), which is tightly integrated with 3D modelling tool Rhinoceros (RH) [16–17]. Grasshopper is an add-on and runs within the RH application. Procedures are created by dragging components onto a canvas. Outputs of these components are then connected to the inputs of subsequent components. Grasshopper is mainly used to build generative algorithms and it acts like a programming tool. Many of Grasshopper's components create 3D geometry. Procedures may also process other types of algorithms including numeric, textual, audio-visual or haptic applications. GH is used because of complex algorithms that can be used out

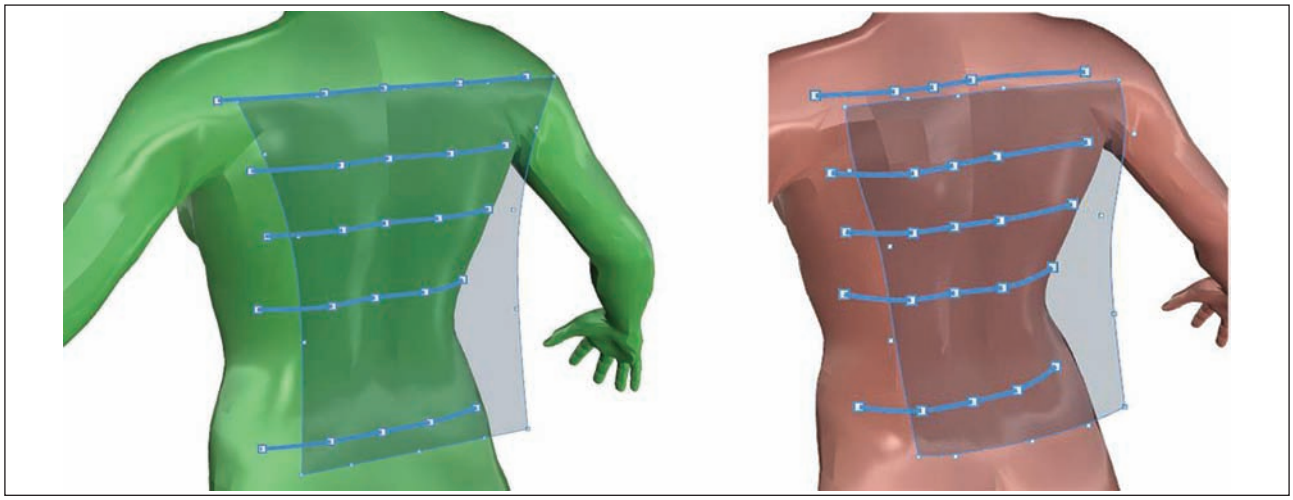

Fig. 8. Cross-section parts on the back for a normal body (left) and deformed body (right)

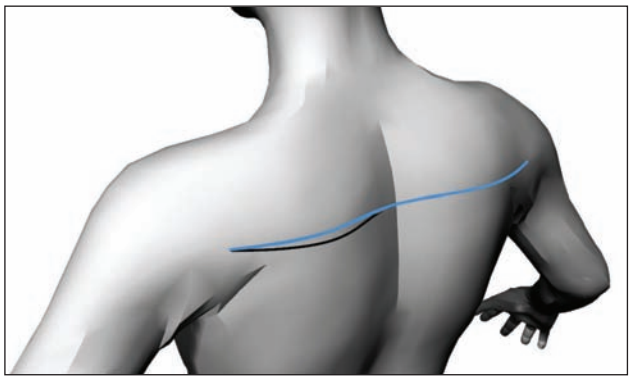

Fig. 9. Scoliotic deformation in the left shoulder area

of the box and can be easily connected and combined. The whole procedure for analyzing digitized surface geometries is based on 10 steps, described in [3, 14].

RESULTS AND DISCUSSION

Both body models, presented in figure 2, were analyzed using the CASP method in the shoulder area, figure 8. Scoliotic deformation in the left shoulder area is represented in figure 9. The blue line follows the curve of the normal body. Deformation in the left shoulder area is seen in the form of a black curve, following the shape of a scoliotic shoulder blade, figure 9.

For the normal model we got the following CASP values, measured in the observed shoulder area:

CASP: (–0.12 ; –0.64 ; 10.30 ; 1.11)

The analysis of the deformed model resulted with these values:

CASP: (–3.06 ; 15.30 ; 185.31 ; 1.17)

Differences in CASP properties are primarily in symmetry, which is expected, since we artificially created the asymmetry. There are also greater values of Curvature and Proportionality. Since it is a composite surface, the Acceleration does not have the same meaning as in elementary surfaces, therefore it will not be considered for this case. Interesting and useful

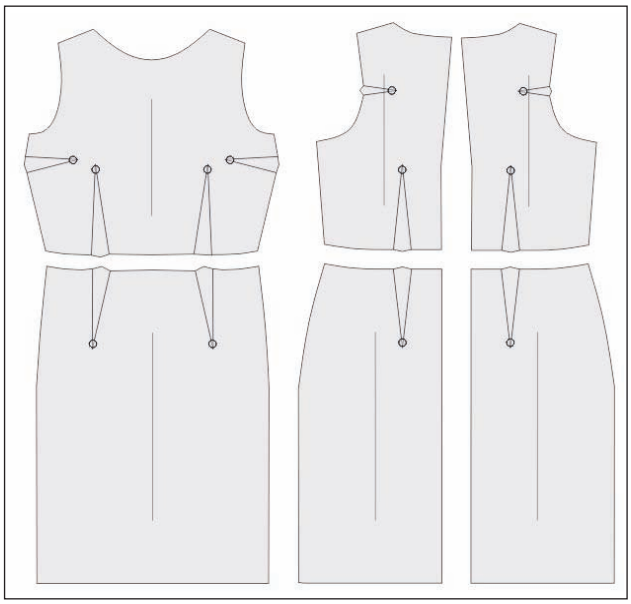

Fig. 10: Basic dress pattern design

are the cross-sections in the examined area of the body. They can be used for the method DEGI (Design with Existing Geometry Implementation) or generally for the analysis of the curvature of the model in a particular cross-section [3].

The dress basic pattern design was constructed according to normal (symmetric) synthetic female body dimensions by using rules of the construction system M. Müller&Sohn and Optitex CAD/PDS system, figure 10 [18–19]. The virtual fitting of the basic dress pattern design on the normal and scoliotic synthetic female bodies are shown in figure 11. It is evident that differences in CASP values are also reflected in the appearance of the dress, figures 11, 13, 14, 15. The deformed body is asymmetric, therefore, the straight seam in the middle of the back, figure 11 (a), because of convex blade, is moved to the right and appearance of the dress enhances asymmetry of the body, figure 11 (b). Also the movement of the darts and their asymmetry according to the body can be

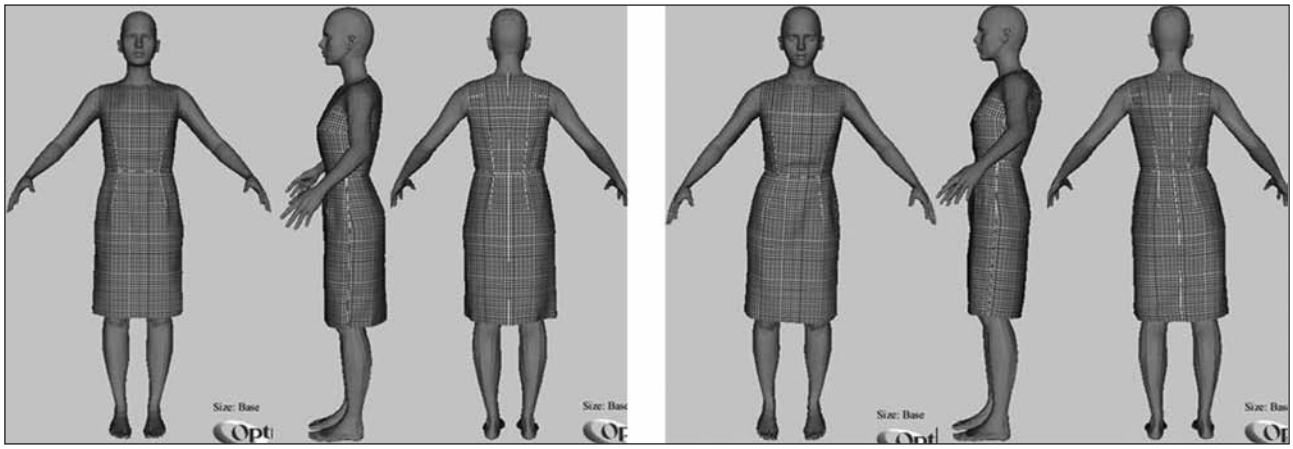

a *b*

Fig. 11. Basic dress pattern design on the normal (a) and scoliotic (b) synthetic female body

seen, as well as shortening of the dress on the right side of the body.

With reconstruction of the basic dress pattern design we wanted to improve the visual appearance and balance of the asymmetric body. For this reason we have observed the shoulder area in both normal and scoliotic body. Using the Optitex software functions we have determined average Tension XY and Tension X above all in the area, marked in figure 12. Graphical results of the tension analysis of combinations related to normal/deformed body and normal/adapted dress are presented in figures 13–15. It can be seen from the tension map that we successfully lowered the tension and therefore also fit and wearing comfort of the garment in the shoulder area.

We have also performed the statistical analysis of results using the F- and t-test regarding the values of

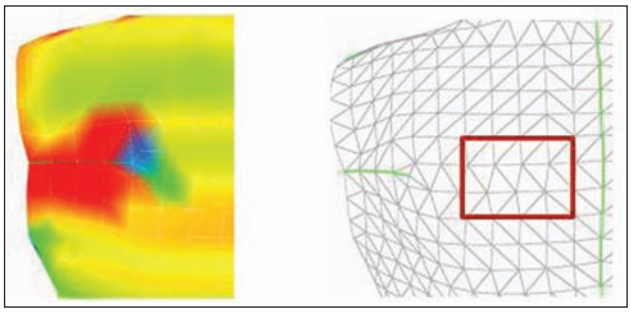

Fig. 12. Determination of Tension XY and Tension X in the investigated left shoulder area

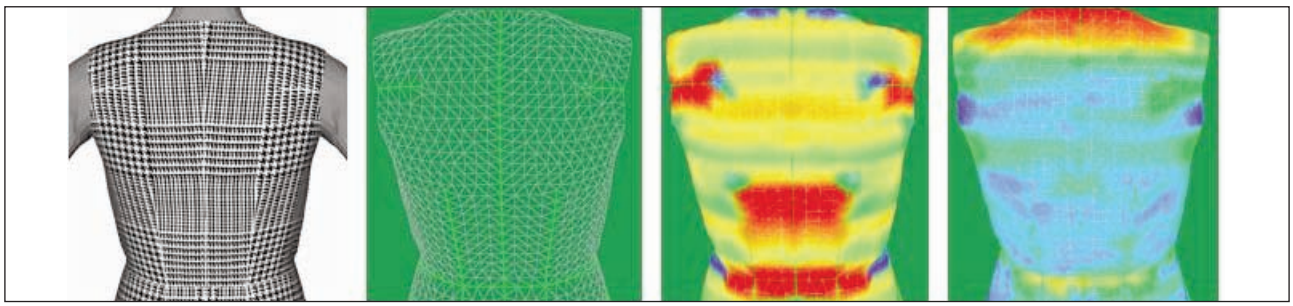

Tension XY 1.45 fg/cm Tension X 0.28 fg/cm

Fig. 13. Tension analysis for a normal body and normal dress

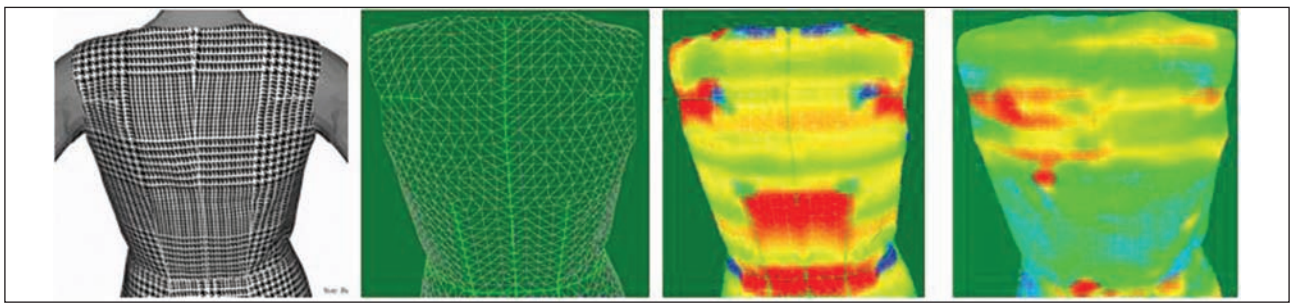

Tension XY 1.46 fg/cm Tension X 1.09 fg/cm

Fig. 14. Tension analysis for a deformed body and normal dress

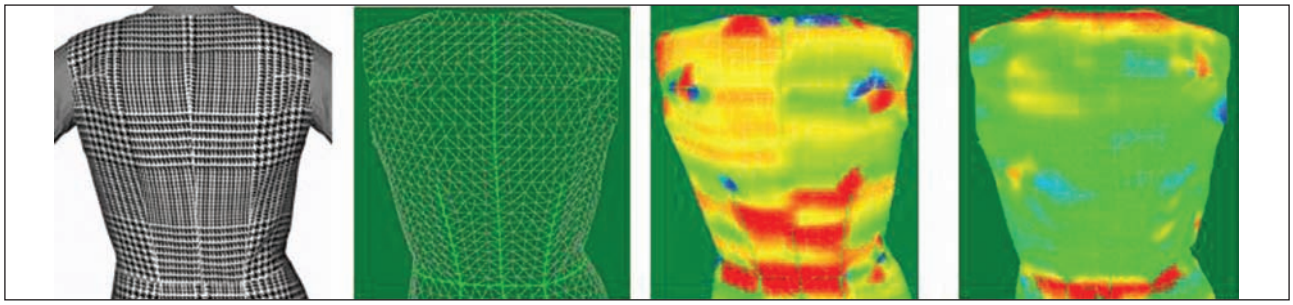

Tension XY 1.45 fg/cm Tension X 0.64 fg/cm

Fig. 15. Tension analysis for a deformed body and adapted dress

Table 1

RESULTS OF STATISTICAL ANALYSIS RELATED TO TENSION XY AND TENSION X						
Comparison between DB-ND and DB-AD						
	F_{calc}	F_{tab}	H_0: $s_1 = s_2$	T_{calc}	T_{tab}	**Significance of difference**
Tension XY	0,27	0,43	Accept	0,49	2,06	Statistically insignificant
Tension X	0,74	0,43	Reject	9,37	2,04	Statistically significant

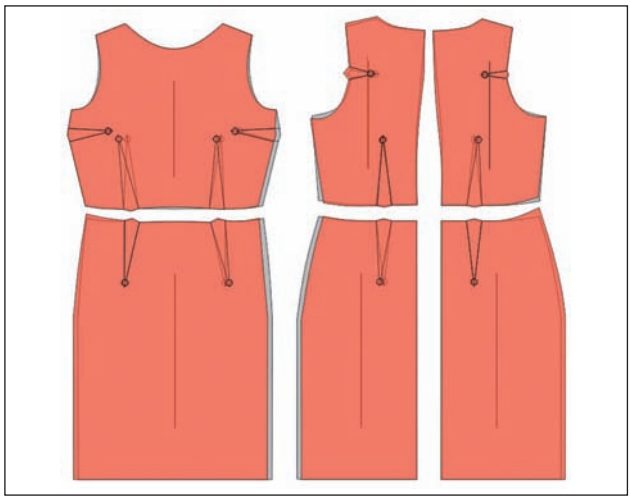

Fig. 16. Comparison between basic dress pattern design for the normal (grey) and scoliotic female (red)

Tension XY and Tension X. Namely, differences are seen above all in transverse direction (direction of the weft in the fabric). The results regarding the comparison of combinations deformed body/normal dress and deformed body/adapted dress are in table 1.

Based on this analysis, and with an inspection of the deformation areas of the body and dress the relocations of the dress side seams, waist seams, back middle seam in the blade area were performed, as well as relocations of the waist, breast and blade darts, figure 16.

Virtual prototype of the adapted basic dress pattern design to a scoliotic female's body is presented in figure 17. When comparing figures 11 (b) and 17 it is clearly visible that reconstruction process of the basic dress pattern design improves the appearance and fit of the dress to a deformed body. The seam in the middle of the back is aligned, darts are symmetrical with respect to the center of the body. Seam line in the waist and dress edge are aligned. We have intentionally chosen the sensitive checkered fabric pattern.

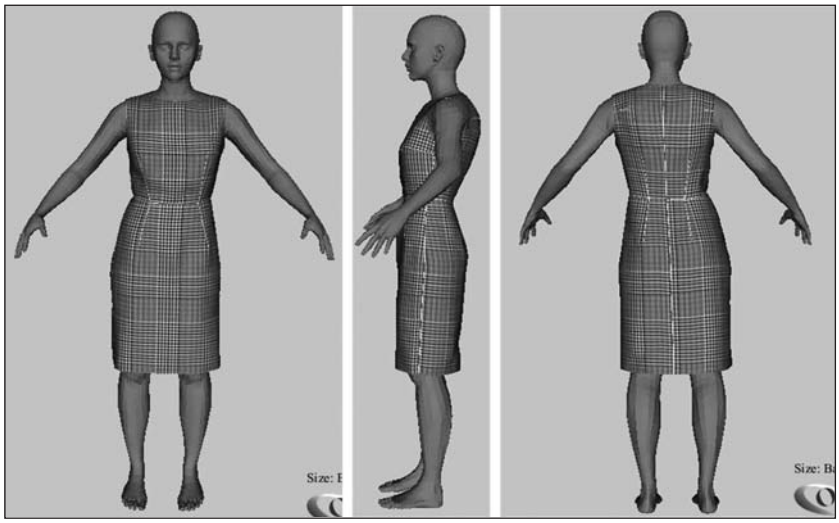

Fig. 17. Adapted (reconstructed) basic dress pattern design on a deformed body

CONCLUSIONS

In this study we have shown that advanced virtual tools and methods, such as CASP, can be used for constructing the garment pattern designs adapted to the 3D body model deformed as a consequence of scoliosis. When designing patterns for garments we commonly use the functionalities of computer-based pattern-design systems (PDS). In this study, we have used the Optitex PDS. The

functionalities works well for patterns, intended for garments for people without body deformations. In cases, related to the pattern design of adapted garments for people with body deformations, such as those seen in scoliotic bodies, we need to apply additional analyses, because commercial PDS packages do not offer functionalities for supporting special requirements. CASP method for evaluation of shape of surfaces, which was originally developed as analysis tool and classification methodology of perceptional surfaces in product design, was successfully used in this study for analyzing the deformed areas in a scoliotic body. The results, CASP values and curves, following the deformed left shoulder blade, were then used for constructing the adapted female's dress. In such a way, an engineered approach was applied and realized in the area of garment design/construction. Beneficial outcomes can be seen as improved optical appearance of the garment and its fit to the body. From the tension maps, presented in figures 13–15, it can be seen that we successfully lowered the tension and therefore also fit and wearing comfort of the garment in the shoulder area. Already minor reduction of tension appearing in a garment contributes significantly to wearing comfort, which is very important in cases of deformed bodies.

With an adapted dress pattern we succeeded to design a dress with better appearance of the seams on the back as well as the fit in the area of shoulder blades. It can be concluded that the potential of such approach can be recognized as a promised one. The garments made using adapted pattern designs fit the persons with scoliosis better, even tight clothes, such as a dress, presented in this article. Such garments can definitely rise the confidence and self-esteem of modern women suffering from scoliosis since they are not forced to use only loose clothes. Our further research will include garments for men suffering from scoliosis. We also intend to extend our studies using CASP method towards the virtual prototyping of adapted garments for people with other body deformations and people with limited body mobility (some preliminary studies already published in [20, 21, 22]).

ACKNOWLEDGMENT

A part of this study belongs to the Adva2Tex ERASMUS+ project, which has been funded with support from the European Commission. This publication reflects the views only of the author, and the Commission cannot be held responsible for any use which may be made of the information contained therein.

BIBLIOGRAPHY

[1] Per Trobisch, Olaf Suess, Frank Schwab; Suess; Schwab (December 2010). *Idiopathic scoliosis*, In: Disch Arztebi Int. 107 (49): pp. 875–884.

[2] *Scoliosis*, available from: https://en.wikipedia.org/wiki/Scoliosis, accessed [29. 06. 2015].

[3] Cupar, A., *Development of classification methodology of perceptional surfaces in product design*, Doctoral Dissertation, University of Maribor, Faculty of Mechanical Engineering, 2015.

[4] *Clothing ideas for scoliosis*, available from: http://www.well-women.com/Clothing.html, accessed [29. 06. 2015].

[5] Strauss, A., *How to Dress with Scoliosis*, available from: http://www.hudsonvalleyscoliosis.com/clothing-for-scoliosis/, accessed [1. 07. 2015].

[6] *Patternmaking for people with postural deviations*, available from: http://www.well-women.com/Clothing.html, accessed [1. 07. 2015].

[7] *Spinal deformities: the essentials*. Edited by Robert F. Heary, Todd J. Albert. New York, Thieme Medical Publishers, 2007.

[8] *Spinal deformities.* Guest Edito Robert B. Winter. The Orthopedic clinics of North America, ISSN 0030-5898, Vol. 25,2. Philadelphia, W.B. Saunders Company, Cop. 1994.

[9] *Scoliosis*, University of Washington, Department of Radiology, available from: http://www.rad.washington.edu/academics/academic-sections/msk/teaching-materials/online-musculoskeletal-radiology-book/scoliosis, accessed [23. 11. 2015].

[10] *Orthotic treatment for scoliosis*, available from: http://centralbraceandlimb.com/ orthotic-treatment-scoliosis/, accessed [1. 07. 2015].

[11] *Makehuman, Open source tool for making 3D characters*, available from: http://www.makehuman.org/, accessed [20. 05. 2015].

[12] *Blender, Open source 3D creation software*, available from: https://www.blender.org/ accessed [20. 05. 2015].

[13] Cupar, A., Pogačar, V., Stjepanović, Z., *Methodology for surfaces analysis and classification*. Universal journal of mechanical engineering, ISSN 2332-3353. [Print ed.], Feb 2014, no. 2, vol. 2, pp. 64–70.

[14] Cupar, A., Kaljun, J., Pogačar, V., Stjepanović, Z., *Methodology framework for surface shape evaluation*. In: Proceedings of the International Conference on Mechanical Engineering (ME 2015, Vienna, Austria, March 15–17, 2015, Recent advances in mechanical engineering series, ISSN 2227-4596, 13, 2015, pp. 58–65.

[15] *CIELAB color model*, available from: http://dba.med.sc.edu/price/irf/Adobe_tg/ models/cielab.html, accessed [16. 02. 2015].

[16] *Grasshopper*, Algorithm modelling for Rhino, available from: http://www.grasshopper3d.com/, accessed [4. 03. 2015].

[17] *Rhinoceros*, available from: https://www.rhino3d.com/, accessed [4. 03. 2015].

[18] System M. Müller & Sohn: *Schnittkonstruktionen für Kleider und Blusen*, Deutsche Bekleidungs-Akademie München, Rundschau Verlag, München, 1992.

[19] *Optitex*, available from: http://www.optitex.com/, accessed [2. 07. 2015].

[20] Rudolf, A., Cupar, A., Kozar, T., Stjepanović, Z., *Study regarding the virtual prototyping of garments for paraplegics*. Fibers and polymers, ISSN 1229-9197, May 2015, vol. 16, no. 5, pp. 1177–1192.

[21] Kozar, T., Rudolf, A., Cupar, A., Jevšnik, S., Stjepanović, Z., *Designing an adaptive 3D body model suitable for people with limited body abilities*. Journal of textile science & engineering, ISSN 2165-8064. [Online ed.], Nov. 2014, vol. 4, iss. 5, pp. 1–13

[22] Rudolf, A., Kozar, T., Cupar, A., Jevšnik, S., Stjepanović, Z., *Development of appropriate garment pattern designs for a sitting position 3D body model*. 10th Conference of Chemists, Technologists and Environmentalists of Srpska Republic, Banja Luka, 2013, pp. 380–388

Authors:

ZORAN STJEPANOVIČ[1]

ANDREJ CUPAR[1]

SIMONA JEVŠNIK[2]

TANJA KOCJAN STJEPANOVIČ[3]

ANDREJA RUDOLF[1]

[1]University of Maribor, Faculty of Mechanical Engineering, Smetanova 17, 2000 Maribor, Slovenia,
e-mail: zoran.stjepanovic@um.si, webpage: http://www.fs.uni-mb.si/

[2]Istanbul Technical University, Faculty of Textile Technologies and Design, Istanbul, Turkey
e-mail: simonajevsnik@gmail.com

[3]DOBA Faculty of Aplied Business and Social Studies Maribor, Slovenia
e-mail: tanjaks@prava-poteza.si